Spring 5-4-2020

Melanocortin-3 Receptor-Expressing Neurons of The Ventral Tegmental Area: Anatomy and Regulation of Feeding and Body Weight

Anna I. Dunigan

MELANOCORTIN-3 RECEPTOR-EXPRESSING NEURONS OF THE VENTRAL TEGMENTAL AREA: ANATOMY AND REGULATION OF FEEDING AND BODY WEIGHT

by

ANNA DUNIGAN

Under the Direction of Aaron Roseberry, PhD

ABSTRACT

Over two-thirds of the US population are overweight or obese with obesity's associated co-morbidities representing 4 out of the 5 leading causes of death. Since the 1970s, a shift in the environment of developed countries has perpetuated overconsumption of calorie-rich foods which is thought to be the primary cause of the obesity epidemic. Thus, understanding neural mechanisms underlying feeding is critical for obesity prevention and treatment. Two of the systems important for feeding regulation are the hypothalamic melanocortin system and the mesocorticolimbic dopamine (DA) system. Increasing evidence indicates that these two systems interact to control feeding but the underlying mechanisms including the main site of their interaction are not understood. Neurons expressing melanocortin-3 receptor in the ventral tegmental area (VTA MC3R neurons) may be a key site for this interaction, as MC3Rs are highly expressed in the VTA, the center of the mesocorticolimbic DA system, and are an important component of the melanocortin system. Hence, I used genetic and viral approaches in mice to characterize the anatomy of VTA MC3R neurons and to determine whether changes in

their activity alter feeding and body weight. I found that VTA MC3R neurons were connected to a discrete set of brain areas involved in regulation of feeding, reward, and aversion and received a surprisingly small amount of input from the hypothalamic arcuate nucleus (Arc), the center of melanocortin system. Further examination of Arc-VTA connectivity revealed that hypothalamic proopiomelanocortin (POMC) and agouti-related protein (AgRP) neurons formed few synapses on the different subtypes of VTA neurons, despite strong labeling by general retrograde tracers injected into the VTA. I also found that VTA MC3R neurons control feeding and body weight in an activity- and sex-dependent manner such that acute activation of VTA MC3R neurons decreased feeding, but only in females, and acute inhibition of these neurons decreased feeding, but only in males, whereas chronic activation transiently decreased feeding and body weight in all mice. These studies greatly contribute to our understanding of the anatomical interactions between the melanocortin and mesocorticolimbic systems and indicate that VTA MC3R neurons may be a key point in these interactions.

INDEX WORDS: VTA, MC3R, Arcuate nucleus, Melanocortin, Feeding, Body weight

MELANOCORTIN-3 RECEPTOR-EXPRESSING NEURONS OF THE VENTRAL TEGMENTAL AREA: ANATOMY AND REGULATION OF FEEDING AND BODY WEIGHT

by

ANNA DUNIGAN

A Dissertation Submitted in Partial Fulfillment of the Requirements for the Degree of

Doctor of Philosophy

in the College of Arts and Sciences

Georgia State University

2020

MELANOCORTIN-3 RECEPTOR-EXPRESSING NEURONS OF THE VENTRAL TEGMENTAL AREA: ANATOMY AND REGULATION OF FEEDING AND BODY WEIGHT

by

ANNA DUNIGAN

Committee Chair: Aaron Roseberry

Committee: Deborah Baro

Daniel N. Cox

Kyle Frantz

Electronic Version Approved:

Office of Graduate Services

College of Arts and Sciences

Georgia State University

May 2020

DEDICATION

I dedicate this dissertation to my family. To my mom and dad for bringing me to a country which makes higher education accessible to all wishing to participate, for allowing me to explore and choose my own way, and for supporting me along each step of that way. To my husband, who patiently walked along with me, picked me up and kept me going. To my son, who was there for some of the experiments and didn't make me sick much! I could not have done any of this without your love, help, and support. Thank you!

ACKNOWLEDGEMENTS

I would like to express my gratitude to my professors and colleagues. I would especially like to thank the members of my dissertation committee, Dr. Deborah Baro, Dr. Daniel N. Cox, and Dr. Kyle Frantz for their guidance, advice, support, patience, and flexibility. I would like to recognize the labs of Dr. Deborah Baro, the late Dr. Tim Bartness, Dr. Hung Shi, Dr. Bingzhong Xue, and Dr. Chun Jiang for granting me access to their equipment and supplies as well as Claudia Sanabria for her help with confocal microscopy. I would also like to thank Dr. Andrew Clancy for stimulating my interest in science, showing me that being a scientist is not a fictional profession, and remaining a friend through the years. I would like to thank my lab mates Melissa Lange, Nia Mitchell, and Geneva Manganiello for helping me maintain the mouse colonies, Andrew Swanson for helpful suggestions and training, and especially Kat West for her continued friendship and support. Finally, I would like to thank my committee chair and mentor, Dr. Aaron Roseberry, for teaching me to think critically, troubleshooting experiments with me, guiding and encouraging me, always being available, and for his support and understanding during difficult times in professional and personal life.

TABLE OF CONTENTS

LIST OF TABLES

LIST OF FIGURES

LIST OF ABBREVIATIONS

5-HT, serotonin

α-MSH, alpha-melanocyte-stimulating hormone

AA, anterior amygdaloid area

AAV, adeno-associated virus

ac, anterior commissure

aca, anterior commissure

AgRP, agouti-related protein

AH, anterior hypothalamic area

ALDH1A1, aldehyde dehydrogenase family 1 member A1

AP, anteroposterior

Arc , arcuate nucleus of the hypothalamus

BFP, blue fluorescent protein

BL(a/p), basolateral amygdala (anterior/posterior)

BM(a/p or A/P), basomedial amygdala (anterior/posterior)

BMI, body mass index

BST(L/M), bed nucleus of stria terminalis (lateral or medial devisions)

CeA, central amygdala

Cg, cingulate cortex

ChR2, channelrhodopsin

Cli, caudal linear nucleus

CNO, Clozapine-N-oxide

CPA, conditioned place aversion

CPu, caudate putamen

D2R, dopamine D2 receptors

DA, dopamine

DAT, dopamine transporter

DMH, dorsomedial hypothalamic nucleus

DP, dorsal peduncular cortex

DR, dorsal raphe

DV, dorsoventral

Ect, ectorhinal cortex

EnvA, avian sarcoma leucosis virus glycoprotein

eYFP, enhanced yellow fluorescent protein

f, fornix

FAA, food anticipatory activity

GAD, glutamic acid decarboxylase

GFP, green fluorescent protein

Gi, gigantocellular reticular nucleus

HDB, nucleus of the horizontal limb of the diagonal band

IC, inferior colliculus

ICjM, major islands of Calleja

Icrtx, insular cortex

Ih, hyperpolarization-activated cation current

IHC, immunohistochemistry

IL, infralimbic cortex

Int, interposed cerebellar nucleus

IP, intraperitoneal

IPAC, interstitial nucleus of the posterior limb of the anterior commissure

Lat, lateral (dentate) cerebellar nucleus

LC, locus coeruleus

LDTg, laterodorsal tegmental nucleus

LGP, lateral globus pallidus

LH, lateral hypothalamus

LHb, lateral habenula

LPB, lateral parabrachial nucles

LPO, lateral preoptic area

LS (LSI/LSD) , lateral septum (intermediate and dorsal segments of the lateral septum)

LV, lateral ventricle

M2, motor cortex

MC3R, melanocortin-3 receptor

MC4R, melanocortin-4 receptor

MCPO, magnocellular preoptic nucleus

MCR, melanocortin receptor

MeA, medial amygdala

MFB, medial forebrain bundle

mGFP, membrane-tethered green fluorescent protein

MHb, medial habenula

ML, mediolateral

mlf, medial longitudinal fasciculus

MnR, median raphe nucleus

MPB, medial parabrachial nucles

MPO, medial preoptic area

MRN, midbrain reticular nucleus

MTu, medial tuberal nucleus

NAcc, nucleus accumbens

NAccC, nuclues accumbens core

NAccSh (m/l), nucleus accumbens shell (medial or lateral)

NEUROD6, neurogenic differentiation factor-6

NPY, neuropeptide Y

NPYR, neuropeptide Y receptor

OC, orbital cortex

OTX2, orthodenticle homeobox 2

PAG, periaqueductal gray

PBP, parabrachial pigmented nucleus

PBS, phosphate-buffered saline

PFC, prefrontal cortex

PH, posterior hypothalamic area

PM, premammillary nucleus

PMnR, paramedian raphe nucleus

PN, paranigral nucleus

POMC, proopiomelanocortin

PPTg, pedunculopontine tegmental nucleus

Pr, prepositus nucleus

PRh, perirhinal cortex

PrL, prelimbic cortex

PSTh, parasubthalamic nucleus

PV, paraventricular thalamic nucleus

PVH, paraventricular nucleus

rG, rabies glycoprotein

RLi, rostral linear nucleus

RMg, raphe magnus nucleus

RMTg, rostromedial tegmental nucleus

RNr, pontine reticular nucleus

ROI, region of interest

RR, retrorubral nucleus and field

RRF, retrorubral field

RVdG, G-deleted rabies virus

S1, somatosensory cortex

SC, superior colliculus

scp, superior cerebellar peduncle

SI, substantia innominata

sm, stria medullaris of the thalamus

SN, substantia nigra

SNC, substantia nigra pars compacta

st, tria terminalis

Su3, supraoculomotor periaqueductal gray

SYP/SYN, synaptophysin

TH, tyrosine hydroxylase

Tu, olfactory tubercle

TVA, avian receptor protein

vGlut2, vesicular glutamate transporter 2

vlPAG, ventrolateral periaqueductal grey

VMAT2, vesicular monoamine transporter 2

VMH, ventromedial hypothalamus

VP, ventral pallidum

VTA, ventral tegmental area

WT, wild type

ZI, zona inserta

1 INTRODUCTION

Obesity is a growing problem in the developed world, including the United States. Today, over two-thirds of US adults are overweight or obese as defined by body mass index (BMI; overweight: BMI ≥25, obese: BMI ≥30) [1]. Many serious co-morbidities are associated with

obesity including 4 out of the top 5 leading causes of death in the United States (heart disease, cancer, lung disease, and stroke) [2; 3]. To put this in numbers, in 2015 alone, excess body weight was responsible for 4 million deaths and 120 million disability-adjusted life years, the number of years lost due to disability or early death, worldwide [2]. In addition to being a considerable health burden, obesity also presents a large economic burden, generating an estimated health care cost of $147 billion in the United States in 2008 [4]. Taken together, obesity presents is a very serious problem that requires immediate attention.

Disruptions in energy homeostasis, the intricate balance between energy intake and expenditure, result in obesity. Since the 1970s, an obesogenic shift in the environment of the United States and other developed countries has been taking place in form of an increase in availability and a decrease in cost of calorie-dense and highly palatable foods (foods rich in fat and sugar), increases in portion size, and an increase in sedentary activities [5-8]. These environmental changes promote energy overconsumption and a decrease in energy expenditure placing the population at risk of obesity. Understanding the mechanisms involved in the regulation of feeding and body weight is critical to the development of novel treatments and behavioral strategies targeted at obesity prevention and reversal.

Feeding is a complex behavior that can be separated into two broad aspects, homeostatic and hedonic or reward-based. Homeostatic feeding, or feeding to maintain the organism's metabolic needs, is primarily regulated by hypothalamic and brainstem homeostatic feeding circuits, whereas consumption of palatable foods irrespective of physiological need is primarily regulated by the DA reward system [9; 10]. The two systems are not autonomous, however, and they interact to regulate both homeostatic and reward-based feeding. For example, in addition to increasing homeostatic feeding, food deprivation increases responding for food reward [11], suggesting that metabolic state can alter food reward sensitivity. Furthermore, the reward system can override homeostatic needs as illustrated by rats that continue to work for palatable fat and sugar, even when sated [12]. The mechanisms underlying this interaction between

homeostatic and reward circuits are still not well understood, however. In this dissertation, I present studies focused on defining the anatomical organization of a subset of mesocorticolimbic neurons potentially playing a central role in the interaction between the homeostatic and the reward systems, and I examine the role these neurons play in the regulation of feeding and body weight.

1.1 The reward system

1.1.1 Overview of the mesocorticolimbic dopamine system

Dopamine is a key neurotransmitter involved in the regulation of many different behaviors including reward, reinforcement, motivated behavior, motor activity, arousal, learning, memory, feeding, and aversion [13-16]. The ventral midbrain contains two regions densely populated with DA neurons: the ventral tegmental area (VTA) and the substantia nigra pars compacta (SNc). These two populations of midbrain DA neurons give rise to two distinct projection systems with different behavioral correlates. The mesostriatal pathway consists of the DA neurons of SNc which project to dorsal striatum and are responsible for regulation of motor activity and coordination, whereas the mesocorticolimbic pathway consists of VTA DA neurons and their efferent projections to the ventral striatum and cortex which play a large role in the regulation of reward and reinforcement. Clinically, dysregulation of DA signaling can result in depression, addiction, motor deficit disorders such as Parkinson's disease, and eating disorders such as anorexia nervosa and binge eating disorder. The studies described in this dissertation focus on the role of VTA neurons and circuits involved in feeding regulation.

The mesocorticolimbic system is known as the reward pathway and is composed of two anatomically distinct circuits, the mesolimbic and the mesocortical. Both pathways consist of DA neurons originating in the ventral tegmental area (VTA) that project to different targets such that the mesolimbic pathway projects to the nucleus accumbens (NAcc) as well as several limbic structures, whereas the mesocortical pathway mostly targets the prefrontal cortex (PFC). At

rest, DA neurons fire tonically in a steady, low-frequency mode setting a stable background dopaminergic tone, but when exposed to unexpected salient stimuli of positive or negative valence DA neurons fire in high-frequency phasic mode which produces high extracellular DA concentrations at efferent targets [17-19]. Activation of the mesocorticolimbic pathway is highly rewarding. For example, rats readily press a lever to electrically stimulate regions along the mesocorticolimbic pathway [20] and some rats even forgo food and starve to continue self-stimulating [21]. This behavior was later shown to be dependent on DA neurotransmission [22]. The full mechanism is much more complex, however, as subsequent experiments showed that repeated cue-reward pairing results in transfer of the DA neuron excitability from reward to the reward predicting cue [23] and decades of investigation have revealed the breadth of behaviors regulated by the mesocorticolimbic DA system including natural and drug rewards, reinforcement, motivation, and aversion [14; 24-27]. This dissertation focuses on the role of the mesocorticolimbic system in the regulation of feeding as this system is an important component of the neural circuitry controlling feeding and food reward [9; 28-30].

1.1.2 The mesocorticolimbic system and feeding

The importance of properly balanced DA levels in feeding is well illustrated by observations of patients with Parkinson's disease, a neurodegenerative disorder affecting DA neurons, whose typically decreased food consumption is reversed to compulsive-like eating of palatable foods by the administration of DA agonists [31]. DA agonists also promoted compulsive-like eating in non-Parkinson's individuals [32]. Human imaging studies showed that the activity of the brain's reward areas increases following ingestion of food or presentation of food images and that this activity is proportional to the self-reported level of pleasure derived from food consumption or is greater in response to images of "fatty foods" compared to lower caloric content foods [33; 34]. Conversely, activation of the reward areas of the brain in response to food consumption is decreased in obese individuals [35] putting forth a hypothesis that obesity may alter the reward

circuitry and decrease the amount of pleasure derived from food resulting in an escalation of caloric consumption. Striatal dopamine D2 receptors (D2R) are decreased in obese individuals compared to lean controls [36] and increase following long-term bariatric surgery-induced weight loss [37], supporting the idea that obesity can alter the mesocorticolimbic system.

Experiments in rodents showed that food cues can stimulate feeding in sated states [38; 39] demonstrating that feeding can take place independent of caloric need. Palatable food is highly rewarding as rats prefer to consume non-caloric saccharin solution rather than self-administer cocaine [40] and these foods are also highly motivating as shown by rats which endure noxious or painful stimuli to gain access to shortcake, pate, peanut butter, soda, and chocolate, even in presence of freely available standard chow [41-43]. Furthermore, food cues reinstate food-seeking, just like drug cues reinstate drug-seeking [44]. DA is essential for food reward and reinforcement behaviors and food-associated cues and stimuli have been shown to change DA neuron activity and neurotransmitter release. For example, consumption, orosensory stimulation, and presentation of food, or food-predictive cues, has been shown to activate DA neurons and stimulate DA release in the NAcc [45-49]. Furthermore, DA antagonism or depletion disrupts food reward-directed behaviors [50]. For example, when given a choice, rats prefer to self-administer palatable food rather than eat freely available chow, but lever pressing for food decreases and chow intake increases upon systemic or intra-NAcc treatment with DA antagonists [51-53].

Although the mesocorticolimbic system is known for its role in reward and motivation, including food reward and food motivated behaviors, it also appears to play an important role in the regulation of homeostatic aspects of feeding. For example, mice lacking tyrosine hydroxylase (TH), a rate-limiting enzyme involved in DA production, are aphagic and hypoactive and starve to death if not treated with a DA precursor L-DOPA [28]. Importantly, this aphagic response to the lack of DA is independent of motor impairments [54]. Furthermore, dopamine receptor blockade decreases free feeding [55-57] and feeding elicited by electrical stimulation of

the lateral hypothalamus (LH) [58]. Similar to palatable foods, free feeding and lever pressing for food increase extracellular DA in NAcc of food-restricted rats [45; 59; 60] and intra-NAcc administration of DA dose-dependently increases food intake in D2R-dependent manner [61]. Taken together, it is clear that the mesocorticolimbic DA system is involved in the regulation of many aspects of feeding and is subject to alteration by obesity.

1.1.3 VTA anatomy and heterogeneity

The VTA is composed of neurons highly heterogeneous in their cytoarchitecture, projections, and electrophysiological and molecular properties. This heterogeneity likely contributes to the mesocorticolimbic system's ability to regulate diverse behaviors. Anatomically, VTA neurons have been segregated into 5 subregions: paranigral (PN), parabrachial pigmented (PBP), interfascicular (IF), rostral linear (RLi), and caudal linear (CLi) nuclei (Figure 1.1) [62; 63]. Recent studies showed that VTA neurons with shared properties are broadly concentrated within one or more of these subregions [64-66].

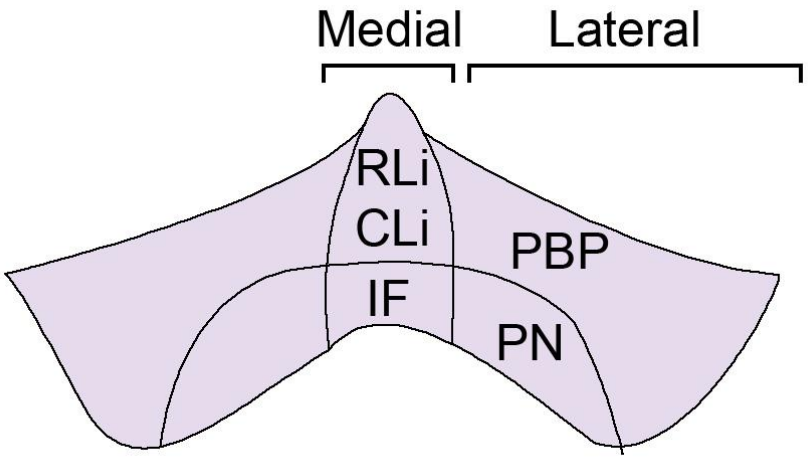

Figure 1.1. VTA subregions.

Diagram showing major subregions of VTA as defined by cellular cytoarchitecture. RLi and CLi share the same mediolateral position but are non-overlapping nuclei present at different

rostrocaudal positions such that RLi is located in the rostral VTA and CLi in the caudal VTA. Adapted from [63].

Dopamine production, release, recycling, and auto-regulation involves several key proteins including TH involved in DA synthesis, vesicular monoamine transporter 2 (VMAT2) responsible for vesicular packaging of DA, DA transporter (DAT) which facilitates DA reuptake from extracellular space following release, and D2Rs expressed on the VTA DA neurons responsible for feedback auto-inhibition. DA neuron heterogeneity has been observed in the molecular markers for these proteins. For example, TH is plentifully expressed in all VTA sub-nuclei, but some of the TH-expressing VTA neurons had been shown to lack VMAT2, DAT, or D2R [65; 67]. Furthermore, VTA neuron populations expressing TH but not releasing DA, as well as those expressing TH mRNA but no detectable protein, have been reported [67; 68]. DA neurons are also heterogeneous in their electrophysiological properties with more lateral neurons possessing properties classically associated with DA neurons such as the presence of a large hyperpolarization-activated cation current (Ih), long action potential durations, and D2R-mediated auto-inhibition while medially distributed neurons have been shown to lack Ih current or D2R auto-inhibition [65; 69]. Recently, much effort has been devoted to classifying VTA neurons according to their molecular properties to understand the roles these heterogeneous populations play in different behaviors.

Although DA neurons are the predominant neuron type in the VTA, the region also contains GABAergic (~30%) and glutamatergic (~2–3%) neurons [68; 70]. Much like VTA DA neurons, VTA GABA and glutamate neurons have been shown to participate in the regulation of both reward-associated and aversive behaviors [67; 71; 72] and also appear to have distinct anatomical distribution and heterogeneous properties. For example, glutamate neurons are most prevalent in the IF and RLi and have been reported to outnumber TH+ neurons in these nuclei [68; 73; 74], whereas VTA GABA neurons are distributed more broadly.

The full scope of VTA heterogeneity is complicated by the fact that different neurotransmitters can be co-expressed in the same VTA neuron. Multiple combinations of co-expressing VTA neurons have been described to date, including neurons co-releasing DA and glutamate, DA and GABA, and even glutamate and GABA. VTA neurons co-expressing TH and vesicular glutamate transporter 2 (vGlut2), a marker of VTA glutamate neurons, are concentrated within the RLi and IF subregions [74] and have been shown to release both DA and glutamate from the same axon [75; 76]. Another population of TH+ neurons which projects to the lateral habenula (LHb) has been shown to co-express glutamate decarboxylase [77], an enzyme involved in GABA synthesis, but not VMAT2 and subsequently only releases GABA onto the neurons of LHb [67; 78; 79]. In the NAcc, GABA release has been observed from TH+ neurons expressing VMAT2 but lacking cellular machinery to produce GABA [80-82]. In this case, instead of *de novo* synthesis of GABA, the neurotransmitter was recycled from the cytoplasm by GABA transporters 1 and 4 and packaged along with DA by VMAT2 [81]. Another unique mechanism of GAD-independent GABA production by TH+ neurons involves synthesis by aldehyde dehydrogenase family 1 member A1 (ALDH1A1) which was shown to be necessary for GABA co-release in the striatum [82]. Lastly, individual VTA neurons co-expressing glutamate and GABA molecular markers have been shown to establish adjacent asymmetric and symmetric synapses onto LHb neurons [79], suggestive of excitatory and inhibitory transmission from a single axon. Furthermore, many other genes, including genes encoding for ion channels, peptides, peptide receptors, calcium-binding proteins, and transcription factors, also show distinct expression patterns in the VTA contributing to the region's molecular heterogeneity (reviewed by [83]).

1.1.4 VTA connectivity

VTA DA, GABA, and glutamate neurons receive input from largely overlapping brain areas with some quantitative, but not qualitative differences in their inputs [84]. Some of the sources of

glutamatergic and GABAergic inputs have been characterized for VTA DA and GABA neurons but are still largely unknown for VTA glutamate neurons. DA neurons of the VTA receive excitatory input from the prefrontal cortex (PFC), pedunculopontine tegmental nucleus (PPTg), laterodorsal tegmental nucleus (LDTg), lateral habenula (LHb), periaqueductal grey (PAG), bed nucleus of the stria terminalis (BST), and dorsal raphe (DR) [85-91] and inhibitory input from rostromedial tegmental nucleus (RMTg), PAG, DR, LH, and ventral pallidum (VP) [89; 92-95]. GABAergic neurons of the VTA receive excitatory input from the LHb and PFC [85; 88] and inhibitory input from the NAcc [96]. Additionally, PAG, DR, LH, and BST make both excitatory and inhibitory synapses with the VTA GABA neurons [89; 93; 94; 97]. VTA GABA neurons project to PFC, NAcc, lateral preoptic area (LPO), magnocellular preoptic nucleus (MCPO), BST, central amygdala (CeA), VP, and DR [98] and VTA 'GABA-only' neurons target cholinergic interneurons of the NAcc [99]. VTA neurons co-expressing TH and VGluT2 have been shown to release both DA and glutamate in the NAcc [76; 100], but also target amygdala, VP/BST, and MCPO [98], suggesting that co-release may also occur in these areas. 'VGlut2-only' neurons project to the VP, BST, MCPO, the olfactory tubercle (OT) [98], and the parvalbumin-expressing neurons of NAcc [101]. Additionally, both VTA glutamate and GABA neurons form local connections onto DA and non-DA neurons [72; 102; 103] and LHb glutamate neurons receive input from 'GABA-only', 'glutamate-only', and the GABA/glutamate co-releasing VTA neurons [79; 98]. Taken together, VTA circuitry is highly complex and heterogeneous and there is a need for identification and classification of molecularly distinct groups of VTA neurons.

1.2 Homeostatic regulation of feeding

1.2.1 Overview of the melanocortin system

The melanocortin system is one of the key brain circuits controlling homeostatic feeding. This system is composed of two non-overlapping populations of neurons, AgRP and POMC neurons (melanocortin neurons), the peptide neurotransmitters released by these neurons

(AgRP and alpha-melanocyte-stimulating hormone, α-MSH), and the melanocortin-3 and -4 receptors (MC3R and MC4R) which bind these peptides. AgRP neurons release an additional neuropeptide, neuropeptide Y (NPY), which also plays a role in feeding regulation but through a separate set of receptors, neuropeptide Y receptors (NPYR) (Figure 1.2). The major population of melanocortin neurons resides in the Arc and another population of POMC neurons is also found in the commissural nucleus of the solitary tract [104-106]. The Arc is located in the mediobasal hypothalamus and is well perfused due to its proximity to the median eminence which puts the melanocortin neurons in a good position to serve as a relay station of peripheral signals of energy state. In fact, many of the receptors for circulating molecules associated with metabolic state including leptin, insulin, and ghrelin are expressed in Arc neurons [107-109]. Furthermore, POMC and AgRP neurons are reciprocally connected with many brain regions, including those involved in feeding regulation such as the paraventricular (PVN), dorsomedial (DMH), lateral (LH), and ventromedial (VMH) hypothalamic nuclei [110], putting these neurons in an ideal position to integrate peripheral and central inputs and produce feed-forward commands driving feeding behavior.

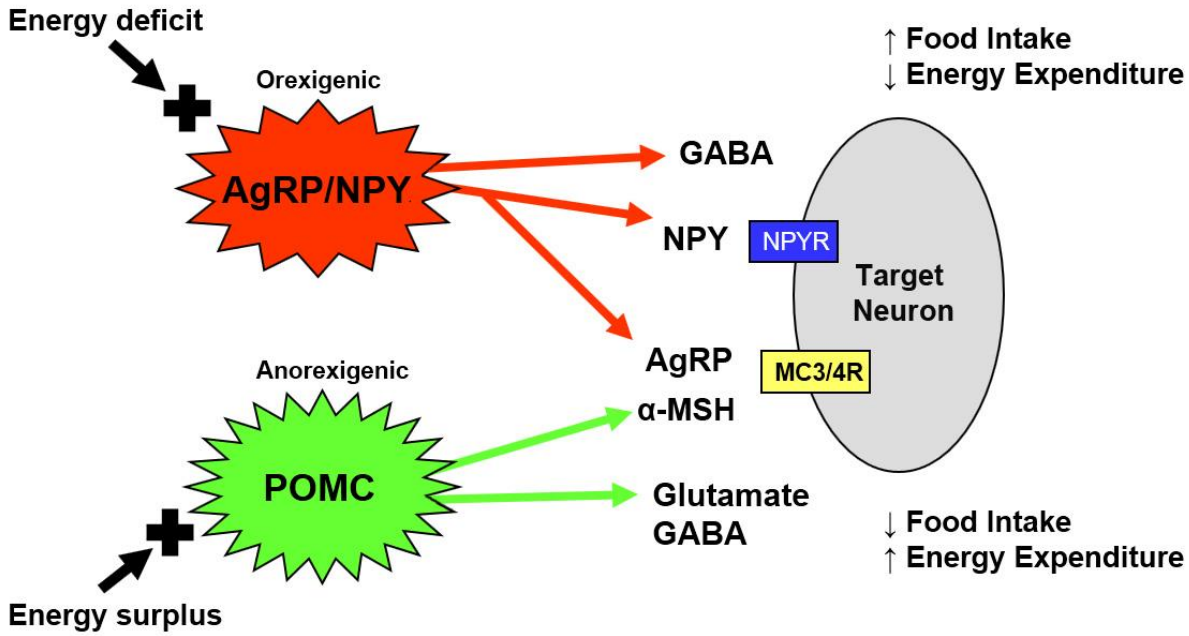

Figure 1.2. Bidirectional regulation of feeding by the melanocortin system

Depicted are neuropeptide and amino acid neurotransmitters released by POMC and AgRP/NPY neurons in response to changes in energy homeostasis. Neuropeptides α-MSH, AgRP, and NPY bind to their receptors (MC3R/MC4R for α-MSH and AgRP and NPYR for NPY) and alter energy homeostasis through their actions on the target neurons.

The neuropeptide α-MSH is produced by proteolytic cleavage of POMC propeptide and acts as an agonist of the central melanocortin receptors (MCRs, MC3R and MC4R), whereas AgRP is an inverse agonist/competitive antagonist of the MCRs. POMC and AgRP neurons monitor energy state and change their activity to alter feeding and body weight. For example, fasting activates AgRP neurons and an increase in AgRP activity drives feeding [111-113]. Increases in activity of POMC and AGRP neurons has the opposite effect on energy homeostasis such that the stimulation of POMC neurons or injection of melanocortin receptor (MCR) agonists decreases food intake and increases energy expenditure and metabolism [114-116], whereas central administration or overexpression of AgRP promotes feeding and weight

gain [111; 114; 117-119]. In addition to neuropeptide-mediated signaling, both POMC and AgRP neurons are also capable of fast neurotransmission via glutamate and/or GABA [120-122] and this neurotransmission has been suggested to play an important role in the ability of AgRP neurons to control feeding [123; 124] (Figure 1.2). Knockout of MC3R or MC4R results in increased weight and fat mass, diabetes, and altered activity [125-128], suggesting that both receptor subtypes are important for energy homeostasis. The phenotypes and feeding behavior of MC3R and MC4R null mice differ, however. Specifically, MC4R-/- mice eat more and gain weight when maintained on chow or high-fat diet, whereas mice lacking MC3R are normophagic on either diet and increase body weight only when fed high-fat diet [125-127; 129].

In humans, dysregulation of the melanocortin system can cause severe obesity and metabolic syndrome. For example, congenital lack of POMC gene products results in early-onset hyperphagia and obesity [130] and MC4R defects are the most common monogenic cause of severe early-onset obesity [131; 132]. Although less common, MC3R mutations have also been implicated in cases of human obesity [133-135], but the physiological function of MC3Rs in the regulation of energy homeostasis is not straightforward and is, therefore, less well understood.

1.2.2 Melanocortin 3 receptor

Unlike MC4Rs which are distributed broadly across the brain [136], MC3R expression is more localized and restricted to hypothalamic and limbic structures with the highest expression in the ventromedial hypothalamus (VMH), medial habenula, and VTA [137]. MC3Rs are also expressed in Arc POMC and AgRP neurons [138; 139] where they appear to have an autoregulatory function [140]. MC3R-/- mice display late-onset obesity concomitant with increased fat mass, decreased lean mass, and stunted growth [125; 126] that is independent of MC4R dysregulation as dual knockout of MC3R and MC4R produces an additive obesity phenotype [126; 141]. MC3R-/- mice maintained on standard chow are hypo- or normophagic

but have increased feed efficiency (i.e., gain more weight per amount of food consumed), decreased locomotor activity, and develop modest hyperinsulinemia [106; 129; 142] which is exacerbated to the levels comparable to MCR4 knockouts by high-fat diet consumption [125; 126; 143], suggesting that MC3R-dependent obesity is caused by metabolic or energy expenditure defects in this mouse model. However, mice expressing a human MC3R double-mutant variant ($MC3R^{hDM/hDM}$), previously associated with obesity and increased energy intake in human children [134], show increased energy intake irrespective of the diet and very subtle energy expenditure defects [144] suggesting that in this translational-application relevant model, increased energy intake contributes to obesity. The phenotypes of these two animal models maintained on chow or high-fat diet are summarized in Table 1.1.

Table 1.1. Diet and genotype dependency of MC3R-deficiency phenotypes.

Genotype / **Phenotype**	**MC3R -/- chow**	**MC3R -/- HFD**	**$MC3R^{hDM/hDM}$ chow or HFD**
Body weight	≈	↑	↑
Food intake	≈ /↓	≈	↑
Feed efficiency	↑	↑	↑
Fat mass	↑	↑	↑
Lean mass	↓	↓	↓
growth	↓	↓	↓
insulin	↑(moderate)	↑	≈
locomotion	↓	↓	≈

≈ not different from wild type control, ↑ increased, and ↓decreased compared to wild type control MC3R -/- data summarized from [125; 126; 129] and $MC3R^{hDM/hDM}$ summarized from [144].

Much of the literature attributes the feeding regulatory role of the melanocortin system to the MC4R, but several studies suggest that both receptor subtypes may be involved, although MC3R's role may be more subtle and condition-specific. For example, AgRP increases food intake in MC4R-/- [145] and central administration of MTII, a non-selective MC3R/MC4R agonist, produces a partial anorexigenic effect in MC4R-/- mice [146], suggesting that orexigenic and anorexigenic effects of melanocortin peptides may be exerted through MC3R. MC3R-/- mice exhibit daytime high-fat diet hyperphagia [106], and defects in the behavioral and metabolic responses to fasting, including fast-induced refeeding [147; 148]. Furthermore, re-expression of MC3Rs in AgRP or DA neurons of MC3R -/- mice altered food intake and food self-administration [149; 150] and MC3R expressed in AgRP neurons have been shown to have a regulatory function as they facilitate GABA release onto anorexigenic MC4R-expressing neurons [148]. MC3R appears to also play a role in maintaining circadian rhythmicity of the central nervous system as MC3R deficiency attenuates food anticipatory activity (FAA), the increase in locomotor activity in anticipation of food, [151] and reduces activity of circadian oscillator genes [151-153]. MC3R defects also affect physical activity, which could potentially contribute to obesity development. For example, MC3R -/- mice have reduced home cage activity and wheel running during the dark phase, their active phase [106; 125; 126; 152; 154]. Although there is significant evidence that MC3R contributes to the regulation of feeding and energy homeostasis, the understanding of the exact role MC3R plays in these behaviors is limited.

1.3 Interaction of the melanocortin and mesocorticolimbic systems

Increasing evidence suggests that the melanocortin and the mesocorticolimbic systems can interact to regulate feeding and body weight. Both POMC and AgRP neurons project to the VTA [155; 156] and, as described earlier, the VTA is one of the top brain regions with the highest expression of MC3Rs [137; 157]. Intra-VTA administration of α-MSH increases

extracellular DA in NAcc [158; 159] and increases behaviors classically known to be DA-dependent such as grooming, rearing, and locomotor activity [158-161]. Global deletion of MC3R alters food self-administration [150] and sex-dependently alters sucrose preference and DA turnover [157]. Furthermore, our laboratory recently showed that α-MSH increased the firing rate of MC3R-expressing VTA neurons, many of which were DA neurons [162], and, in the past, we showed that melanocortin receptor agonists injected into the VTA decrease the intake of both standard chow and palatable sucrose solutions, and decrease sucrose self-administration, whereas injection of melanocortin receptor antagonists into the VTA increase chow intake, body weight, and sucrose self-administration [163-165]. Together, these findings suggest that melanocortins can act in the VTA to regulate both homeostatic and reward-related aspects of feeding and that this interaction is likely mediated by MC3Rs. However, despite abundant expression of MC3Rs in the VTA, few studies have focused on the extra-hypothalamic function of MC3R or on the neurons expressing this receptor. Because VTA neurons expressing MC3Rs are likely to be the main point of interaction between melanocortin and mesocorticolimbic systems, I set out to identify the circuitry of VTA neurons expressing MC3Rs and examined the role this VTA population plays in feeding.

1.4 *Summary of the introduction*

Obesity is largely caused by overconsumption of calorie-dense foods and is a problem of a national, if not global, scale. The neural mechanisms controlling feeding are not fully understood and need to be studied for successful development and implementation of strategies to combat obesity. To date, many studies examined independent roles of the hypothalamic melanocortin system responsible for the regulation of homeostatic feeding and the mesocorticolimbic DA system known for its role in reward. However, much evidence suggests that the two systems are interconnected and interdependent. Additionally, the exact roles of VTA neurons, MC3Rs, or the neurons expressing this receptor in energy homeostasis are still

not well understood. Here I describe my studies aimed at identifying the neural circuitry of the interaction between the melanocortin and mesocorticolimbic systems and the effect of changes in activity of VTA MC3R neurons on feeding and body weight.

2 WHOLE-BRAIN EFFERENT AND AFFERENT CONNECTIVITY OF MOUSE VENTRAL TEGMENTAL AREA MELANOCORTIN-3 RECEPTOR NEURONS

Anna I. Dunigan[1], Andrew M. Swanson[1], David P Olson[3], and Aaron G. Roseberry[1,2]

[1]Department of Biology and [2]Neuroscience Institute, Georgia State University, Atlanta, GA 30303, USA

[3]Department of Pediatrics, University of Michigan, Ann Arbor, MI 48109, USA

Running Title: Whole-brain connectivity of VTA MC3R neurons

Author Contribution: AMS conducted the retrobead trace experiment including image acquisition and data analysis, AID performed all other experiments and data analyses.

2.1 Abstract

The mesolimbic dopamine system is involved in the regulation of multiple behaviors, including feeding, and evidence demonstrates that the melanocortin system can act on the mesolimbic dopamine system to control feeding and other behaviors. The melanocortin-3 receptor (MC3R) is an important component of the melanocortin system, but its overall role is poorly understood. Because MC3Rs are highly expressed in the ventral tegmental area (VTA) and are likely to be the key interaction point between the melanocortin and mesolimbic dopamine systems, we set out to identify both the efferent projection patterns of VTA MC3R neurons and the location of the neurons providing afferent input to them. VTA MC3R neurons were broadly connected to neurons across the brain but were strongly connected to a discrete set of brain regions involved in the regulation of feeding, reward, and aversion. Surprisingly, proopiomelanocortin (POMC) and agouti-related protein (AgRP) neurons in the arcuate nucleus made few direct synapses onto VTA MC3R neurons or any of the other major neuronal subtypes in the VTA, despite being extensively labeled by RetroBeads injected into the VTA.

These results greatly contribute to our understanding of the anatomical interactions between the melanocortin and mesolimbic systems and provide a foundation for future studies of VTA MC3R neurons and the circuits containing them in the control of feeding and other behaviors.

2.2 Introduction

The mesolimbic dopamine (DA) system, comprised of the DA neurons of the ventral tegmental area (VTA) and their afferent and efferent projections, is involved in the regulation of a wide range of behaviors, including natural and drug rewards, reinforcement, motivation, and aversion [14; 16; 24]. Moreover, the mesolimbic DA system is an important component of the neural circuitry controlling feeding and food reward [9; 10; 29]. For example, food consumption, orosensory stimulation, and presentation of food or food-predictive cues all increase neuronal activity in the VTA [49; 166] and stimulate DA release in one of the major VTA targets, the nucleus accumbens (NAcc) [45-48]. Alterations in DA signaling, induced either pharmacologically [57; 167] or via genetic means [54], significantly affect feeding and responding for food reward, independent of the effects on activity. The mechanisms by which the mesolimbic DA system regulates feeding are poorly understood, however.

The hypothalamic melanocortin system is a well-characterized component of the neural circuitry controlling feeding. This system is comprised of the POMC and AgRP neurons of the arcuate hypothalamus (Arc), their neuropeptides, alpha-melanocyte-stimulating hormone (α-MSH) and AgRP, and the central MC3Rs and MC4Rs. Furthermore, the role of the melanocortin system in the neural control of feeding has been studied extensively [104-106; 168]. Although most of these studies have focused on the actions of the melanocortin system within the hypothalamus, it also interacts with the mesolimbic dopamine system to regulate feeding and body weight. For example, both POMC and AgRP neurons project to the VTA [155; 156], and the VTA is one of the brain regions with the highest expression of MC3Rs [137], with MC3Rs being expressed in both dopamine and non-dopamine neurons in the VTA [157]. Intra-VTA

injection of α-MSH analogs also increases DA release in efferent target regions [159; 161; 169; 170] and increases DA dependent behaviors such as grooming, rearing, and locomotion [158-160]. Furthermore, intra-VTA administration of melanocortin receptor agonists and antagonists alters feeding, body weight, and food self-administration [163-165]. These findings suggest that the melanocortin system may interact with the mesolimbic dopamine system to regulate feeding and other behaviors and that the VTA MC3Rs may play a central role in this interaction. The circuits underlying the behavioral responses to α-MSH and AgRP acting in the VTA are not known, however, and overall, we have a poor understanding of the exact role that MC3Rs play in the control of feeding. Thus, in these studies, we sought to advance our understanding of the anatomy of this system by using viral tracing approaches to identify the efferent and afferent connectivity of neurons in the VTA that express MC3Rs (VTA MC3R neurons).

2.3 Materials and Methods

2.3.1 Reagents and viral vectors

AAV2/5-EF1a-DIO-hChR2 (H134R)-eYFP was obtained from the UNC Vector Core (Chapel Hill, NC). The pAAV-hSyn-FLEx-mGFP-2A-Synaptophysin-mRuby plasmid was a gift from Liqun Luo and was obtained from addgene (Addgene plasmid #71760; http://n2t.net/addgene:71760; RRID: Addgene_71760). The pHelper and pAAV-RC plasmids used for AAV preparation were generous gifts of Ralph DiLeone. Envelope-A pseudotyped, G-deleted rabies virus expressing mCherry (RvdG-mCherry) [171], AAV2/1-CMV-eSyn-DIO-TVA950-eYFP (1.13E+12 GC/ml) and AAV2/1- EF1α -DIO-H2B-tagBFP-Flagx3-T2Am-cB19G (1.01E+11 GC/ml) [84] were from the Salk Institute Gene Transfer Targeting and Therapeutics Core (La Jolla, CA). Sterile bacteriostatic saline, ketamine, xylazine, and meloxicam were from Patterson Veterinary Supply, Inc. (Sterling, MA). The fluorescent RetroBeads were from Lumafluor, Inc. Neurotrace fluorescent Nissl stain was from Thermo-Fisher (Waltham, MA).

2.3.2 AAV-FLEx-mGFP-SYN-mRuby preparation

AAV(2/2)-FLEx-mGFP-SYN-mRuby was prepared using a triple transfection, helper free method and was purified as previously described [172]. Briefly, HEK293 cells were transfected with equal amounts of pAAV-hSyn-FLEx-mGFP-2A-Synaptophysin-mRuby, pHelper, and pAAV-RC using a standard calcium phosphate transfection protocol. ~80 hours post-transfection, the cells were collected, resuspended in freezing buffer (150 mM NaCl, 50 mM Tris, pH 8.0), frozen and stored at -80^{o}C until preparation. Cells underwent two freeze-thaw cycles followed by a 30-minute incubation in benzonase (50 U/ml final) at 37^{o}C. The lysate was then layered on an iodixanol gradient and was spun at 184,000xg (50,000 rpm in a Beckman Type 70Ti rotor) for 3 hours 20 minutes at 10^{o}C. The 40% fraction was collected and replaced with sterile 1X phosphate-buffered saline (PBS) using Amicon Ultra-15 Centrifugal Filter Unit Concentrators (100 kDalton; Millipore, Inc.). Viral titer was calculated using the AAV pro Titration Kit (Clontech, Inc.) per the manufacturer's instructions. The final purified viral particles were aliquoted and stored at -80^{o}C, except during use, when they were stored at 4^{o}C.

2.3.3 Animals

Male and female transgenic mice expressing Cre recombinase in MC3R neurons (MC3R-Cre mice) on a mixed C57/129 background were used for tracing VTA MC3R neuron projections and inputs, and for the synaptophysin-based synaptic connectivity confirmation. MC3R-Cre mice were generously provided by David Olson (University of Michigan, Ann Arbor), and have been previously characterized and validated [162; 173]. C57/129 mice (stock no. 000664; The Jackson Laboratory) or MC3R-Cre negative littermates were used as controls. Neuropeptide Y-GFP (NPY-GFP; stock no. 006417) [174], tyrosine hydroxylase-Cre (TH-Cre, stock no. 008601) [175], vesicular glutamate transporter-2-IRES-Cre (vGlut2- Cre; stock no. 016963) [176], and glutamic acid decarboxylase-IRES-Cre (GAD-Cre; stock no. 010802) [177] mice, all on a C57Bl6/J or mixed C57/129 background, were obtained from The Jackson

Laboratory (Bar Harbor, ME). Mice were single housed in ventilated polycarbonate Animal Care System cages in a temperature- and humidity-controlled room under a 12/12 light/dark cycle (lights on at 6:00 or 7:00 am) with *ad libitum* food and water. All protocols and procedures were approved by the Institutional Animal Care and Use Committee at Georgia State University and conformed to the NIH *Guide for the Care and Use of Laboratory Animals*.

2.3.4 Stereotaxic surgery

Viral vectors or Red RetroBeads were injected into the VTA using standard flat-skull stereotaxic techniques. 7-10 week old mice were anesthetized with isoflurane (1.5–5%) and placed in a stereotaxic apparatus (David Kopf Instruments). The VTA was targeted using the following coordinates (relative to bregma): A/P -3.3, M/L +/-1.32, DV -4.55 and -4.45 from the skull surface, at a 12° angle to the midline. Injections were done bilaterally or unilaterally in equal volumes at two depths (viral vectors) or a single depth (DV-4.50, Retrobeads) at a speed of 50-100 nl/min using a Nanoliter 2010 microinjector (World Precision Instruments, Sarasota, FL) and glass pipettes with ~30-60 µm diameter tips. For unilateral injections, the injection sides were counterbalanced between animals to avoid potential side bias. The pipettes were left in the brain for 3 minutes following the first injection and 5 minutes following the final injection to allow for diffusion from the injection site. For pain management, the mice received meloxicam (1 mg/kg) at the onset of the surgery and again 24 hours post-surgery. AAV-DIO-ChR2-eYFP was injected unilaterally in a total volume of 300 nL (150 nL per injection site), and mice were sacrificed 4 weeks later. For the synaptophysin-mRuby experiments, mice received unilateral injections of 300 nL AAV-FLEx-mGFP-SYN-mRuby (150 nL/site) or 400nL of a 1:3 mix of AAV-DIO-ChR2-eYFP and AAV-FLEx-mGFP-SYN-mRuby (200 nL/site), and the mice were sacrificed 10 weeks later. For the RetroBead experiments, 100 nL of Red RetroBeads diluted 1:5 in sterile saline was injected bilaterally and the mice were sacrificed 4 weeks later. For the RVdG-mCherry experiments, 300 nL (150 nL/site/side) of 1.5:1 volume mixture of AAV-RbG-

hBFP and AAV-TVA-eYFP (diluted 1:100 from the original AAV received) was injected bilaterally. Three weeks later, 126 nL of RVdG-mCherry (63 nL/site) was injected into the same coordinates and the mice were sacrificed 7 days later.

2.3.5 Tissue processing and histology

Mice were deeply anesthetized with ketamine/xylazine (93/7 mg/kg) and transcardially perfused with ice-cold PBS followed by 4% paraformaldehyde. The brains were dissected, post-fixed with 4% paraformaldehyde at 4°C overnight, washed with 1X PBS, and incubated in 30% sucrose (in 1X PBS) for 2-3 days until the brains sunk. The brains were then flash-frozen in ethanol/dry ice-cooled isopentane and stored at -80°C until sectioning. The brains were sectioned, mounted on glass slides, and coverslipped using ProLong Diamond Antifade Mountant with or without DAPI (ThermoFisher Scientific) or lab-prepared gelvatol containing 10% DABCO. All slides were allowed to cure for at least 24 hours before imaging. For the efferent and afferent traces, 40 µm thick coronal sections were collected on a cryostat at 200 µm intervals (every 5th section) between +2.10 mm and -6.24 mm relative to bregma. For the synaptophysin experiment, 20 µm thick coronal sections containing the brain regions of interest were collected on the cryostat at 200 µm intervals (every 10th section). For the RetroBead experiment, 40 µm thick coronal sections were collected through the VTA and arcuate nucleus (Arc) at 200 µm intervals (every 5th section). For the RVdG experiment to determine the connectivity between Arc POMC and AgRP neurons and VTA neuron subtypes, 40 µm thick coronal sections were collected through the VTA at 200 µm intervals (every 5th section), and through the Arc at 80 µm intervals (every other section). The sections used for the quantification of the whole-brain VTA MC3R inputs and outputs were counterstained with Green Fluorescent Nissl stain (NeuroTrace 500/525, Invitrogen/ThermoFisher Scientific) at 1:100 dilution using manufacturer's instructions.

POMC neurons were labeled using standard immunological techniques. Brain sections were incubated for 6 hours at room temperature in blocking buffer (5% normal goat serum, 0.2% Triton X-100, 0.1% bovine serum albumin in 1X PBS), washed in 1X PBS for 5 minutes, and were incubated with rabbit polyclonal anti-POMC antibodies (Cat. # H-029-30, Phoenix Pharmaceuticals) diluted 1:1500 in antibody incubation buffer (0.2% Triton X-100, 1% bovine serum albumin in 1X PBS) overnight at 4°C. Sections were washed with 1X PBS 3 times for 5 minutes and were incubated with Alexa Fluor 647 conjugated goat anti-rabbit antibodies (Cat. # 111-605-045, Jackson Immuno Research) diluted 1:300 in antibody incubation buffer for 4 hours at room temperature. Sections were then washed with 1X PBS 3 times for 5 minutes, mounted on glass slides and coverslipped as described above.

2.3.6 Image acquisition

Images used for the analysis of VTA MC3R axon density, synaptophysin puncta quantification, and whole-brain VTA MC3R afferent cell count were acquired at 10x, 20x, or 60x magnification on an Olympus BX41 fluorescent microscope equipped with an Olympus DP73 camera. The 10x and 20x magnification images used for scoring VTA MC3R axon density or RVdG-mCherry-labeled cell counts were acquired in a grid pattern and were stitched together post-acquisition using the ImageJ2 *Stitching* plugin [178]. 20x and 60x magnification images used for software-based VTA MC3R density quantification, synaptophysin puncta quantification, or counting of densely populated RVdG-mCherry-labeled cells were manually acquired at different focal planes (~3-6 focal planes) and were stacked together post-acquisition into a single image using the Fiji *Stack Focuser* plugin in ImageJ [179]. For the experiments examining the connectivity between the VTA and the Arc, the images were acquired using Laser Scanning Confocal Microscope (Carl Zeiss LSM 780) at 20x magnification with 0.7 magnification factor. Macrostructure features and nuclei of the brain sections were delineated with the use of Neurotrace according to the Paxinos Mouse Brain Atlas [180], and brain areas were grouped

into regions and sub-regions based on the Allen Brain Atlas classification (http://mouse.brain-map.org/).

2.3.7 VTA MC3R axon density quantification

To identify whole-brain efferent targets of VTA MC3R neurons, 10x magnification images of coronal brain sections were used. The delineated brain regions between +1.78 mm and -6.24 mm relative to bregma were assigned density scores of 1 to 4 using the following scoring rubric: 1 (very low) - very few fibers covering the area, 2 (low) - dispersed fibers covering the area, 3 (moderate) - part of the area is densely covered by fibers, and 4 (strong) - most of the area is densely covered by fibers. In most cases, brain areas containing eYFP+ axons were spread over multiple brain sections. For this reason, scores were averaged across all sections containing the individual region within an animal and then averaged across all animals.

For software-based analysis of axon density in selected brain regions, we acquired 20x magnification images using the same acquisition parameters across sections within an individual animal. The individual axons were isolated with Fiji *Tubeness* plugin [181]. The brain region of interest (ROI) was delineated, isolated, and the area of the region was measured using ImageJ [182]. The ImageJ Fiji *Internal coverage area* macro [183] was used to quantify the axon density as reflected by the ratio of squares (3 pixels in size) with and without a signal. The quantified axon density was normalized to the measured area of the ROI and the resulting density of each brain region was normalized to the density in the VTA to allow comparison between animals.

2.3.8 Synaptophysin puncta quantification

Images were taken at 60x magnification at three different rostral-caudal sections (rostral, middle, and caudal) of each brain area to fully represent the entire length of each nucleus analyzed. The Synaptophysin-mRuby puncta quantification was then automated with the use of

the *Analyze Particles* Fiji plugin in ImageJ [184] with *Watershed* separation [185]. The results were averaged within each animal and then within each group (MC3R-Cre and WT).

2.3.9 Whole-brain quantification of RVdG-mCherry labeled cells

VTA sections at 20x magnification between -2.92 mm and -4.48 mm relative to bregma were used for manual count of starter cells using ImageJ *Cell Counter* plugin [184]. Cells were identified as starter cells if they expressed both cytoplasmic mCherry (RvdG-mCherry) and nuclear blue fluorescent protein (AAV-RbG-hBFP). Sections adjacent to the VTA were also analyzed for the presence of blue fluorescent protein (BFP) and starter cells to any off-target starter cells. 10x and 20x (when necessary) magnification images of the 40 µm coronal sections with delineated brain regions were used for manual count of whole-brain VTA MC3R afferent inputs with the aid of ImageJ *Cell Counter* plugin [184].

2.3.10 Data analysis

All data are presented as means ± SEM. Data were graphed using IgorPro (Wavemetrics, Inc., Lake Oswego, OR, USA), and statistical analyses were performed using IBM SPSS Statistics 25. A significance level was set at $p<0.05$ *a priori* for all analyses. Synaptophysin-mRuby puncta counts were analyzed using two way repeated measures ANOVA. One way ANOVA was used to analyze the number of RetroBead-labeled neurons in the Arc and the connectivity between Arc and VTA subpopulations was analyzed using two way ANOVA. ANOVAs were followed by LSD *post hoc* tests corrected for multiple comparisons. T-tests were used to compare starter cells in MC3R-Cre vs WT mice in the control rabies experiment and to make gender comparisons for the starter cell, total cell, and input per starter counts. The sex comparisons for the VTA MC3R inputs from the individual areas were made in two different ways: using a 2-way repeated measures ANOVA and performing individual t-tests comparing the number of RVdG-mCherry-labeled neurons in each region between males and females. Neither of the approaches revealed any significant sex differences.

2.4 Results

2.4.1 Efferent projections from VTA MC3R neurons

We initially sought to identify the efferent projection patterns of VTA MC3R neurons. To examine the efferent anatomy of VTA MC3R neurons, we injected AAVs expressing cre-dependent channelrhodopsin-eYFP (ChR2-eYFP) unilaterally into the VTA of both male and female MC3R-cre mice (Figure 2.1A). The mice were sacrificed 5 weeks later and 40µm coronal sections were collected across the entire rostro-caudal extent of the brain and analyzed for the presence of eYFP+ axons using standard epifluorescence microscopy. In all mice, eYFP+ cells bodies were largely restricted to the VTA and were present in all VTA subnuclei (scattered in the PBP and densely populated in the PN and IF; Figure 2.3A), similar to the previously reported distribution of VTA MC3R neurons [157; 162]. eYFP+ axons were observed in efferent target regions between +1.78 and -6.24 mm relative to bregma, with no labeling identified in brain regions rostral or caudal to these regions (see examples of labeling in sagittal sections in Figure 2.1). Although we included equal numbers of males and females in these experiments, we did not see any apparent sex differences in the density of eYFP+ axons in any of the brain regions, so the brains of animals of both sexes were grouped for analysis.

We initially used a qualitative approach to describe the presence of axons across different brain regions. Axon density scores of 1 to 4 were assigned to each brain region by the investigator based on the apparent axon density in each brain region. Average axon density scores for all brain regions containing VTA MC3R neuron projections are shown in Figure 2.2. Overall, the brain regions receiving input from VTA MC3R neurons reflect the projection patterns that have been identified for other VTA neuron subpopulations [74; 98; 186; 187]. The most prominent VTA MC3R neuron projection areas were in forebrain regions with ascending fibers concentrated in the medial forebrain bundle (MFB) traveling through the lateral hypothalamus (LH, Figure 2.1). The strongest VTA MC3R axon densities were observed in the

NAcc (Figure 2.1D, 2.2, 2.3B), olfactory tubercle (Tu; Figure 2.1D, 2.2, 2.3B,F), lateral septum (LS; Figure 2.1D, 2.2, 2.3B), ventral pallidum (VP), substantia innominata (SI; Figure 2.1C, 2.2, 2.3F), bed nucleus of stria terminalis (BST; Figure 2.2, 2.3G), LH (Figure 2.1C, 2.2, 2.3H), lateral habenula (LHb; Figure 2.1D, 2.2, 2.3I) and basolateral amygdala (BL; Figure 2.1B, 2.2, 2.3J). Sample images of VTA MC3R axon labeling in each of these brain regions are shown in Figure 2.3, and the distributions of VTA MC3R axons across the brain are described below.

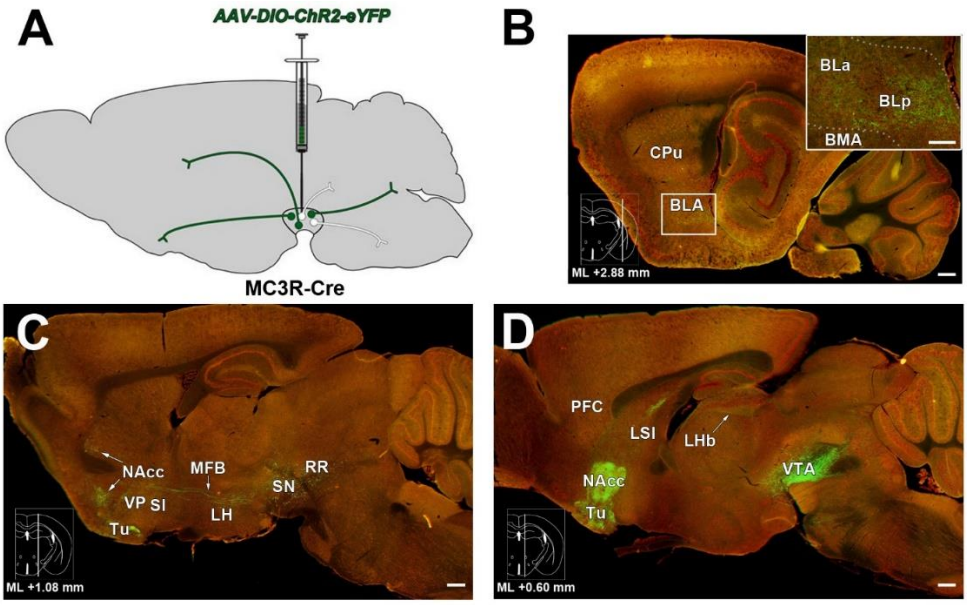

Figure 2.1. Major efferent projection targets of VTA MC3R neurons

A. Schematic illustrating strategy to achieve VTA MC3R axon labeling. **B-C.** Sagittal brain sections stained with NeuroTrace (red) showing ChR-eYFP+ axons (green) in major target areas of the VTA MC3R neurons. Atlas insets on the bottom left of each image show the mediolateral location of each sagittal section and the distance relative to midline. **B.** Lateral-most section of the series. *Inset*: Higher magnification view of the area in the white box. **C.** Middle section of the series. **D.** Medial-most section of the series. Scale bars: 200 µm. Abbreviations: ***BLa/BLp***-anterior and posterior basolateral amygdala, ***BMA/BMP***- anterior and posterior basomedial amygdala, ***RR***- retrorubral nucleus and field, ***SN***-substantia nigra.

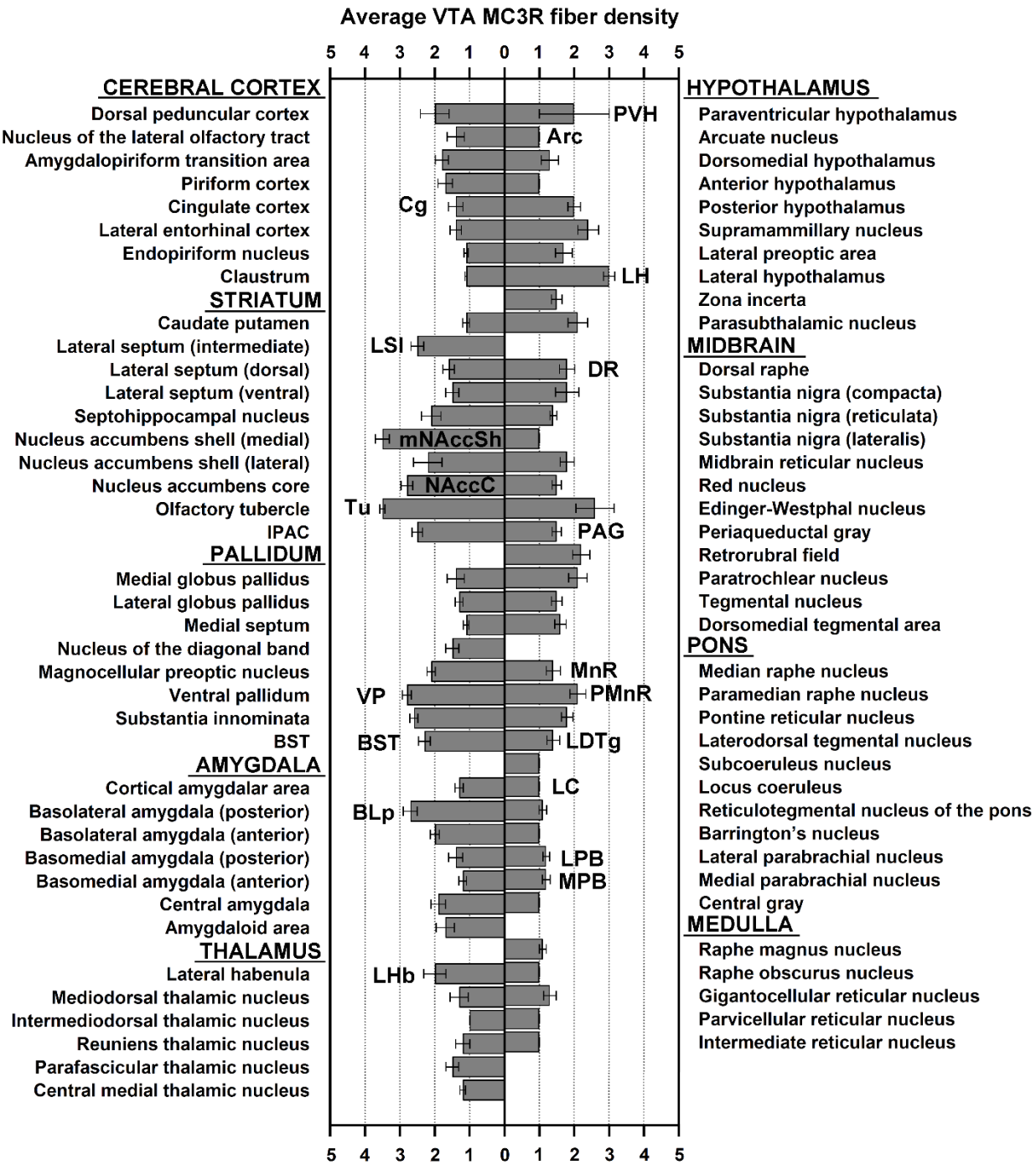

Figure 2.2. Qualitative analysis of VTA MC3R axon density across the brain.

Average ChR-eYFP+ axon density scores of different brain areas in MC3R-Cre mice. The scores were assigned based on the following predetermined rubric: 1 (very low)-very few axons covering the area, 2 (low)-dispersed axons covering the area, 3 (moderate) - part of the area is densely covered by axons, and 4 (strong) - most of the area is densely covered by axons. n = 6 mice. Abbreviations: ***IPAC***- interstitial nucleus of the posterior limb of the anterior commissure.

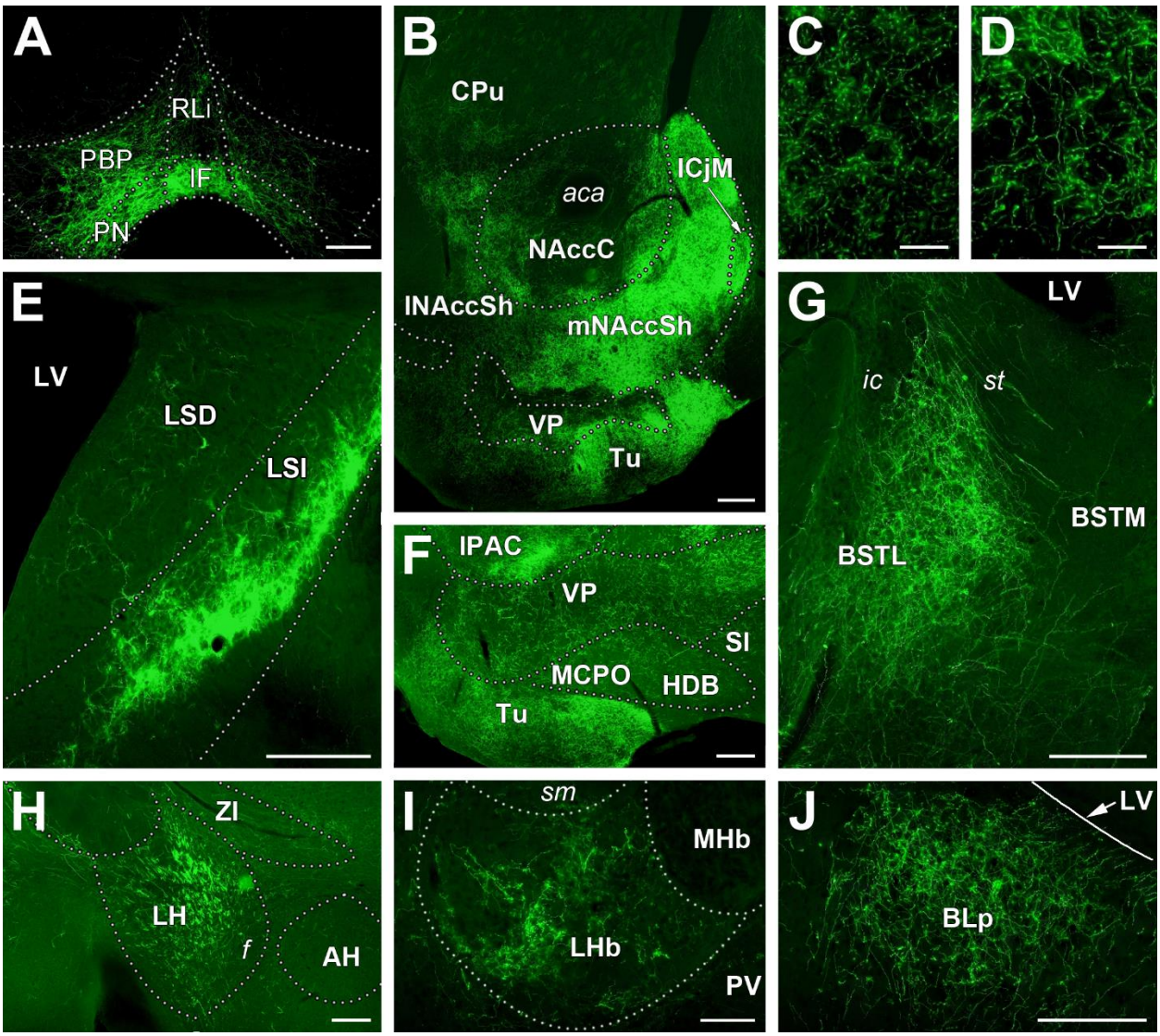

Figure 2.3. Sample images of the major efferent projection targets of VTA MC3R neurons.

Representative coronal sections showing ChR-eYFP+ axon distributions in the major efferent targets of VTA MC3R neurons. **A.** eYFP+ axons and cell bodies in the VTA. Major subnuclei of

the VTA are delineated. **B.** NAcc and Tu. **C-D.** Higher magnification images of eYFP+ axons in the NAcc (**C**) and the Tu (**D**) with branched appearance and varicosities characteristic of synaptic contact. **E.** LSI. **F.** VP, SI, medial Tu, and IPAC. **G.** Lateral BST. **H.** LH: note the thick cords of fibers of passage of the medial forebrain bundle located in the dorsal LH. **I.** LHb. **J**. BLp. Midline is to the right of the images for B, E-J. Scale bars: 100 µm (A-B, E-F); 10 µm (C-D). Abbreviations: ***AH*** –anterior hypothalamic area, ***BST(L/M)***- lateral or medial divisions of the bed nucleus of stria terminalis, ***HDB***- nucleus of the horizontal limb of the diagonal band, ***ICjM***- major islands of Calleja, ***LSI/LSD***- intermediate and dorsal segments of the lateral septum, ***mNAccSh/lNAccSh***- medial shell or lateral shell of NAcc, ***MCPO***- magnocellular preoptic nucleus, ***MHb***- medial habenula, ***PV***- paraventricular thalamic nucleus, ***ZI***- zona inserta; **VTA subnuclei:** ***IF***- interfascicular, ***PBP***- parabrachial pigmental, ***PN***- paranigral, ***RLi***-rostrolinear; fiber tracts and other structures: ***aca***- anterior commissure, ***f***- fornix, ***LV***– lateral ventricle, ***sm***- stria medullaris of the thalamus, ***st***- stria terminalis.

Cerebral cortex. VTA MC3R projections to the cerebral cortex were weak, with only a few eYFP+ axons present in each labeled cortical area. Most of the brain areas receiving input from the VTA MC3R neurons were in the cortical plate with the regions associated with olfaction (dorsal peduncular cortex, nucleus of the lateral olfactory tract, amygdalopiriform transition area, and piriform cortex) receiving stronger input (Figure 2.2). Anterior cingulate cortex (Cg) was the only region of the prefrontal cortex (PFC) containing eYFP+ axons and axon density within Cg was very weak with only a few eYFP+ axons observed in a portion of Cg-containing sections examined.

Striatum. Within the striatum, most eYFP+ axons were concentrated in the ventral striatum and the lateral septal complex with very weak labeling seen in the dorsal striatum (Figure 2.1-2.2). The regions receiving the densest projections from the VTA MC3R neurons were the NAcc, Tu, and the LS (Figure 2.1D, 2.2, 2.3B, E, F) with NAcc and Tu being the top

two regions receiving the most VTA MC3R neuron input across the entire brain. NAcc and Tu-projecting VTA MC3R neuron axons were concentrated in the medial aspects of these nuclei and, on occasion, appeared to be organized in patches (Figure 2.1C, D; 2.3B, F). The medial shell of the NAcc received the densest projections from the VTA MC3R neurons followed by the NAcc core (NAccC) and the lateral shell (Figure 2.1, Figure 2.2, and Figure 2.3B). The major island of Calleja located between the medial shell and the LS was densely populated with eYFP+ axons (Figure 2.3B). The caudate putamen (CPu) and septohippocampal nucleus of the dorsal striatum were weakly to moderately labeled by the VTA MC3R neuron axons (Figure 2.2). The rostro-caudal range of CPu labeling was very broad and encompassed most of the length of the nucleus, whereas eYFP+ axons were only seen in 2-3 septohippocampal nucleus-containing sections and usually were found in the intermediate to caudal portions of the nucleus. Most often, few eYFP+ axons were scattered in the CPu per section analyzed and occasionally a moderately labeled patch of eYFP+ axons was present at the interface between CPu and lNAccSh (Figure 2.3B).

Septum. Within the lateral septal complex, the intermediate segment of the LS received the strongest VTA MC3R projections and was one of the top 10 most prevalent VTA MC3R neuron target areas (Figure 2.2). In all animals, eYFP+ axons in the LS were concentrated in the caudal portion of the nucleus (between 0.14 and -0.1mm relative to bregma) and were arranged in a dense band located on the border with the dorsal segment of the nucleus (Figure 2.1D, 2.3E). Both dorsal and ventral segments of the LS also contained VTA MC3R neuron axons, but the labeling in these regions was scattered and weak to moderate in strength (Figure 2.2, Figure 2.3E).

Pallidum. The most prominent pallidal targets of the VTA MC3R neurons were structures of the ventral and caudal pallidum including the VP, SI, and the BST (Figure 2.1C, 2.2, 2.3B, F, G). The eYFP+ axons were present along the entire rostro-caudal extent of VP including the pallidal islands intermingled along the Tu parenchyma (Figure 2.3B, F). Similar to VP, SI

received moderate VTA MC3R neuron projections that covered the entire rostro-caudal extent of the nucleus. Unlike the densely packed or patchy organization of the eYFP+ axons in the ventral striatum and the LS, the axons in the VP and SI were loosely spread over the entire nucleus (Figure 2.3B, F). BST was moderately innervated by the VTA MC3R neurons and axons were present along the entire rostro-caudal extent of the nucleus, including the very caudal intra-amygdaloid division. The densest eYFP+ axons were concentrated in the lateral division of the BST, while axons within the medial portion were sparse (Figure 2.3G).

Amygdala. Within the amygdala, the most prevalent VTA MC3R neuron target was the basolateral amygdala which was moderately innervated by eYFP+ axons (Figure 2.2, Figure 2.3J). VTA MC3R neurons sent denser projections to the posterior division of the nucleus (BLp) compared to the anterior portion (BLa; Figure 2.1B). Low to moderate eYFP+ axon density was observed in the central amygdala (CeA), while the basomedial amygdala received sparse VTA MC3R neuron innervation (Figure 2.1B). We did not see any eYFP+ axons in the medial amygdala (MeA).

Thalamus. In the thalamus, VTA MC3R neurons projected exclusively to the polymodal associated cortex related nuclei including the LHb, reuniens nucleus, central medial thalamic nucleus, intermediodorsal thalamic nucleus, and parafascicular thalamus (Figure 2.2). LHb was the most prominent thalamic VTA MC3R neuron target receiving moderate eYFP+ axon projections (Figure 2.1D, 2.2, 2.3I). The remaining thalamic nuclei lacked or were weakly labeled by VTA MC3R neuron axons (Figure 2.2).

Hypothalamus. Within the hypothalamus, more eYFP signal was observed in the lateral zone compared to the medial zone or the periventricular zone/region. The LH contained moderate to high density of VTA MC3R neuron axons whereas the remaining nuclei in the lateral zone including lateral preoptic area (LPO), zona incerta, and parasubthalamic nucleus (PSTh) contained low to moderate amount of eYFP+ axons (Figure 2.2, 2.3H). It should be noted that during the scoring of the LH, the thick concentrations of eYFP+ axons that appeared

to be organized into chords were not included in the density analyses as these likely belong to fibers of passage traveling through the LH as part of the medial forebrain bundle (MFB, Figure 2.1C, 2.3H). The supramammillary nucleus of the medial hypothalamic zone contained low to moderate VTA MC3R neuron projections whereas the remaining hypothalamic nuclei including the anterior, posterior, dorsomedial, paraventricular nuclei (PVH) and the Arc contained very sparse eYFP+ axons (Figure 2.2).

Midbrain, Pons, and Medulla Oblongata. In general, the density of the VTA MC3R neuron axons decreased towards the caudal extent of the brain. Within the midbrain, sparse to moderate eYFP+ axon density was observed in the retrorubral field, dorsal raphe (DR), and substantia nigra pars compacta, and along most of the rostro-caudal extent of the midbrain reticular nucleus (MRN, Figure 2.1C, 2.2). Moderate labeling was observed in the paramedian raphe and pontine reticular nucleus while other pontine nuclei such as the laterodorsal tegmental nucleus (LDTg), locus coeruleus (LC), and lateral and medial parabrachial nuclei (LPB, MPB, respectively) only showed sparse VTA MC3R neuron axons (Figure 2.2).

We also utilized a more quantitative approach to determine the eYFP+ axon density in the brain regions showing the highest density of axons in the qualitative analysis. For this analysis, a single image was acquired from the VTA and each of the top 9 VTA MC3R neuron projection targets using the same acquisition parameters across each section. Pixels containing eYFP+ axons were isolated and quantified using ImageJ and Fiji plugins (Figure 2.4A, see methods). The axon density in each brain region was normalized to the area of the region analyzed and then to the VTA axon density to control for the number of neurons infected to be able to compare density between brain regions and to average between animals. Representative pixel-isolated images used for software-based quantification are shown in Figure 2.4C. These quantitative results closely matched those obtained using the more qualitative density analysis, validating these results (compare Figure 2.2 and 2.4B). The brain

regions with the highest axon density were LSI, NAccSh, and LHb (Figure 2.4B), which broadly agree with the qualitative analysis in Figure 2.2.

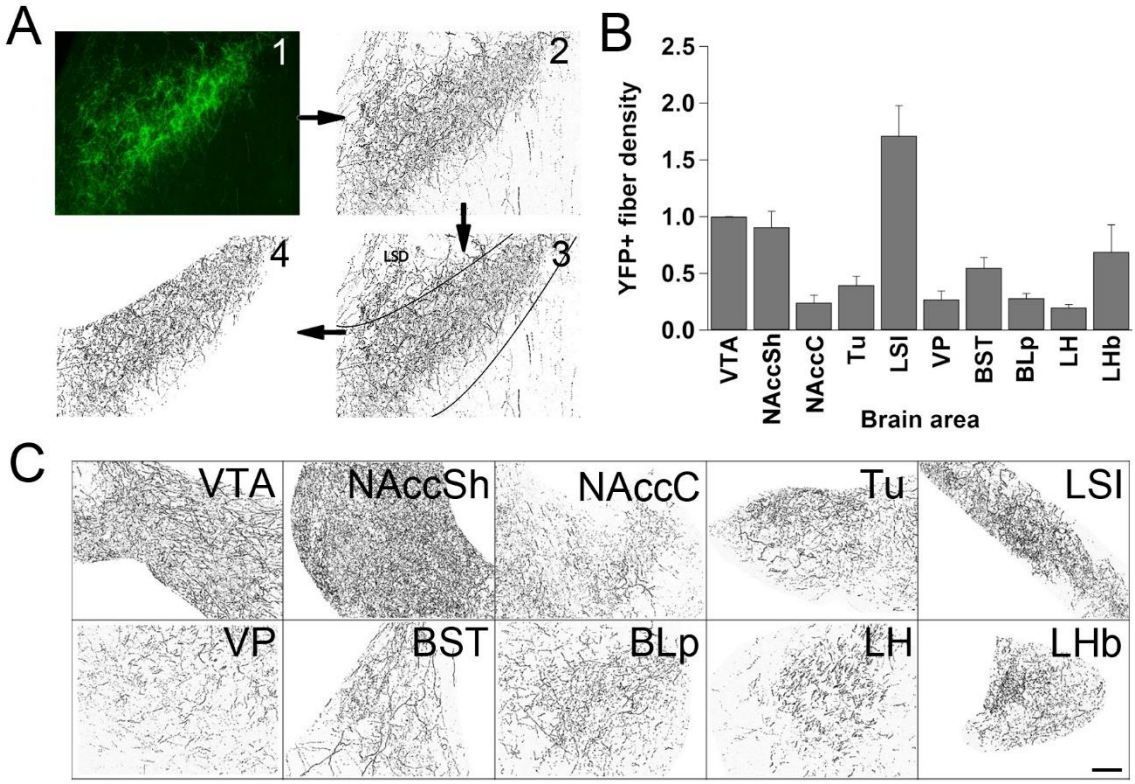

Figure 2.4. Quantitative analysis of VTA MC3R neuron axon densities in major efferent projection targets.

A. Summary of the procedure used for software-based quantification of VTA MC3R neuron axons in their major projection targets: (1) a single image per brain area per animal was acquired from coronal sections using the same acquisition parameters. (2) Pixels containing eYFP+ signal were isolated. (3) The region of interest (ROI), an area containing the nucleus being measured, was delineated and the area was measured. (4) eYFP+ axon density was measured as the ratio of dark to white pixels. **B.** Average VTA MC3R axon density normalized to the ROI area and then to the density in the VTA. n=6. **C.** Representative pixel and ROI-

isolated images used for software-based quantification. Midline is to the right of the image for A and to the left of the image for C. Scale bars: 50 µm

2.4.2 VTA MC3R axons synapse in their major projection target regions

Although the presence of eYFP+ axons indicates that VTA MC3R neurons synapse in these target brain regions, it is possible that the fibers were only fibers of passage that do not form synapses in the labeled regions. In most of the regions containing eYFP+ axons, branching fibers with bulging varicosities were observed (see NAcc and Tu in Figure 2.3C, D), suggestive of synaptic contact, but we sought to confirm that VTA MC3R neurons indeed synapse in each of the major target regions. To confirm the presence of synapses, MC3R-Cre and wild type (WT) mice were unilaterally injected in the VTA with AAVs expressing a Cre-dependent membrane-tethered GFP (mGFP) and synaptophysin-mRuby connected by the T2A linker (Figure 5A) [188]. In addition, a subset of mice received a 1:3 mixture of AAV-DIO-ChR2-eYFP and AAV-DIO-synaptophysin-mRuby to facilitate identification of VTA MC3R axons. The synaptophysin-mRuby signal was normalized to the fluorescence present in the WT mice to account for high background fluorescence present in some brain regions. Clear synaptophysin-mRuby-positive boutons were identified in each of the brain regions analyzed, and in some cases, mRuby+ boutons were observed along a GFP+ axon (Figure 2.5C). Quantitative analysis of mRuby puncta revealed a significant brain area*genotype interaction ($F(9, 54)=8.449$, $p<0.001$) and *post hoc* tests revealed that synaptophysin-mRuby+ puncta were significantly higher in the NAccSh ($p=0.010$), NAccC ($p=0.010$), Tu ($p=0.027$), LSI ($p=0.037$), and LHb ($p=0.016$) of MC3R-Cre mice compared to the background fluorescence present in WT mice (Figure 2.5B). mRuby puncta were also higher in the VP, BST, BLp, and LH in MC3R-Cre mice than in the WT mice, but these differences did not reach statistical significance (Figure 2.5B). This likely reflects the high levels of background fluorescence in these areas as clear synaptophysin-mRuby+ puncta were identified along mGFP/eYFP+ axons in each of these brain

regions (Figure 2.5C). Thus, VTA MC3R neurons appear to synapse in each of the brain regions receiving strong innervation from VTA MC3R neurons that were identified using ChR2-eYFP labeling.

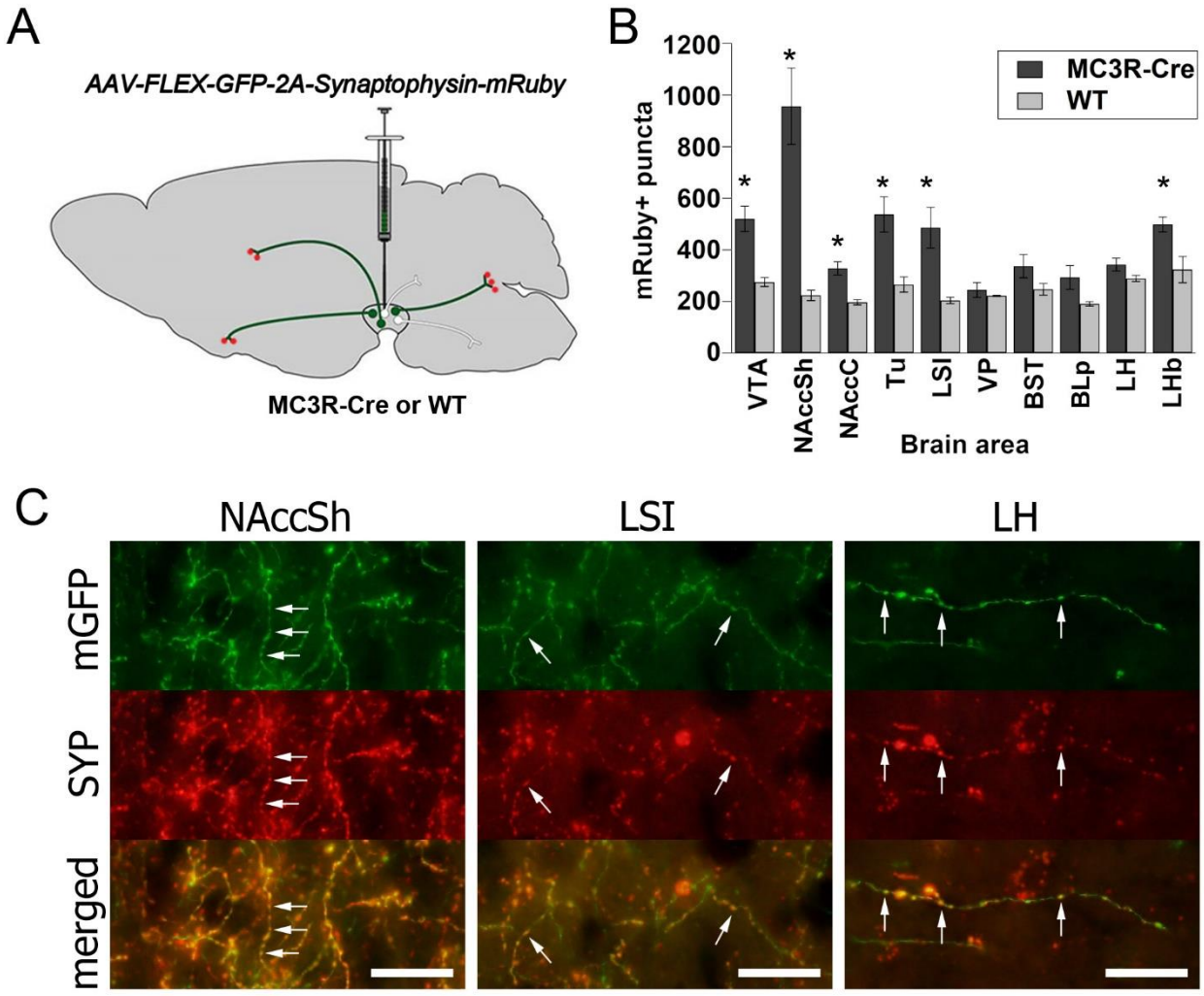

Figure 2.5. Synaptophysin-based confirmation of VTA MC3R synaptic terminals in the major efferent projection targets.

A. Schematic illustrating strategy to achieve synaptophysin-mRuby expression in VTA MC3R axon terminals. **B.** Average synaptophysin-mRuby+ puncta in MC3R-Cre (n=5) and wild type (WT; n=3) mice. **C.** Representative images from NAccSh, LSI, and LH showing synaptophysin-

mRuby+ puncta (red) along mGFP/eYFP+ axons (green). Arrows: examples of synaptophysin-mRuby puncta along an eYFP+ axon. Scale bars: 10 µm. * p<0.05 vs. WT. Abbreviations: **SYP**-synaptophysin.

2.4.3 Afferent inputs to VTA MC3R neurons

We next set out to identify the brain regions providing afferent input to VTA MC3R neurons by making use of EnvA-pseudotyped, G-deleted rabies viruses (RVdG) expressing mCherry [84; 189; 190]. Two AAVs expressing either Cre-dependent TVA-eYFP or Cre-dependent rabies glycoprotein G and blue- fluorescent protein (rG-BFP) [84] were injected into the VTA of male and female MC3R-Cre mice, and RVdG was injected into the same site three weeks later. The mice were sacrificed after 7 days of incubation with RVdG, and 40 µm sections were obtained across the entire rostro-caudal extent of the brain (Figure 2.6A).

The specificity of the RVdG has been previously validated [84], but we wanted to confirm its specificity in our system as well. The AAV helper viruses expressing Cre-dependent TVA-eYFP and rG-BFP were injected into the VTA of WT mice (n=2) 3 weeks before the RVdG injection (n=2) and brains were harvested 1 week later. A small number of mCherry-labeled neurons were observed in the VTA of control animals (Figure 2.6B, C) consistent with the small amount of Cre-independent TVA expression reported previously [84; 191]. No cells expressing BFP were observed in the VTA, however, (Figure 2.6B, C, blue channel) and no RVdG-mCherry labeled neurons were identified outside the VTA, confirming that all RVdG labeled neurons identified in MC3R-Cre mice provide direct input to VTA MC3R neurons. We also confirmed that the injections were restricted to the VTA to exclude the possibility that RVdG-mCherry labeled neurons project to MC3R-expressing neurons outside the VTA. Greater than 88% of starter cells, defined as cells expressing both mCherry and BFP, were located in the VTA in both male and female mice (Figure 2.6D). Off-target starter cells represented less than 12% of all starter

cells and most often were located in the Edinger–Westphal nucleus, red nucleus, substantia nigra pars compacta, MRN, and RRF with no more than 10 cells per off-target site and most sites showing only 1-4 starter neurons. Although we initially analyzed all data by sex, there were no sex differences in the number of inputs per starter (Figure 2.6E), total inputs (data not shown), or inputs from individual brain regions (data not shown). As a result, the data from both sexes were combined for the remainder of the analyses.

The number of RVdG-mCherry labeled cells normalized to the number of VTA starter cells in brain regions providing more than 0.25% of the total number of RVdG labeled cells identified are shown in Figure 2.7, and a whole-brain series of representative coronal sections containing RVdG-mCherry-labeled cells is shown in Figure 2.8. In addition, the numbers of RVdG labeled neurons in each brain region across the entire brain are presented in Table 0.1 (Appendix A). Although RVdG-mCherry labeled non-starter cells (*i.e.* mCherry-positive, BFP-negative) were observed in the VTA, we excluded the VTA from the total input cell count because the cells expressing low levels of TVA may have been directly infected by RVdG and, as a result, could not be distinguished from those providing local input to VTA MC3R neurons. The greatest number of retrogradely labeled neurons were seen in the DR, LH, VP, NAcc, lateral parabrachial nucleus (LPB), LHb, superior colliculus (SC), and median raphe nucleus (MnR) (Figure 2.7-2.9). Together, these top eight brain regions were responsible for ~46% of the total input to VTA MC3R neurons, and examples from each of these brain regions are shown in Figure 2.9. The distributions of cells providing afferent input to VTA MC3R neurons are described below.

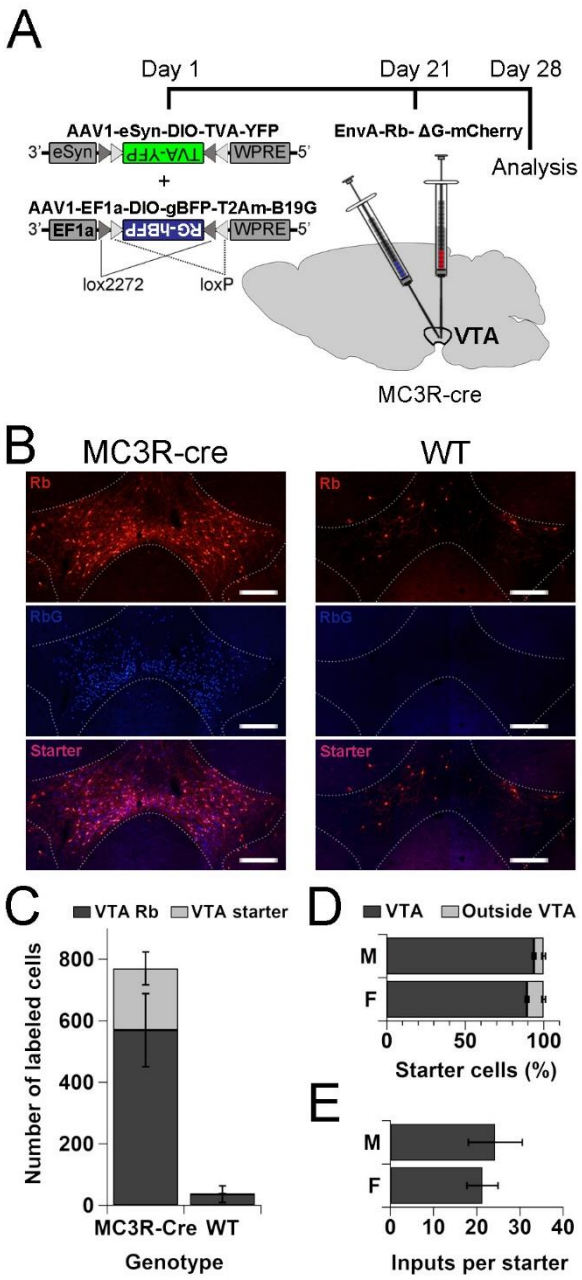

Figure 2.6. Strategy and validation of cell-type-specific monosynaptic rabies virus-mediated tracing from VTA MC3R neurons.

A. Schematic illustrating the strategy used to achieve monosynaptic cell-type specific retrograde labeling of neurons providing synaptic input to VTA MC3R neurons. **B.** Representative images of mCherry, BFP, and merged images taken from coronal VTA sections of VTA MC3R-Cre (left panel) or wild type mice (WT, right panel) injected with helper AAVs and RVdG-mCherry. **C.** Average numbers of VTA starter cells (RVdG-mCherry + rG-BFP; light grey) and neurons expressing RVdG-mCherry only (dark gray) in MC3R-Cre (n=6) and WT mice (n=2). **D.** Percent starter cells within (dark gray) or outside (light gray) the VTA in male and female MC3R-Cre mice (male n=3, female n=3). **E.** Ratio of the total number of RVdG-mCherry-labeled neurons in the entire brain to the number of starter neurons in male and female MC3R-Cre mice (male n=3, female n=3). There were no sex differences in the input/starter ratio (p=0.71). Scale bars: 100 µm.

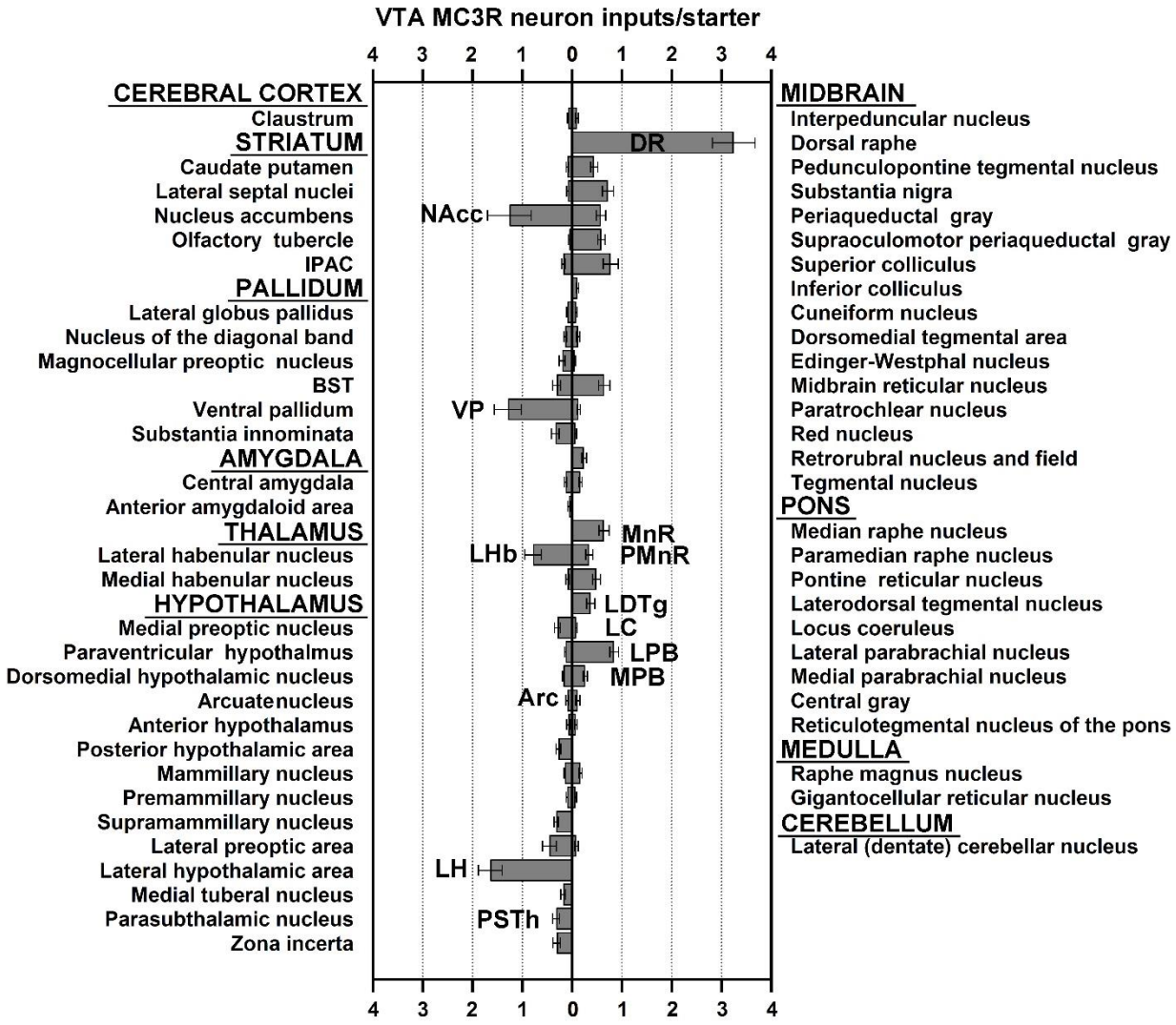

Figure 2.7. RVdG-mCherry labeled inputs to VTA MC3R neurons across the brain.

Average number of RVdG-mCherry-labeled neurons in different brain regions of male and female MC3R-Cre mice normalized to the total number of starter cells. Only the regions providing >0.25% of total input are shown. Inputs for all brain regions are shown in Appendix A. Male n=3, female n=3.

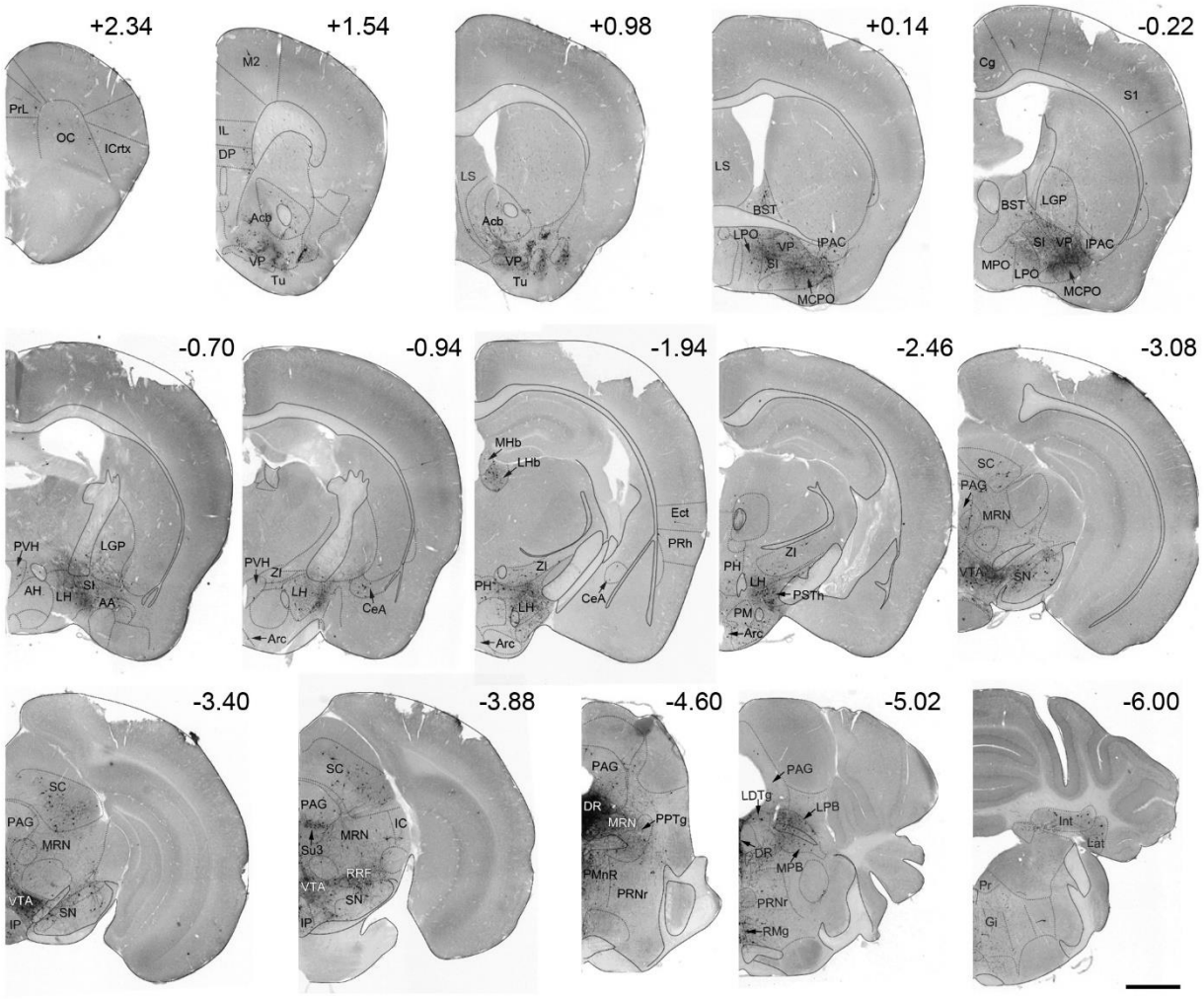

Figure 2.8. Sample whole-brain series of coronal images showing RVdG-mCherry labeled neurons providing afferent input to VTA MC3R neurons.

Representative whole-brain coronal sections showing RVdG-mCherry-labeled neurons (black) in different brain regions of a MC3R-Cre mouse. Brains sections are outlined with dotted lines and fiber tracts are outlined with solid lines. Numbers in the top right corner indicate the section's position relative to bregma. Scale bar: 1 mm. Abbreviations: ***AA***- anterior amygdaloid area, ***DP***- dorsal peduncular cortex, ***Ect***- ectorhinal cortex, ***Gi***- gigantocellular reticular nucleus, ***IC***- inferior colliculus, ***Icrtx***- insular cortex, ***IL***- infralimbic cortex, ***Int***- interposed cerebellar nucleus, ***IP***- interpeduncular nucleus, ***Lat***- lateral (dentate) cerebellar nucleus, ***LGP***- lateral

globus pallidus, ***M2***- motor cortex, ***MPO***- medial preoptic area, ***OC***- orbital cortex, ***PH***- posterior hypothalamic area, ***PM***- premammillary nucleus, ***PAG***- periaqueductal gray, ***PMnR***- paramedian raphe nucleus, ***PPTg***- pedunculopontine tegmental nucleus, ***Pr***- prepositus nucleus, ***PRh***- perirhinal cortex, ***PrL***- prelimbic cortex, ***PRNr***- pontine reticular nucleus, ***RMg***- raphe magnus nucleus, ***RRF***- retrorubral field, ***S1***- somatosensory cortex, ***Su3***- supraoculomotor periaqueductal gray.

Cerebral cortex and cerebellum. The structures of the cerebral cortex and the cerebellum provided very sparse input to the VTA MC3R neurons (1.75%±0.12% and 0.47%± 0.16 % of total input, respectively). All of the cortical and cerebellar nuclei containing RVdG-mCherry-labeled cells displayed scarce labeling, with fewer than 20 mCherry-labeled neurons per area (Figure 2.8, Table 0.2 in Appendix B). A very small number of labeled neurons were present in the prefrontal cortex including the cingulate, prelimbic, infralimbic, and orbital cortices (Figure 2.8, Appendix A). The very sparsely labeled olfactory areas included the anterior olfactory nucleus, dorsal peduncular cortex, dorsal tenia tecta, nucleus of the lateral olfactory tract, and piriform cortex. The single cortical nucleus with the greatest amount of retrogradely labeled neurons, although still very sparsely labeled, was the claustrum of the cortical subplate (Figure 2.8, Appendix A). In the cerebellum, few cells were present in the cerebellar nuclei including the interposed, dentate, and fastigial nuclei (Figure 2.7-2.8, Appendix A).

Striatum. Striatal areas were responsible for 6.9% ± 1.2% of total input to the VTA MC3R neurons with most of the striatal input coming from the ventral striatum. NAcc was very highly populated with retrogradely labeled neurons which were highly concentrated and organized into patches within the mNAccSh. Conversely, the RVdG-mCherry labeling in the NAcc core and lateral shell was sparse (Figure 2.7-2.8, 2.9A, Appendix A). The remaining nuclei of the ventral striatum including the Tu, the lateral stripe of the striatum, and the interstitial nucleus of the posterior limb of the anterior commissure (Figure 2.9B) provided very low to low amount of

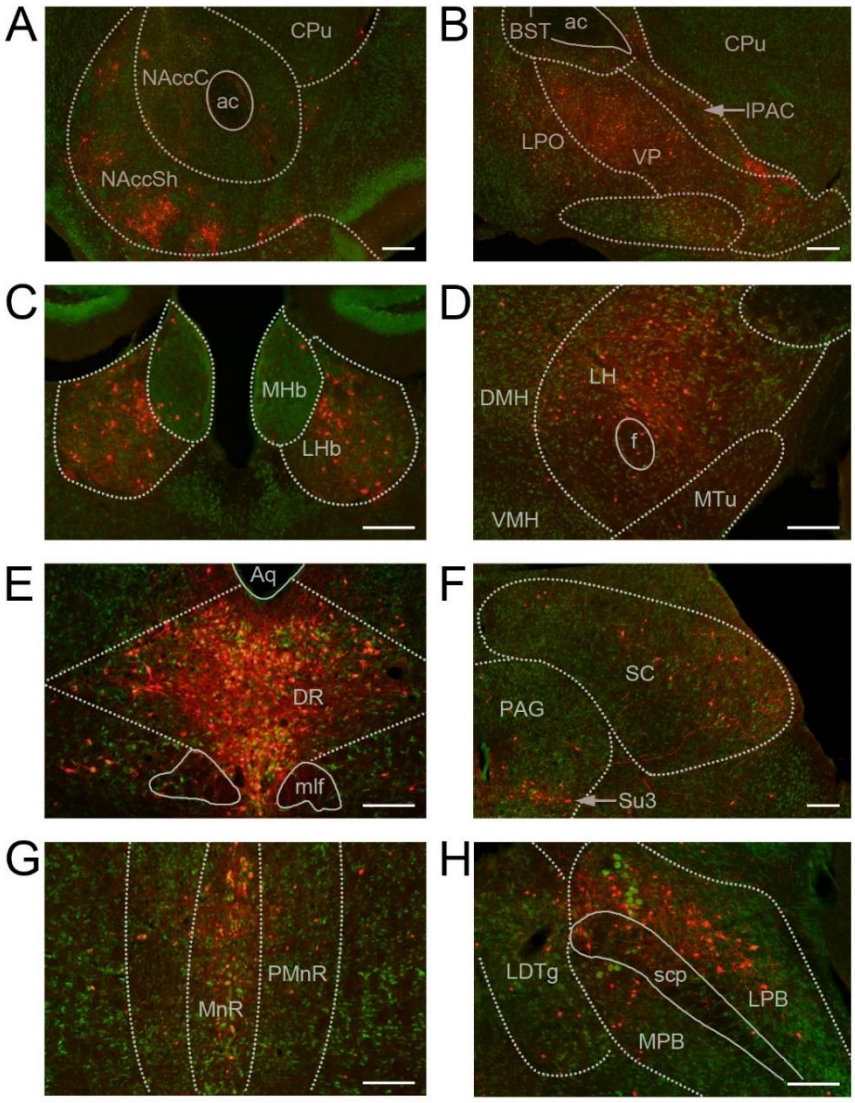

Figure 2.9. Sample images of the major areas providing afferent input to VTA MC3R neurons. RVdG-mCherry labeled neurons are shown in red in coronal sections stained with NeuroTrace Nissl stain (green) **A**. NAcc **B.** VP and LPO. **C**. LHb **D**. LH. **E**. DR. **F**. SC and PAG, **G**. MnR and PMnR. **H**. Parabrachial nucleus. Brain regions are outlined with dotted lines, and fiber tracts are outlined with continuous lines. Scale bars: 100 µm. Abbreviations: ***DMH***- dorsomedial hypothalamic nucleus, ***MTu***- medial tuberal nucleus, ***VMH***- ventromedial hypothalamus; fiber tracts and other structures: ***ac***- anterior commissure, ***mlf***- medial longitudinal fasciculus, ***scp***- superior cerebellar peduncle.

afferent input to VTA MC3R neurons (Figure 2.7-2.8, Appendix A). The nuclei of the lateral septal complex including lateral septal nuclei, septofimbrial, and septohippocampal nuclei as well as the CPu (Figure 2.9A, B) of the dorsal striatum contained very few labeled neurons (Figure 2.7-2.8, Appendix A)

Pallidum. 10.2% ± 0.9% of total afferent input to the VTA MC3R neurons came from the pallidum. Most of the pallidal input originated from the ventral division of the region. Within this division, VP was very highly populated with RVdG-mCherry+ neurons (Figure 2.9B), whereas the labeling within the other structures such as SI and the magnocellular preoptic nucleus was low (Figure 2.7-2.8, Appendix A). The BST of the caudal pallidum also contained a low amount of RVdG-mCherry+ cells (Figure 2.9B) whereas the structures of dorsal pallidum such as the medial and lateral globus pallidus as well as those of the medial pallidum including medial septal nucleus, nucleus of the diagonal band, and the triangular septal nucleus contained very sparse labeling (Figure 2.7, Appendix A).

Amygdala. Structures of the amygdala and extended amygdala supplied very little input to the VTA MC3R neurons providing only 1.3% ± 0.1% of the total input. The CeA contained sparse RVdG-mCherry-labeled cells and was responsible for almost half of the amygdalar input to the VTA MC3R neurons (Figure 2.7-2.8, Appendix A). Other amygdalar nuclei including the MeA, BLA, and BMA, as well as the anterior amygdaloid area, intercalated amygdaloid nucleus, and amygdalostriatal transition area contained very few retrogradely labeled neurons (Appendix A).

Thalamus. 4.6% ± 05% of VTA MC3R input was supplied by the thalamus. Most of the afferent thalamic innervation of the VTA MC3R neurons came from the polymodal associated cortex related structures with the LHb containing the highest number of retrogradely labeled neurons of all thalamic structures (Figure 2.7-2.8, 2.9C, Appendix A). Medial habenula (Figure 2.9C) as well as the other polymodal associated cortex related nuclei including the nuclei of the

lateral, anterior, medial, midline, intralaminar thalamic groups, and the reticular thalamic nucleus contained very sparse RVdG-mCherry labeling (Figure 2.8, Appendix A).

Hypothalamus. Hypothalamic nuclei provided 21.2% ± 1.1% of the total VTA MC3R neuron input. We observed a lateral to medial gradient in the amount of hypothalamic input, with the most labeled neurons in the lateral zone and the fewest in the medial, periventricaular zone. In the periventricular zone/region, sparse labeling was observed in the medial preoptic, paraventricular, and dorsomedial nuclei with very sparse labeling in the remaining nuclei (Figure 2.7-2.8, Appendix A). To our surprise, but consistent with the lateromedial gradient, we found very few RVdG-mCherry-labeled cells in the Arc (Figure 2.7-2.8, Appendix A). In the medial hypothalamic zone, weak RVdG-mCherry labeling was observed in the posterior hypothalamic area, the mammillary nucleus and very weak labeling was seen in the ventromedial hypothalamus, premammillary and the tuberomammillary nuclei (Figure 2.7-2.8, Appendix A). In the lateral hypothalamic zone, LPO provided a moderate amount of input to the VTA MC3R neurons (Figure 2.7-2.8, 2.9B, Appendix A). Very strong input to the VTA MC3R neurons came from LH (Figure 2.9D), whereas the low amount of retrogradely labeled neurons were present in the zona incerta, and PSTh with very sparse labeling in the subthalamic nucleus (Figure 2.7-2.8, Appendix A).

Midbrain, Pons, and Medulla Oblongata. Together, the midbrain and pons provided a little over half of all input (37.1% ± 2.9% and 15.0% ± 0.4%, respectively). In the midbrain, very high RVdG-mCherry labeling was present in the dorsal raphe (DR) which was the brain area providing the highest input to the VTA MC3R neurons (Figure 2.7-2.8, 2.9E, Appendix A). The SN was moderately populated with RVdG-mCherry+ neurons with more abundant labeling in pars compacta than in pars reticulata (Figure 2.7-2.8, Appendix A). The pedunculopontine tegmental nucleus and interpeduncular nucleus both displayed low/very low labeling, and the periaqueductal gray including the supraoculomotor nucleus contained a moderate number of labeled neurons (Figure 2.7-2.8, 2.9F, Appendix A). Many RVdG-mCherry+ cells were present

in the SC, but only a few were present in the inferior colliculus (IC; Figure 2.7-2.8, 2.9F, Appendix A). The MRN was moderately populated with retrogradely labeled neurons and low levels of labeled cells were seen in the RRF and the dorsomedial tegmental area (Figure 2.7-2.8, Appendix A). Multiple other midbrain areas were sparsely populated with retrogradely labeled neurons (Appendix A).

Most of the hindbrain input was derived from pons. The most prominent pontine input was from the LPB which contained many RVdG-mCherry+ neurons whereas the MPB was labeled sparsely (Figure 2.7-2.8, 2.9H, and Appendix A). MnR displayed moderate levels of labeling with low levels seen in the paramedian raphe (Appendix A, Figure 2.7, Figure 2.8, Figure 2.9G). Low levels of RVdG-mCherry-labeled cells were also present throughout the pontine reticular nucleus and the LDTg, and very sparse labeling was present in the locus coeruleus (Figure 2.7-2.8, Appendix A). Many other pontine areas contained sparse RVdG-mCherry labeling (Appendix A), and a low amount of labeling was observed in the raphe magnus nucleus of the medulla oblondata with the remaining areas of the region labeled very sparsely labeled (Figure 2.8, Appendix A).

2.4.4 Afferent Input from the Arcuate Nucleus to VTA MC3R Neurons

One surprising result of the analysis of the afferent inputs was the near absence of RVdG-mCherry labeled neurons in the Arc which contains POMC and AgRP neurons that would be expected to provide the ligands for MC3Rs (α-MSH and AgRP). Also, previous studies have shown that general retrograde tracers injected into the VTA label POMC neurons in the Arc [155] and that AgRP axons are present in the VTA [156]. Therefore, we conducted additional retrograde tracing experiments to further examine the potential projections from Arc POMC & AgRP neurons to the VTA. We initially injected RetroBeads into the VTA of transgenic mice expressing GFP in NPY neurons (NPY-GFP mice) to confirm the previous reports that Arc POMC and AgRP neurons project to the VTA. POMC and AgRP neurons labeled with

RetroBeads were identified using immunohistochemistry for POMC and GFP labeling in NPY/AgRP neurons. NPY-GFP was used to identify AgRP neurons because all AgRP neurons express NPY [192; 193] and AgRP neurons are difficult to identify using standard immunohistochemical techniques. Injection of fluorescent microspheres into the VTA resulted in 614 +/- 90 labeled neurons/mouse in the Arc (sampled from every 5th section) (Table 1), with NPY/AgRP neurons comprising 27.2 +/- 1.1% and POMC neurons comprising 12.5+/-1.0% of the total number of labeled neurons (Figure 2.10B, Table 1). There was a significant main effect of neuron cell type ($F(2,14)=11.057$, $p=0.002$) that was due to higher co-expression of RetroBeads with non-POMC, non-NPY/AgRP neurons ("other") compared to POMC ($p=0.001$) or NPY/AgRP neurons ($p=0.16$), but no significant difference between the number of labeled POMC or NPY/AgRP ($p=0.083$, Figure 2.10B). Sample images of POMC and NPY/AgRP neurons containing RetroBeads are shown in Figure 2.10 A*i-iv*.

Table 2.1. Absolute number and percent of total Arc neurons labeled by RetroBeads and RVdG

Genotype	**#POMC***	**#NPY/AGRP***	**# OTHER***	**%POMC**	**%NPY/AgRP**	**%OTHER**
RetroBeads (n=5)	74 ± 9	165 ± 23	300 ± 54	12.5 ± 1.0	27.2 ± 1.1	51.9 ± 8.4
MC3R-Cre (n=5)	2 ± 1	0.00	2 ± 1	54.3 ± 14.6	0.00	45.7 ± 14.6
TH-Cre (n=6)	4 ± 2	0.00	5 ± 1	28.3 ± 11.5	2.4 ± 2.4	69.3 ± 11.5
vGlut2-Cre (n=5)	8 ± 3	1 ± 1	18 ± 7	39.8 ± 10.9	7.7 ± 5.7	52.5 ± 8.9
GAD-Cre (n=4)	3 ± 1	1 ± 0	7 ± 2	29.4 ± 5.1	3.1 ± 1.8	67.4 ± 4.2

* Retrobead labeled neurons were counted in every 5th Arc section, whereas RVdG-mCherry labeled neurons were counted in every other Arc section.

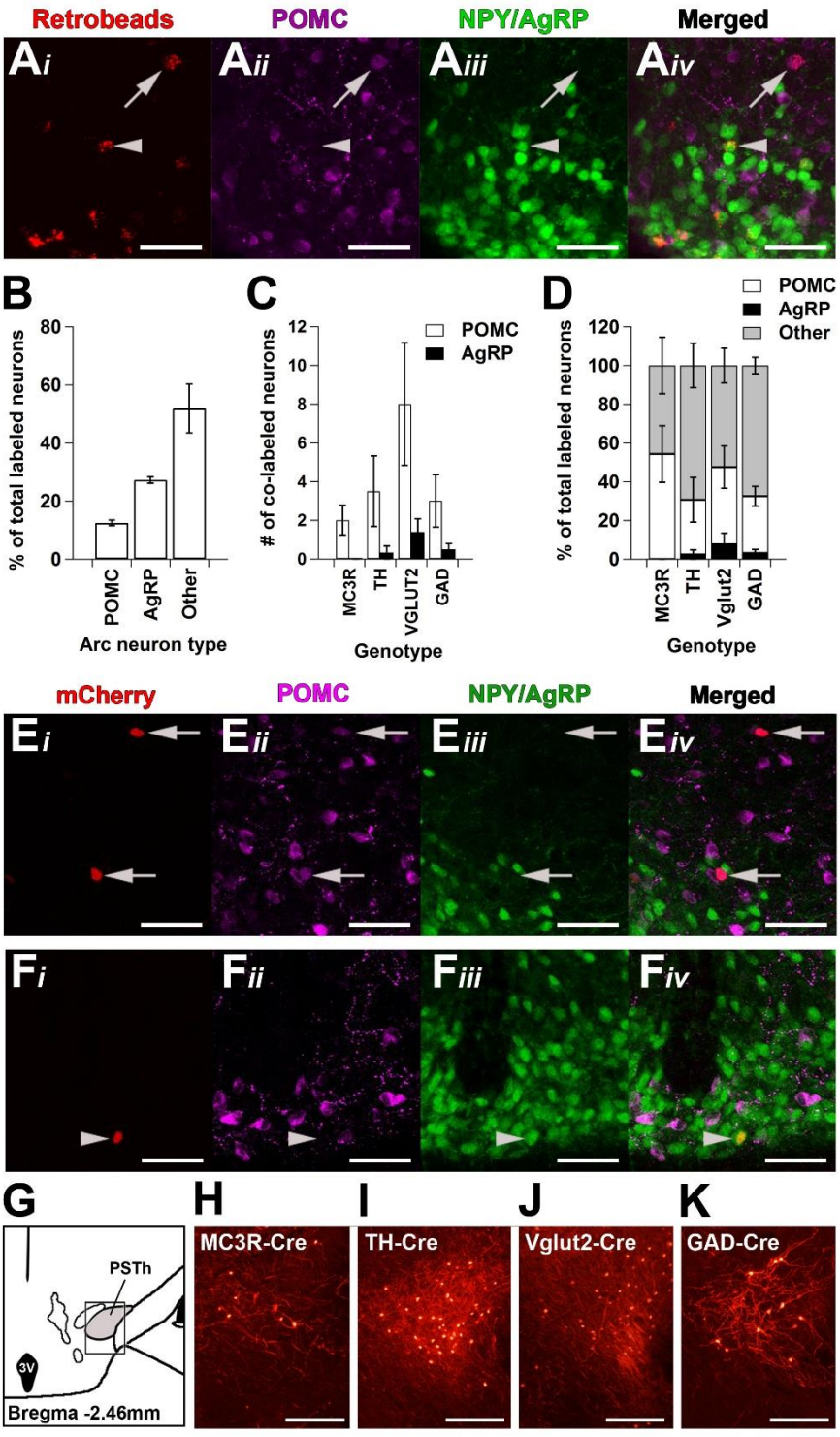

Figure 2.10. Arc POMC and AgRP neurons project to the VTA but form few direct synapses with any of the major VTA neuron subtypes.

A-B. Arc POMC and AgRP neurons were labeled by RetroBeads injected into the VTA. **A*i*-A*iv***. Representative images showing Retrobead-labeled POMC and NPY/AgRP neurons **A*i***. RetroBeads (red) **A*ii***. POMC (magenta), **A*iii*.** NPY/AgRP (green), and **A*iv*.** merged images. Arrow indicates a RetroBead-labeled POMC neuron and arrowhead indicates a RetroBead-labeled NPY/AgRP neuron **B**. Percent of total RetroBead-labeled Arc neurons that were POMC, NPY/AgRP, or non-POMC, non-NPY/AgRP ('other') neurons (n=5). The cell counts were obtained from every 5th Arc section. **C-F**. Sample Arc images and quantification of RVdG-mCherry-labeled neurons in the Arc from MC3R-Cre (n=5), TH-Cre (n=6), vGlut2-Cre (n=5), and GAD-Cre (n=4) mice **C**. Total number of POMC (white) or NPY/AgRP (black) neurons labeled by RVdG-mCherry from VTA MC3R, TH, vGlut2, or GAD neurons. The total cell counts were obtained from every other Arc section. **D**. Percent of total POMC (white), NPY/AgRP (black), or other (gray) Arc neurons labeled by RVdG-mCherry from VTA MC3R, TH, vGlut2, or GAD neurons. Error bars for each cell type are at the top of each bar. **E*i*-F*iv*.** Representative Arc images of sections from a vGlut2-Cre mouse (**E**) or a TH-Cre mouse (**F**), **E*i*, F*i***: RVdG-mCherry; **E*ii*, F*ii***: POMC; **E*iii*, F*iii***: NPY/AgRP; **E*iv*, F*iv***: Merged images. Arrows indicate a RVdG-labeled POMC neuron and arrowhead indicates a RVdG-labeled AgRP neuron. **G-K.** Confirmation of functional tracing by RVdG in the PSTh in mice used for quantification of synaptic connectivity between Arc and VTA neuronal populations. **G.** Atlas section showing the location of PSTh images (box). **H-K**. Sample images of the PSTh in sections from MC3R-Cre (**H)**, TH-Cre (**I)**, vGlut2-Cre (**J)**, and GAD-Cre (**K)** mice. Scale bars: 50 µm (A, E, F) and 100 µm (G-H).

The lack of RVdG-labeled neurons in the Arc following RVdG injection into the VTA of MC3R-Cre mice combined with the robust labeling of POMC and AgRP neurons by the fluorescent microspheres injected to the VTA suggested that POMC and AgRP neurons may synapse onto other VTA neuron subpopulations. Thus, we utilized RVdG to test whether POMC or AgRP neurons synapse onto MC3R, dopamine (DA), GABA, or glutamate neurons in the

VTA using MC3R-Cre, TH-Cre (DA), GAD-Cre (GABA), or vGlut2-Cre (glutamate) mice. Each of the mouse lines was crossed to NPY-GFP mice to visualize both NPY/AgRP and POMC (using IHC) neurons within the same brain sections. Male and female mice of each genotype were injected with the helper AAVs expressing TVA and RG-BFP, followed by RVdG as described for the whole-brain input mapping experiments (Figure 2.6A), and coronal sections containing the VTA and Arc were collected. The VTA sections were visualized to confirm correct injection location and the presence of starter cells, and every other Arc section was examined for the presence of RVdG-mCherry, POMC and NPY/AgRP neurons (Figure 2.10E-F). As a positive control, the PSTh, which is located within the same sections containing the Arc and has been shown to provide input to all of these populations of VTA neurons [84], was examined for the presence of mCherry to confirm functional tracing by RVdG (Figure 2.10G-K). Analysis of the number of labeled neurons in the different genotypes examined revealed a significant main effect of genotype ($F(3,48)=4.115$, $p=0.011$) due to higher Arc RVdG-mCherry labeling in the neurons retrogradely traced from vGlut2 neurons compared to other VTA neuron groups ($p=0.002$ *vs* MC3R, $p=0.009$ *vs* TH, $p=0.036$ *vs* GAD). Although both POMC and NPY/AgRP neurons in the Arc were labeled by RVdG-mCherry in all genotypes tested, there were few labeled POMC or NPY/AgRP neurons observed for each of the starter cell types (Figure 2.10C, E-F, Table 2.1). Overall, only ~2-8 POMC (~30-50% of all Arc RVdG-mCherry expressing cells) and 0-2 NPY/AgRP neurons (~0-8% of all Arc RVdG-mCherry expressing cells) were labeled across all of the Arc sections examined (Figure 2.10C-D, Table 2.1). And in contrast to the data obtained with the fluorescent microspheres, most of the RVdG labeled neurons co-localized with POMC and not NPY/AgRP neurons for all genotypes examined (Figure 2.10C-D, Table 2.1). There was a significant main effect of cell type ($F(2, 48) =7.002$, $p=0.002$) with fewer NPY/AgRP neurons co-expressing RVdG-mCherrry compared to non-POMC, non-NPY/AgRP neurons ($p=0.001$) but there were no differences in the number of POMC or NPY/AgRP neurons labeled with RVdG-mCherry ($p=0.051$). Thus, it appears that although POMC and AgRP

neurons project to the VTA, few of them form direct synapses onto VTA neurons, suggesting that Arc POMC and AgRP neurons may predominantly release their neuropeptides extra-synaptically within the VTA.

2.5 Discussion

In these studies, we have defined the efferent projection patterns of VTA MC3R neurons, and we have identified the location of all neurons providing afferent input to these cells. We have also demonstrated that POMC and AgRP neurons in the Arc form few direct synapses (as identified by RVdG tracing) onto any of the major neuron subtypes in the VTA, including VTA MC3R neurons, despite the robust labeling of POMC, AgRP, and other undefined Arc neurons after injection of general retrograde tracers into the VTA. The results of these studies defining the anatomy of VTA MC3R neurons provide valuable information, as these neurons are likely to be an important site of interaction between the melanocortin and mesolimbic dopamine systems in the neural control of feeding and body weight.

One of the most surprising and interesting results of these studies was the very low amount of direct synaptic input from Arc POMC and AgRP neurons to any of the VTA neuron subtypes tested, including VTA MC3R neurons (Figure 2.7,2.10C-F), despite the large number of Arc neurons labeled by RetroBeads injected into the VTA (Figure 2.10A-B), and the previous identification of Arc POMC and AgRP neuron projections to the VTA [155; 156]. This was also unexpected because the endogenous ligands for MC3Rs, α-MSH and AgRP, are produced by Arc POMC and AgRP neurons, so it would be expected that Arc POMC & AgRP neurons would release these neuropeptides at direct synapses in the VTA. Unlike classical fast neurotransmitters (glutamate and GABA), neuropeptide release may occur not only at a synapse but also at extra-synaptic release sites along the axon. Neuropeptides can then act near their release site or can travel over long distances to exert their effect on neurons far from the release site (*i.e.* volume transmission) [194; 195]. Based on the robust number of

RetroBead-labeled cells in the Arc (our Figure 2.10A-B, and [155]) combined with the presence of AgRP terminals in close proximity to the VTA TH neurons [156], and the low number of RVdG labeled cells observed, it appears that POMC and AgRP neurons likely utilize extra-synaptic neuropeptide transmission in the VTA. Peptide release into the extracellular space along with its diffusion and the lack of reuptake machinery results in long extracellular half-life [196] which is consistent with the ability of α-MSH to suppress feeding for prolonged periods. This possibility is also supported by the previous demonstration that the majority of dense-core vesicles in POMC and AgRP neuron terminals in the paraventricular nucleus were located in extra-synaptic release sites [197].

Another important point that arises from these results is the potential under-representation of neuropeptide transmitting neurons in studies utilizing RVdG to identify inputs to specific neuronal populations. RVdG has been widely used to examine the afferent inputs to distinct neuronal populations in the brain. Thus, it appears that results from these prior studies should be interpreted carefully to allow for the likelihood that the labeled neurons only represent neurons providing direct, fast, classical neurotransmitter-mediated inputs and may exclude other neuropeptide containing neurons, although this will need to be examined on an individual basis.

VTA MC3R neurons received input from and projected to a wide variety of brain regions (Figure 2.1-2.2, 2.7-2.8), roughly resembling the previously described circuit connectivity patterns of different populations of VTA neurons [74; 84; 93; 98; 191]. VTA MC3R axons and retrogradely labeled neurons were concentrated in the medial aspects of the ventromedial striatum (Figure 2.3B, F) consistent with the ventromedial position of VTA MC3R neurons [157; 162] and the previously characterized mediolateral topographic organization of VTA neuron projections and inputs [198; 199]. Overall, the brain regions providing input to VTA MC3R neurons were more widely distributed across the brain than the efferent projections of these cells, and some areas showed reciprocal connections, whereas other areas only received projections or provided input (Figure 2.11). For example, in the striatum, both the NAccSh and

NAccC were reciprocally connected to the VTA MC3R neurons whereas the Tu and LSI only received input from VTA MC3R neurons. Some of the other reciprocally innervated brain regions of note were VP, CeA, LHb, PVH, LH, and SN. In contrast, the VTA MC3R neuron target areas which provided very little input back to the VTA MC3R included Tu, LSI, BST, SI, and BLA/BMA, whereas the LPO, DR, periaqueductal gray, pedunculopontine tegmental nucleus, SC, MnR, LDTg, LPB, and MPB provided more input to the VTA MC3R neurons than they received.

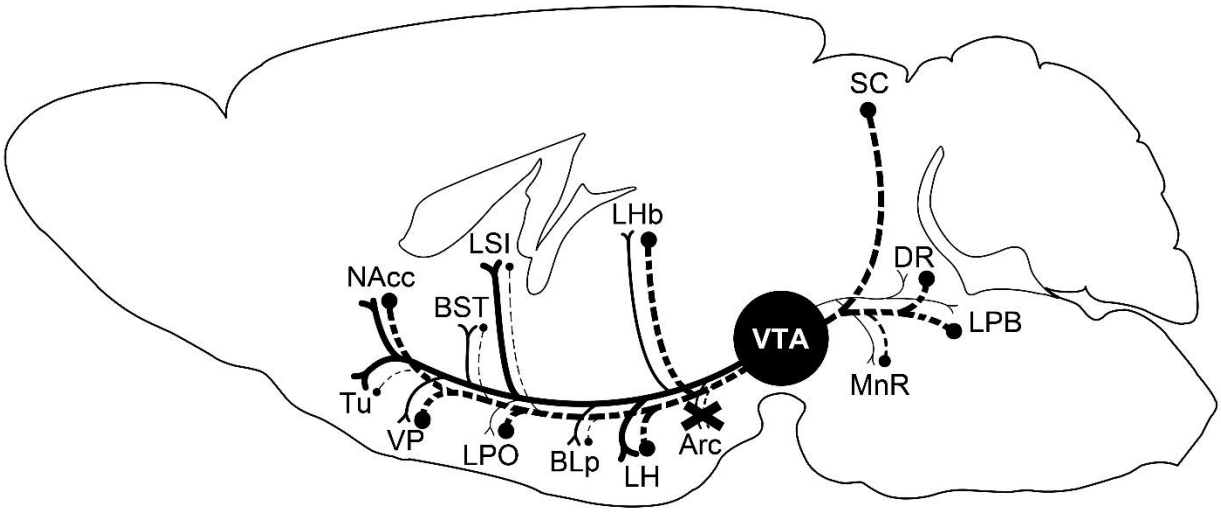

Figure 2.11. Summary of the major efferent projections targets and the areas providing afferent input to VTA MC3R neurons.

Solid lines represent efferent projections of the VTA MC3R neurons and dashed lines represent afferent input to VTA MC3R neurons. The thickness of the lines represents the density of projections or the number of neurons in the area providing input to VTA MC3R neurons. The “x: over Arc projections indicates the low afferent and efferent connectivity between Arc and the VTA.

There were a number of brain regions identified in these studies that were notable for either the presence or absence of efferent output from or afferent input to VTA MC3R neurons. The first notable finding was the near lack of labeling in the PFC. Although VTA MC3R neurons are present in all subnuclei of the VTA, they are highly concentrated in the ventromedial region including PN, IF, RLi, CLi (Figure 2.3A, 2.6B). Both the ventromedial location of the VTA MC3R neurons and their electrophysiological properties [162] are consistent with a unique population of medial neurons identified by Lammel *et al.* which project to the mPFC, NAcc medial shell and core, and basolateral amygdala [65]. VTA MC3R neurons differed from the population identified by Lammel *et al.* [65], however, in that their cortical projections were very sparse. And consistent with the low amount of cortical input to the VTA DA, glutamate, and GABA neurons reported previously [84], PFC input to the VTA MC3R neurons was also sparse (Supplemental Table 1).

Another brain region that stood out, both in the density of VTA MC3R axons (Figure 2.2-2.4) and the reproducibility of their unique band-like appearance (Figure 2.3E) was the intermediate segment of LS. LS GABAergic neurons that project to the LH bidirectionally regulate food intake such that their activation inhibits feeding, whereas their inhibition increases feeding [200]. Thus, VTA MC3R neurons could modulate these LS GABA neurons to regulate feeding, although this remains to be tested. The ventromedial location of the VTA MC3R neurons and the band-like appearance of their LSI projections appear to overlap with previously described VTA neural populations including a population of TH+ neurons co-expressing Neurogenic Differentiation Factor-6 (NEUROD6), transcription factor orthodenticle homeobox 2 (OTX2), CALBINDIN1, and aldehyde dehydrogenase 1a1 (ALDH1A1) [201; 202], as well as a population of TH+ neurons co-expressing CCK and another one co-expressing vGlut2 [202]. The potential molecular overlap between these neuronal populations with VTA MC3R neurons still needs to be established, but if confirmed, this could facilitate the study of LSI-projecting DA neurons.

VTA MC3R neuron axons and synaptic puncta were identified in the LH (Figure 2.3-2.5) raising the possibility that, in addition to a potential indirect effect on LH via the LSI, VTA MC3R neurons may directly modulate LH neural circuitry and associated behaviors (Figure 2.2-2.5). Optogenetic stimulation of LH GABA neurons, including those projecting to the VTA, induces feeding and reward-associated behaviors [203; 204], whereas selective ablation of these neurons reduces feeding, body weight gain, and motivation to obtain palatable reward [203] and stimulation of glutamatergic LH projections to the VTA results in conditioned place aversion [205]. LH receives VTA GABAergic input, but little to no VTA glutamatergic input [98; 206] raising the possibility that VTA MC3R neurons could decrease feeding and food reward via direct inhibition of LH GABA neurons, including those projecting back to the VTA, as LH neurons also provided a strong reciprocal innervation to the VTA MC3R neurons (Figure 2.7-2.9). Future studies are required to understand the functional implication of the reciprocal connections between VTA MC3R neurons and the LH including the types of neurons that are interconnected between the two nuclei and the behaviors regulated by this network.

VTA MC3R neurons were also bidirectionally connected to the LHb (Figures 2.2, 2.7), raising the possibility that VTA MC3R neurons might participate in the regulation of aversive behaviors. LHb neurons are activated by aversive stimuli and inhibit VTA DA neurons [92; 207; 208] to produce aversive or avoidance behaviors [208]. VTA DA/GABA and glutamate neurons also project back to the LHb and regulate LHb output and resulting behaviors such that VTA glutamatergic signaling activates LHb circuitry and promotes aversion [71], whereas stimulation of VTA GABA release in the LHb promotes reward [67]. Thus, VTA MC3R neurons could alter reward and aversive behaviors through the release of GABA or glutamate in the LHb, but future studies will be required to test this possibility.

The PBN, which is known for its role in taste regulation [209; 210] and appetite suppression [211-213], was notable for the strength of its input to VTA MC3R neurons (Figure 2.7). Although PBN is best known for its projections to the forebrain structures involved in

appetite regulation, [214-216] both VTA DA and GABA neurons have been shown to receive direct input from the PBN [93; 210] including PBN neurons involved in responding to pain, fear, and satiety stimuli [213; 217]. Additionally, VTA projecting PBN neurons have been shown to be responsive to both sweet and bitter stimuli [210] suggesting that PBN may regulate both reward and aversion-associated behaviors through its action in the VTA. Further studies will be necessary to determine the role of PBN-VTA MC3R neuron circuit in feeding, taste, aversion, and reward processing, however.

Although these studies have provided important information on the efferent and afferent connectivity of VTA MC3R neurons, there are still some important unanswered questions. First, the neurotransmitter phenotype of VTA MC3R neurons projecting to the efferent targets is unknown. MC3Rs are expressed in both dopamine and non-dopamine neurons in the VTA [157], so it remains to be determined which neurotransmitters are released by VTA MC3R neurons at the different efferent targets. It is also unknown whether VTA MC3R neuron projections to the different regions identified play specific roles in independent aspects of behavior or if they act in a concerted fashion. Further study will be required to answer these and other questions, however.

In summary, we have shown here that VTA MC3R neurons send strong projections to and receive afferent inputs from a discrete set of brain regions involved in the regulation of feeding, reward, and aversion. We have also shown that, although Arc neurons provide strong projections to the VTA, they form few direct synapses on any of the VTA neuron subtypes examined, suggesting that the transmission of α-MSH and AgRP to the VTA likely happens via extra-synaptic release. This work greatly contributes to our understanding of the anatomy of the interaction between the melanocortin and the mesolimbic systems and contributes to the growing body of work focused on understanding how molecularly distinct VTA neuron groups and their circuits control behavior. In addition, defining the anatomical organization of VTA

MC3R neurons will allow for a more detailed analysis of the role that these neurons, and the circuits they are embedded in, play in the control of feeding and other behaviors.

3 SEX DEPENDENT ALTERATIONS IN FEEDING AND BODY WEIGHT FOLLOWING ACTIVATION AND INHIBITION OF VTA MC3R NEURONS

Anna I. Dunigan[1], David P. Olson[3], and Aaron G. Roseberry[1,2]

[1]Department of Biology and [2]Neuroscience Institute, Georgia State University, Atlanta, GA

[3]Department of Pediatrics, University of Michigan, Ann Arbor, MI

3.1 Abstract

The melanocortin and the mesolimbic dopamine systems are two neural circuits highly implicated in the control of feeding and body weight, and increasing evidence indicates that these systems interact to regulate food-related behaviors. Because melanocortin-3 receptors are highly expressed in the VTA, we set out to determine the role of VTA neurons expressing these receptors (VTA MC3R neurons) in the regulation of feeding and body weight. DREADD receptors were used to acutely and chronically activate and inhibit VTA MC3R neurons, and changes in food intake and body weight were measured in both male and female mice. Acute activation and inhibition of VTA MC3R neurons inhibited feeding in a sex-dependent manner, such that activation inhibited feeding only in females and inhibition inhibited feeding only in males. Chronic activation of VTA MC3R neurons also produced a transient decrease in feeding and body weight in all mice, whereas inhibition of VTA MC3R neurons showed a trend towards an increase in feeding and body weight. VTA MC3R neurons dynamically regulate feeding and body weight in a sex-dependent manner, indicating that VTA MC3R neurons may be a key point of interaction between the melanocortin and the mesolimbic dopamine systems in the control of feeding and body weight.

3.2 Introduction

Obesity is a growing problem in the US and has been increasing worldwide. As much as 70% of US population is estimated to be overweight or obese [218; 219] and obese individuals are at higher risk for developing serious medical conditions such as insulin resistance and type II diabetes, cardiovascular disease, some cancers, and life-threatening respiratory conditions [220]. Furthermore, obesity treatment generates an estimated annual health care cost of $150 billion [4]. Despite the prevalence and burden of obesity and its associated disorders few effective therapies currently exist to combat it. Consequently, there is a great need to advance our understanding of the neural mechanisms that control feeding and body weight, which could lead to new, viable strategies to combat obesity.

Feeding is a complex behavior, and most research examining the control of feeding has focused on two broad aspects of feeding: homeostatic feeding (feeding to satisfy basic physiological needs) and hedonic or reward-based feeding (feeding based on the reward or pleasure of foods, especially palatable foods rich in fat and/or sugar).

The melanocortin system is a major component of the neural circuitry controlling homeostatic feeding, and it is comprised of the neuropeptides α-melanocyte-stimulating hormone (α-MSH) and agouti-related peptide (AgRP), the neurons in the arcuate nucleus of the hypothalamus (Arc) that release these neuropeptides (proopiomelanocortin (POMC) and AgRP neurons), and the central melanocortin-3 and melanocortin-4 receptors (MC3R and MC4R) that respond to α-MSH and AgRP. Activation of POMC and AgRP neurons has opposite effects on feeding behavior such that the activation of POMC neurons or injection of MC3/4R agonists decreases food intake and body weight [114-116], whereas activation of AgRP neurons and central administration or overexpression of AgRP stimulates food intake and weight gain [111; 114; 117-119]. Although both MC3Rs and MC4Rs are involved in the effects of α-MSH and AgRP on feeding and energy homeostasis [106; 125-128], the exact role of MC3Rs in these

processes is not well understood. MC3Rs may be an important contributor to energy homeostasis, however, as central administration of AgRP increases food intake in MC4R-/- mice [145], MTII has a partial anorexigenic effect in MC4R-/- mice following a fast [146], and MC3R -/- mice have an altered physiological response to fasting and pregnancy [147-149] and show altered food self-administration [150]. Furthermore, re-expression of MC3Rs only in AgRP [149] or dopamine neurons [150] in a MC3R -/- background altered food intake and food self-administration [149; 150]. Thus, although there is significant evidence for a role of MC3Rs in controlling feeding and energy homeostasis, overall we have a limited understanding of the exact role that MC3Rs play in these behaviors.

The mesolimbic dopamine (DA) system, which consists of VTA DA neurons and their afferent and efferent projections, has been implicated in a wide range of behaviors, including natural and drug rewards, reinforcement, motivation, and aversion [14; 16; 24]. Moreover, the mesolimbic system is also an important component of the neural circuitry controlling feeding and food reward [9; 28-30]. Consumption of food, orosensory stimulation, and presentation of food or food-predictive cues, all increase neuronal activity in the VTA and stimulate DA release in the nucleus accumbens [45-47; 221]. In addition, alterations in DA signaling significantly affect feeding and responding for food reward, independent of effects on activity [54; 57; 167]. Although the importance of DA signaling in regulation of feeding is clear, the mechanism by which the mesolimbic DA system controls feeding is poorly understood. Additionally, little is known about how other circuits involved in feeding regulation interact with the mesolimbic DA system to control feeding.

Although most research considers homoeostatic and reward-related feeding as independent, there is increasing evidence that the melanocortin system can interact with the mesolimbic dopamine system to control feeding and body weight. Both POMC and AgRP neurons project to the VTA [155; 156] and the VTA is a region with some of the highest expression of MC3Rs in the brain [137; 157]. Our laboratory has also previously shown that

intra-VTA injection of melanocortin receptor agonists decreased the intake of both normal chow and palatable sucrose solutions and decreased sucrose self-administration, whereas injection of melanocortin receptor antagonists into the VTA increased chow intake and body weight and increased sucrose self-administration [163-165]. In addition, MC3R -/- mice show altered food self-administration [150] and altered sucrose preference and changes in dopamine turnover that were dependent on sex [157]. These findings demonstrate that melanocortins can act in the VTA to regulate both homeostatic and reward-related aspects of feeding. Because MC3R is the predominant receptor subtype in the VTA, VTA neurons expressing this receptor are a good candidate for the site of interaction of the melanocortin and the mesolimbic systems as well as a site of integration of circuits regulating homeostatic and reward-based feeding. In these studies, we have used transgenic mice expressing Cre recombinase in MC3R neurons [173] combined with DREADD receptor technology to test whether acute or chronic activation or inhibition of MC3R-expressing neurons in the VTA (VTA MC3R neurons) alters feeding and body weight.

3.3 Materials and Methods

3.3.1 Reagents

Sterile bacteriostatic saline, ketamine, xylazine, and meloxicam were from Patterson Veterinary Supply, Inc. (Greeley, CO). Clozapine-N-oxide (CNO) was from Tocris, Inc (Minneapolis, MN). pAAV-hSyn-DIO-hM3Dq-mCherry and pAAV-hSyn-DIO-hM4Di-mCherry plasmids [111] were direct gifts from Dr. Bryan Roth. pAAV-hSyn-DIO-mCherry (Addgene plasmid # 50459; RRID:Addgene_50459) was a gift from Bryan Roth and was obtained from Addgene. The pHelper and pAAV-RC (2/2) plasmids were a generous gift from Ralph DiLeone. All other reagents were from common commercial sources.

3.3.2 Adeno-associated virus (AAV) preparation

AAVs were prepared using a triple transfection, helper-free method and were purified as previously described [172]. Briefly, HEK293 cells were transfected with equal amounts of pAAV

(hM3Dq, hM4Di, or mCherry), pHelper, and pAAV-RC using standard calcium phosphate transfection procedures. Cells were collected ~80 hours post-transfection, resuspended in freezing buffer (150 mM NaCl, 50 mM Tris, pH 8.0), frozen and stored at -80^{o}C until preparation. Cells then underwent 2 freeze-thaw cycles and were incubated with benzonase (50 U/ml final) at 37^{o}C for 30 minutes. The lysate was added to a centrifuge tube containing 15%, 25%, 40%, and 60% iodixanol gradient and was spun at 184,000xg (50,000 rpm in a Beckman Type 70Ti rotor) for 3 hours 20 minutes at 10^{o}C. The 40% fraction was collected and exchanged with sterile 1X PBS using Amicon Ultra-15 Centrifugal Filter Unit Concentrators (100 kDalton; Millipore, Inc.). Viral titers were calculated using the AAV pro Titration Kit (Clontech, Inc.) per the manufacturer's instructions. The final purified viral particles were aliquoted and stored at -80^{o}C, except during use, when they were stored at 4^{o}C.

3.3.3 Animals

Male and female transgenic mice expressing Cre recombinase in MC3R neurons ('MC3R-Cre mice') on a mixed C57/129 background were used in all experiments. MC3R-Cre mice were generously provided by David Olson (University of Michigan, Ann Arbor), and have been previously characterized and validated [162; 173]. Mice were 12-15 weeks old at the onset of the acute experiments. Mice were housed in ventilated polycarbonate Animal Care System cages in a temperature- and humidity-controlled room under a 12:12 light/dark cycle (lights on at 7:00 or 8:00 am) with *ad libitum* food and water throughout the experiment. Mice were group-housed until 2 weeks prior to surgery and were then individually housed until the conclusion of the experiment. Mice weighted between 18 and 30 grams (18-22 grams for females and 25-30 grams for males) at the beginning of the experiment. All protocols and procedures were approved by the Institutional Animal Care and Use Committee at Georgia State University and conformed to the NIH *Guide for the Care and Use of Laboratory Animals*.

3.3.4 Stereotaxic surgery

AAV's were injected into the VTA of MC3R-Cre mice using standard flat-skull stereotaxic techniques. 7-10 week old mice were anesthetized with isoflurane (1–5%) and placed in a stereotaxic apparatus (David Kopf Instruments, Tujunga, CA, USA). The VTA was targeted using the following coordinates (relative to bregma): A/P-3.3, M/L+/-1.32, DV-4.55 and 4.45 from the skull surface, at a 12° angle to the midline. 150 nL of AAV solution was injected bilaterally at each of the two depths (300 nL total/side) at a speed of 50 nl/min using a Nanoliter 2010 microinjector (World Precision Instruments, Sarasota, FL) fitted with glass pipettes with ~30-60 □m diameter tips. The pipettes were left in the brain for 3 minutes following the first injection and 5 minutes following the second injection to allow for AAV diffusion. For pain management, the mice received meloxicam (1 mg/kg) at the onset of the surgery and again 24 hours post-surgery. The mice were given 5 weeks for recovery to allow for full DREADD expression prior to the onset of testing.

3.3.5 Food intake and body weight measurement

Standard laboratory chow (Purina rodent diet #5001, PMI Nutrition International; 3.36 kcal/g) was used in all experiments. Mice were acclimated to eat out of a 10 cm petri dish placed at the bottom of a cage for 1 week prior to the onset of the experiments. For measurement of food intake, mice were given a set amount of food which was then weighed at specific time points to determine the amount of food eaten. The bedding was sifted during each measurement to collect food dust in order to account for spillage, with the exception of the acute feeding experiments, when spillage was not accounted for due to time constraints and to assure minimal interference during the experiment. For measurement of body weight, mice were placed in a small box, weighed, and then were kept in the box for a short duration (<1 min) while the food was weighed before being returned to their cage.

3.3.6 General Experimental Design

All mice were tested in both the acute and chronic phases of the experiment and all remained in good health through the experiment. Mice were separated into body weight-matched groups prior to surgery and were then randomly injected with one of the three AAVs. Following a 5 week recovery period, baseline food intake and body weight were collected for 4 days followed by the first acute CNO experimental day. Two days later, the second acute CNO injection was performed. Following the acute study, the mice were allowed to recover for 1 week prior to onset of the chronic injections. The body composition of relative fat and lean masses was obtained using in vivo time-domain nuclear magnetic resonance with a MiniSpec Body Composition Analyzer (Bruker, Spring, TX) 4 days prior to onset of chronic CNO treatment (baseline) and 1 day after the last CNO treatment day. In the acute phase of the experiment, food intake was measured during the non-test days. After the termination of the study, all mice were euthanized via transcardiac perfusion and brains collected for *post hoc* analysis of DREADD receptor expression. CNO was initially dissolved in DMSO, diluted with sterile saline (to 10% DMSO), aliquoted and stored at -20^{o}C until use. Upon use, the CNO was diluted to 0.1 mg/mL with sterile saline (1% DMSO final) and used for the injections. The same DMSO/saline mixture (1% DMSO) was used as the vehicle control for all injections. IP injections were done in a volume of 10 µL/g body weight and the injection sides were alternated between each injection. The researcher performing all aspects of the study was blind to the animal's treatment group until all of the data had been collected and DREADD/mCherry expression was confirmed. The experiments were repeated in 5 independent cohorts of mice, with the size of the cohorts ranging from 9 to 16 mice per cohort.

3.3.7 The effects of acute CNO treatment

On the day of the acute experiment, baseline body weight and the food intake (24 hr) were measured an hour before dark onset, and all food was removed from the cage. 30 minutes

before dark onset, mice received an intraperitoneal (IP) injection of vehicle or CNO (1mg/kg) and food was re-introduced into the cage 3 minutes before dark onset. Food intake was measured at 1,2,3,4, and 24 hours post-injection and body weight was measured 24 hours post-injection. The animals were allowed 2 days to recover and the experiment was repeated. Injections were performed in a counterbalanced manner to control for injection order with half of the mice receiving CNO injections on the first test day and the other half receiving CNO on the second test day.

3.3.8 Effects of chronic CNO treatment and body composition measurement

Baseline body weight and food intake data were collected for 4 days prior to the onset of chronic treatment. The mice were then injected (IP) twice daily with CNO (1 mg/kg) for 5 days followed by 3 more days of recovery during which no injections were given. The injections were administered at 10am and 6pm (lights off at 7pm) daily. Food intake and body weight data were collected between 5pm and 6pm.

3.3.9 Histological confirmation of DREADD expression

At the end of all experiments, mice were deeply anesthetized with ketamine/xylazine (93/7 mg/kg) and transcardially perfused with ice-cold phosphate-buffered saline (PBS) followed by 4% paraformaldehyde. The brains were dissected, post-fixed with 4% paraformaldehyde at 4°C overnight, washed with 1X PBS, and incubated in 30% sucrose (in 1X PBS) for 2-3 days until the brains sunk. The brains were then flash-frozen in ethanol/dry ice-cooled isopentane and stored at -80°C until sectioning. 40 µm thick coronal sections were collected at 200 µm intervals through the entire VTA on a cryostat, mounted on glass slides, and coverslipped using mounting media containing DABCO. Images were collected at 20x on an Olympus BX41 fluorescent microscope equipped with an Olympus DP73 camera. The images were collected in a grid to visualize the entire VTA and were stitched together post-acquisition using the ImageJ *Stitching*

plugin [178]. The number of mCherry positive neurons in the VTA and outside of the VTA were manually quantified using ImageJ cell count plugin [184].

3.3.10 Excitatory DREADD (hm3Dq) activation of c-fos

A separate cohort of MC3R-Cre mice was injected with AAV-hSyn-DIO-hM3Dq-mCherry or AAV-hSyn-DIO-mCherry into the VTA for analysis of CNO-induced activation of c-fos. Mice received an IP injection of CNO (1mg/kg) 4-5 weeks post-surgery and were transcardially perfused 2 hours later. The brains were dissected, processed, and the sections were collected as described above. Brain sections were blocked for 6 hours at room temperature in blocking buffer (5% normal goat serum, 0.2% Triton X-100, 0.1% bovine serum albumin in 1X PBS), washed in 1X PBS for 5 minutes, and were incubated with rabbit anti-c-fos antibodies (Cat. # ABE457, Millipore) diluted 1:1000 in antibody incubation buffer (0.2% Triton X-100, 1% bovine serum albumin in 1X PBS) overnight at 4°C. Sections were washed with 1X PBS 3 times for 5 minutes each and were incubated with Alexa Fluor 488 conjugated goat anti-rabbit antibodies (Invitrogen) diluted 1:1000 in antibody incubation buffer for 4 hours at room temperature. Sections were then washed with 1X PBS 3 times for 5 minutes each, were mounted on glass slides and coverslipped with mounting media containing DABCO. Images of VTA sections containing mCherry and Alexa Fluor 488 (c-Fos) signals were acquired using a 20x objective with 0.7X zoom on a confocal microscope (LSM 720; Carl Zeiss, Oberkochen, Germany). The numbers of neurons expressing mCherry, c-Fos, and those co-expressing mCherry and c-Fos were manually quantified using the ImageJ cell count plugin.

3.3.11 Data analysis, statistics, and experimental design

All data are presented as means ± SEM. Data were graphed using IgorPro (Wavemetrics, Inc., Lake Oswego, OR, USA), and statistical analyses were performed using IBM SPSS Statistics 25. A general linear model with repeated measures analysis was used with group (hM3Dq, hM4Di, mCherry control), treatment (vehicle *vs* CNO), time, and in some cases,

sex (male *vs* female), as independent variables, followed by LSD *post hoc* tests corrected for multiple comparisons. A significance level was set at $p<0.05$ *a priori* for all analyses. The results of all statistical analyses are shown in Table 0.2 (Appendix B) for reference.

For all experiments, mice were included in the data analyses only if DREADDs were bilaterally expressed in the VTA, the mouse did not have a clearly visible brain lesion at the injection site, and off-target (e.g. outside the VTA) labeling was <15% of the total number of cells labeled. Some individual mice had poor injections with only a few labeled neurons. To ensure that we only included the mice with sufficient labeling to produce a behavioral response, we compared the total number of labeled neurons identified in the VTA in an individual mouse to the mean labeling for the group and excluded mice in which the labeling was 1 standard deviation below the group mean. To calculate the means for DREADD-expressing neurons, Gi and Gq groups were combined to obtain a common mean since these groups showed similar expression levels. The control group mean was standalone because the mCherry expression in this group was much higher than in the other two groups. These selection criteria were set prior to data unblinding and analysis.

The experiments were performed in 5 independent cohorts of mice. Information on all of the cohorts of mice tested in these studies, including those that were excluded, is provided in Table 3.1. This information is included for full transparency and reproducibility.

Table 3.1. Detailed description of experimental animals used in the acute and chronic phases of the experiment.

Cohort #	**# started**	**# excluded and reason**	**# included per sex**	**# included per group**
All animals	59	8-lesions 12-unilateral 6-low labeling 8- >15% off target	12 male 13 female	11 Ctrl 7 Gq 7 Gi
Cohort 1	10	3-lesions 2-unilateral labeling 1-low labeling	1 male 3 female	1 Ctrl 2 Gq 1 Gi
Cohort 2	9	4-lesions 3- >15% off target	1 male 1 female	1 Ctrl 1 Gq
Cohort 3	11	1-lesion 2-unilateral labeling 2- >15% off target	3 male 3 female	3 Ctrl 1 Gq 2 Gi
Cohort 4	13	6- unilateral labeling 1- low labeling 2- >15% off target	3 male 1 female	3 Ctrl 1 Gi
Cohort 5	16	2-unilateral labeling 4- low labeling 1- >15% off target	4 male 5 female	3 Ctrl 3 Gi 3 Gq

3.4 Results

In these studies, we tested whether acute or chronic activation or inhibition of VTA MC3R neurons affected feeding and body weight. AAVs expressing the excitatory DREADD receptor, hM3Dq-mCherry, the inhibitory DREADD receptor, hM4Di-mCherry, or mCherry alone, in a Cre-dependent manner were bilaterally injected into the VTA of MC3R-Cre mice (Figure 3.1A, B) [162; 173]. CNO (1 mg/kg) was then used to activate or inhibit VTA MC3R neurons and changes in feeding and body weight were measured. For all experiments, DREADD-mCherry expression was confirmed to be restricted to the VTA for each mouse at the end of the experiment. Representative images showing VTA expression of mCherry for each group are shown in Figure 3.1 C-E, and the mCherry expression pattern was consistent with that shown previously for MC3R expression in the VTA [157; 162].

Although the ability of DREADD receptors to excite and inhibit VTA neurons has been previously established through electrophysiology and IHC [222-224], we confirmed hM3Dq's ability to excite VTA MC3R neurons by examining changes in c-Fos immunoreactivity following CNO administration. Because of low basal c-Fos expression, we were unable to use this technique to validate hM4Di, but hM4Di has been previously shown to inhibit VTA DA neurons [223; 224]. CNO greatly increased c-Fos immunoreactivity in the VTA neurons expressing hM3Dq-mCherry (Figure 3.1F-I) compared to the VTA neurons from the control mice expressing mCherry (Figure 3.1J-M). Consistent with a previous report [222], we also observed an increase in c-Fos signal in the VTA neurons lacking hM3Dq-mCherry, suggesting excitation through local connectivity or circuit network activity (Figure 3.1I).

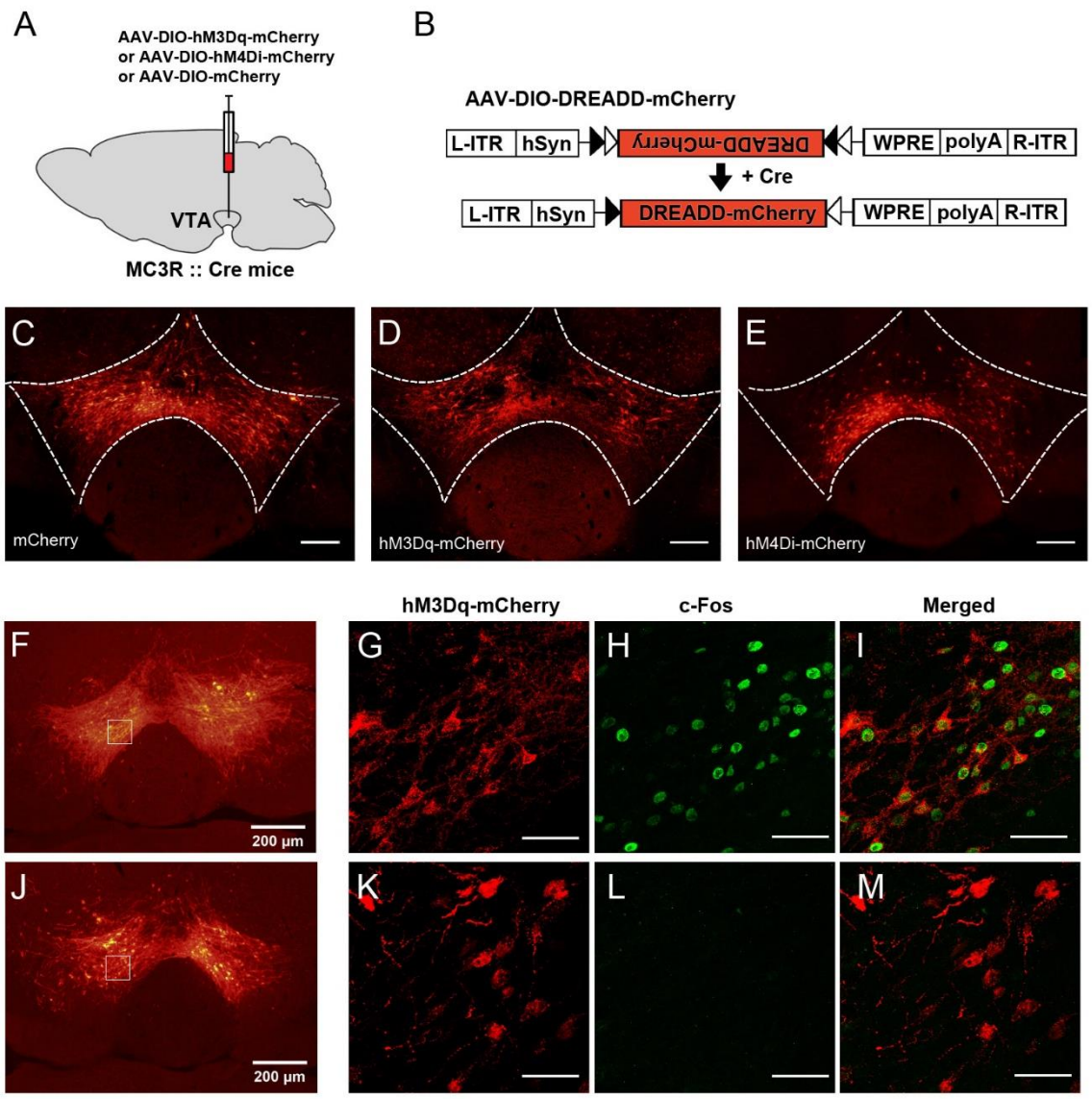

Figure 3.1. Selective expression of the DREADD receptors and DREADD-mediated activation of VTA MC3R neurons in MC3R-cre mice.

Graphical representation of DREADD delivery into the VTA. **B.** General viral vector design for AAV-DIO-hM3Dq-mCherry, AAV-DIO-hM4Di-mCherry, and AAV-DIO-mCherry. **C-E.** Representative VTA sections showing mCherry control (C), hM3Dq-mCherry (D), and hM4Di-mCherry (E) expression in the VTA of MC3R-cre mice. **F-M.** cFos immunoreactivity two hours after CNO injection (1 mg/kg, i.p.) in VTA neurons expressing hM3Dq-mCherry (F-I) or mCherry control (J-M). Rectangles in F and J delineate anatomical location of high magnification images

in G-I and K-M, respectively. Scale bars: 100 μm (C-E), 50 μm (G-M). L-ITR, left-inverted terminal repeat; hSyn, human synapsin promoter; R-ITR, right-inverted terminal repeat; WPRE, woodchuck hepatitis post-transcriptional regulatory element.

We initially tested whether acute activation or inhibition of VTA MC3R neurons affected home cage chow consumption or body weight. When all mice were analyzed together (independent of sex), there was a clear trend for both activation and inhibition of VTA MC3R neurons to decrease food intake for the first 4 hours and for inhibition of VTA MC3R neurons to decrease feeding at 24 hours, but these differences were not statistically significant (Figure 3.2A). Similarly, both activation and inhibition of VTA MC3R neurons resulted in a reduction in the amount of 24-hour weight gain compared to both their vehicle-injected controls and to control mice, but these differences did not reach statistical significance (Figure 3.2B).

We next examined whether there were sex differences in the acute response to activation or inhibition of VTA MC3R neurons. Addition of sex as a variable in the analysis revealed significant drug*group*sex and time*drug*group*sex interactions. As with the analysis independent of sex, there were no effects of CNO in control mice (Figure 3.2C-D). *Post hoc* analyses demonstrated that activation of VTA MC3R neurons significantly inhibited intake in female mice at 2 and 24 hours, with a strong trend toward inhibited intake at 3 and 4 hours (Figure 3.2F), whereas activation of VTA MC3R neurons in males increased 24-hour food intake with no effect at other time points (Figure 3.2E). In contrast to the activation data, inhibition of VTA MC3R neurons significantly inhibited food intake at all of the time points in male mice but had no effect in females (Figure 3.2G-H). Thus, acute activation and inhibition of VTA MC3R neurons alters feeding in a sex-dependent manner.

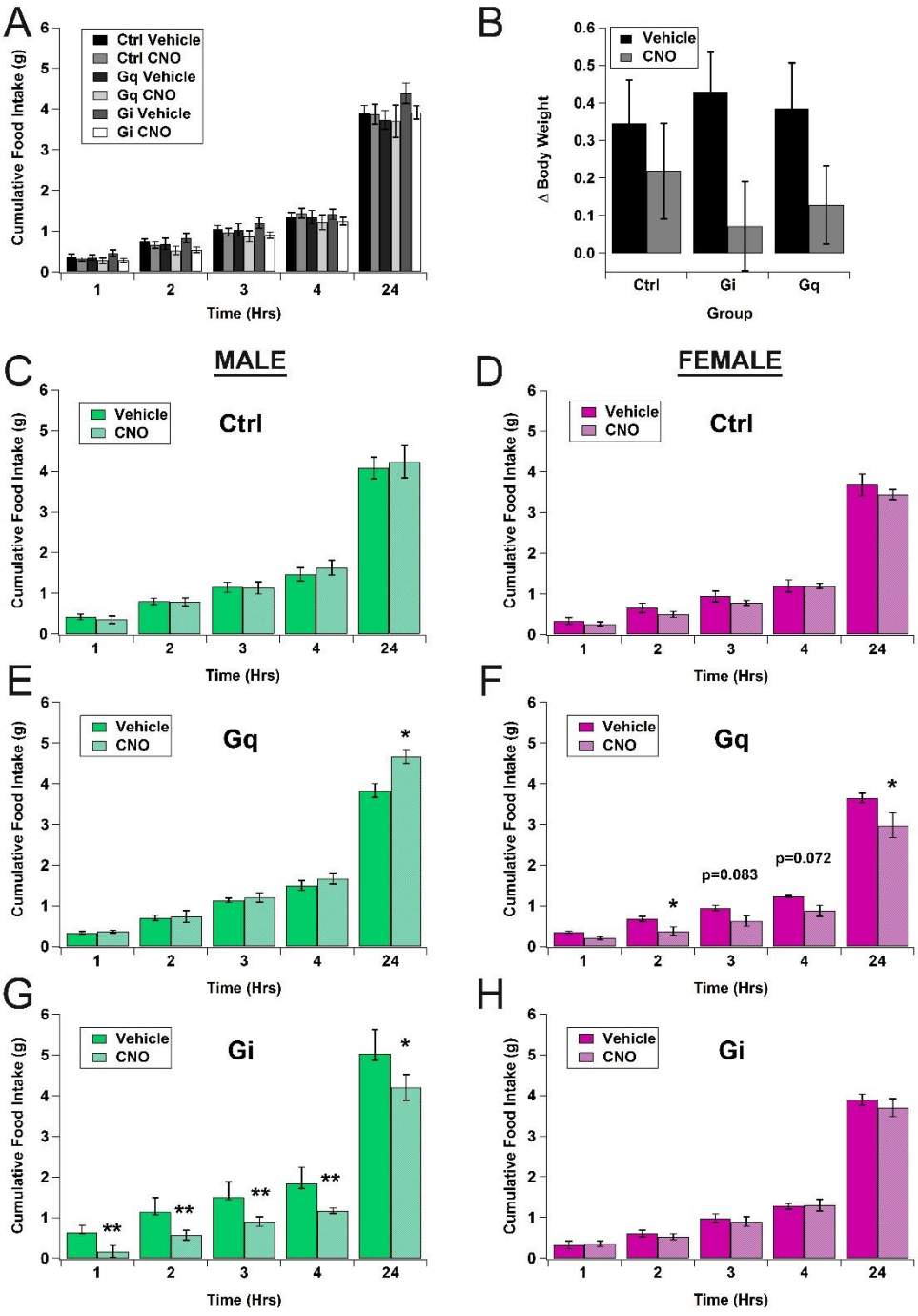

Figure 3.2. Effects of acute activation and inhibition of VTA MC3R neurons on food intake and body weight.

A. Mean cumulative food intake for all mice (independent of sex) injected with vehicle or CNO (1 mg/kg). **B.** Mean 24-hour change in body weight for all mice (independent of sex). **C-H.** Mean

cumulative food intake for male (C, E, G) and female (D, F, H) mice (green = male, magenta = female). **C-D**. Control (mCherry). **E-F**. VTA MC3R neuron activation ('Gq'). **G-H**. VTA MC3R neuron inhibition ('Gi'). All—control: n=11, Gq: n=7, Gi: n=7. Control male n=6; Gq male n=3; Gi male n=3; Control female n=5; Gq female n=4; Gi female n=4. * $p<0.05$ vs. vehicle, ** $p<0.005$ vs. vehicle.

We next tested whether chronic activation or inhibition of VTA MC3R neurons altered food intake or body weight. For chronic treatment, mice were injected with CNO (1 mg/kg) twice a day for 5 days (3 hours into the light phase and 1 hour prior to the onset of the dark phase) and food intake and body weight were measured every 24 hours. Analysis of daily food intake for all mice independent of sex revealed a significant time*group interaction for both absolute intake and when intake was normalized to each mouse's baseline intake to address variability in food intake between mice. *Post hoc* analyses demonstrated that there were no significant group differences in baseline food intake, whereas chronic activation of VTA MC3R neurons significantly inhibited food intake on the first treatment day compared to the chronic inhibition of VTA MC3R neurons (Figure 3A-B). There was also a non-significant trend for decreased intake compared to control mice on day one and to both control and VTA MC3R neuron inhibition on day two (Figure 3.3A-B). Somewhat surprisingly, food intake rapidly returned to baseline, control levels on treatment day 3 for VTA MC3R neuron activation and remained at baseline, control levels throughout the rest of the treatment. There was also a trend for increased food intake with VTA MC3R neuron inhibition, but these differences did not reach statistical significance.

As would be expected based on the feeding data, there were also significant time*group interactions for the changes in body weight following VTA MC3R neuron activation (Figure 3.3C-D). VTA MC3R neuron activation caused significantly more weight loss than both control and VTA MC3R neuron inhibition on treatment days 1 and 2 with a slow recovery to control levels over the rest of the treatment period (Figure 3.3C-D). VTA MC3R neuron inhibition also

appeared to have higher body weights compared to controls across the treatment period, but these differences did not reach statistical significance.

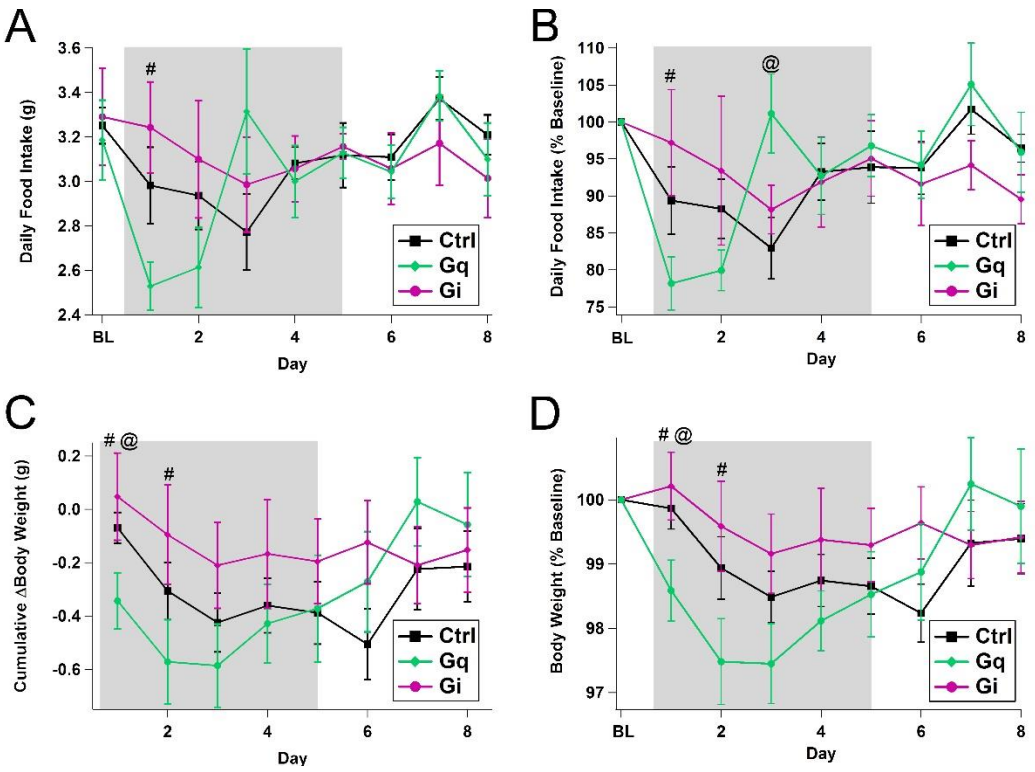

Figure 3.3. Effects of chronic activation and inhibition of VTA MC3R neurons on food intake and body weight.

A-B. Mean daily food intake for all mice (independent of sex) following 2x daily injections of CNO (1 mg/kg) for 5 days. **A.** Absolute daily food intake. **B.** Food intake normalized to baseline. **C-D.** Mean body weight for all mice (independent of sex). **C**. Cumulative change in body weight starting from baseline (day 0). **D**. Mean body weight normalized to baseline ('BL'). Gray box highlights chronic CNO treatment. Control ('Ctrl', black squares) n=11; VTA MC3R neuron activation ('Gq', green circles) n=7; VTA MC3R neuron inhibition ('Gi', magenta circles) n=7. # $p<0.05$ Gq vs. Gi, @ $p<0.05$ Gq vs. ctrl.

Within-group *post hoc* tests also demonstrated the effects of injections for each treatment group. Control mice had a significant reduction in both food intake and body weight over the initial days of CNO treatment (Figure 3.4 A-B), likely due to the stress of the handling and repeated injections. Activation of VTA MC3R neurons had a robust inhibition of both food intake and body weight at early time points, with a rapid return to baseline food intake on day 3 and a slower recovery of body weight (Figure 3.4 C-D). Interestingly, VTA MC3R neuron inhibition overall had no effect on food intake or body weight (Figure 3.4 E-F).

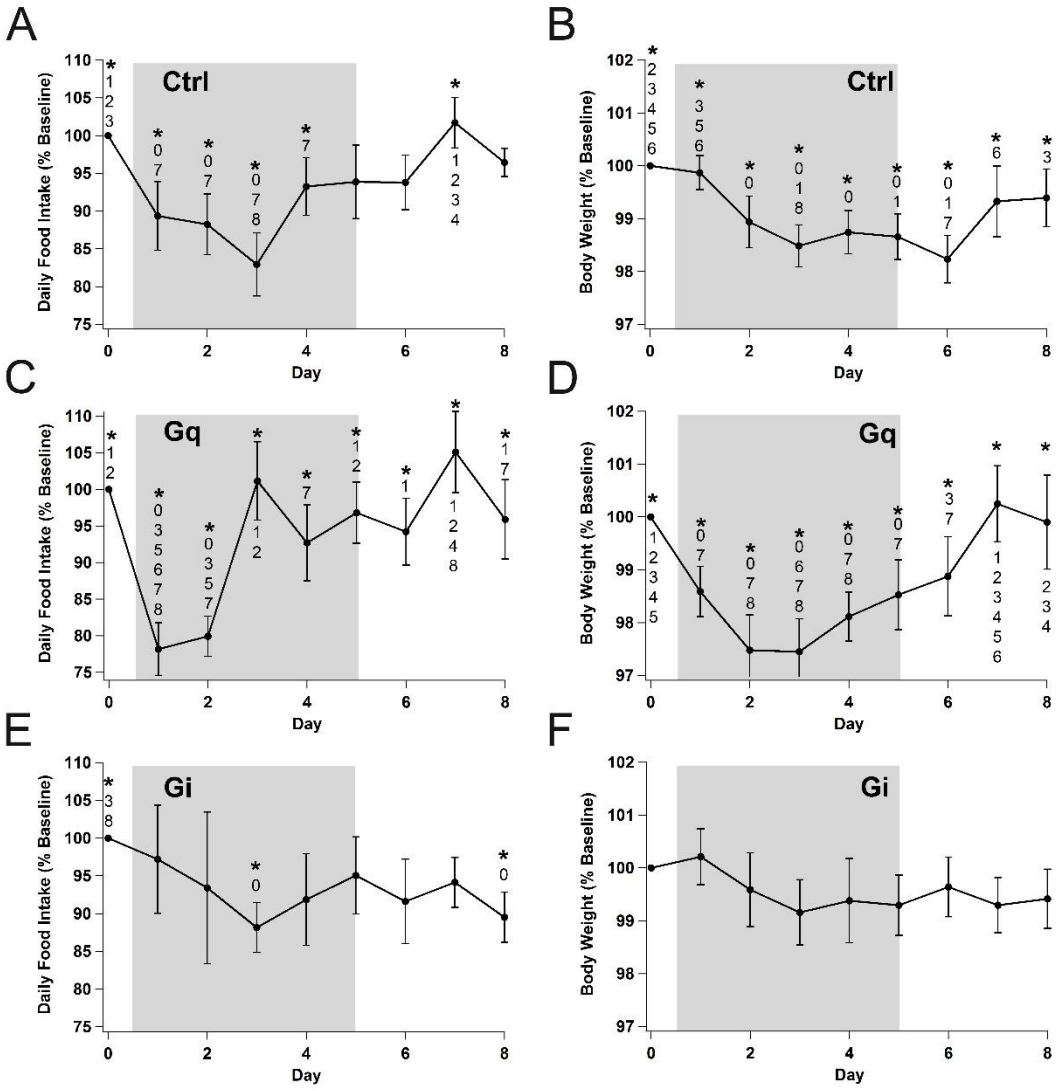

Figure 3.4. Within-group effects of chronic activation and inhibition of VTA MC3R neurons on food intake and body weight.

A-B. Mean food intake (A) and body weight (B) of control ('Ctrl') mice. **C-D.** Mean food intake (C) and body weight (D) following VTA MC3R neuron activation ('Gq'). E-F. Mean food intake (E) and body weight (F) following VTA MC3R neuron inhibition ('Gi'). All data are normalized to baseline. Gray box highlights chronic CNO treatment. Day 0 is baseline. Ctrl n=11, Gq n=7,Gi n=7. Numbers indicate the days significantly different from the marked day (*$p<0.05$).

Because we saw sex differences in the response to acute activation and inhibition of VTA MC3R neurons, we next examined whether there were also sex differences in the responses to chronic activation or inhibition of VTA MC3R neurons. Group comparisons separated by sex are shown in Figure 3.5, and comparisons of male *vs.* female responses for each group are shown in Figure 3.6. Although the addition of sex as a variable in the analyses did not show significant main effects of sex, a closer examination of the data revealed interesting potential sex differences. In males, VTA MC3R neuron activation robustly decreased food intake for the first two days of CNO treatment and resulted in a prolonged decrease in body weight relative to both controls and VTA MC3R neuron inhibition (Figure 3.5 A, C). In addition, VTA MC3R neuron inhibition also appeared to increase both food intake and body weight in males for the first two days of CNO treatment compared to controls (Figure 3.5 A, C). Interestingly, VTA MC3R neuron activation and inhibition had no effect in female mice compared to controls (Figure 3.5 B-D), although there may have been a slight increase in weight loss with VTA MC3R neuron activation. These sex differences were most obvious when examining the effects of VTA MC3R neuron inhibition, where males and females differed greatly in their responses to the first two treatment days (Figure 3.6 E-F). There were no apparent differences between males and females for VTA MC3R neuron activation (Figure 3.6 C-D) or in controls (Figure 3.6 A-B), although control females did eat slightly less and lost slightly more

weight than control males, possibly due to increased sensitivity to the stress of the handling and injections.

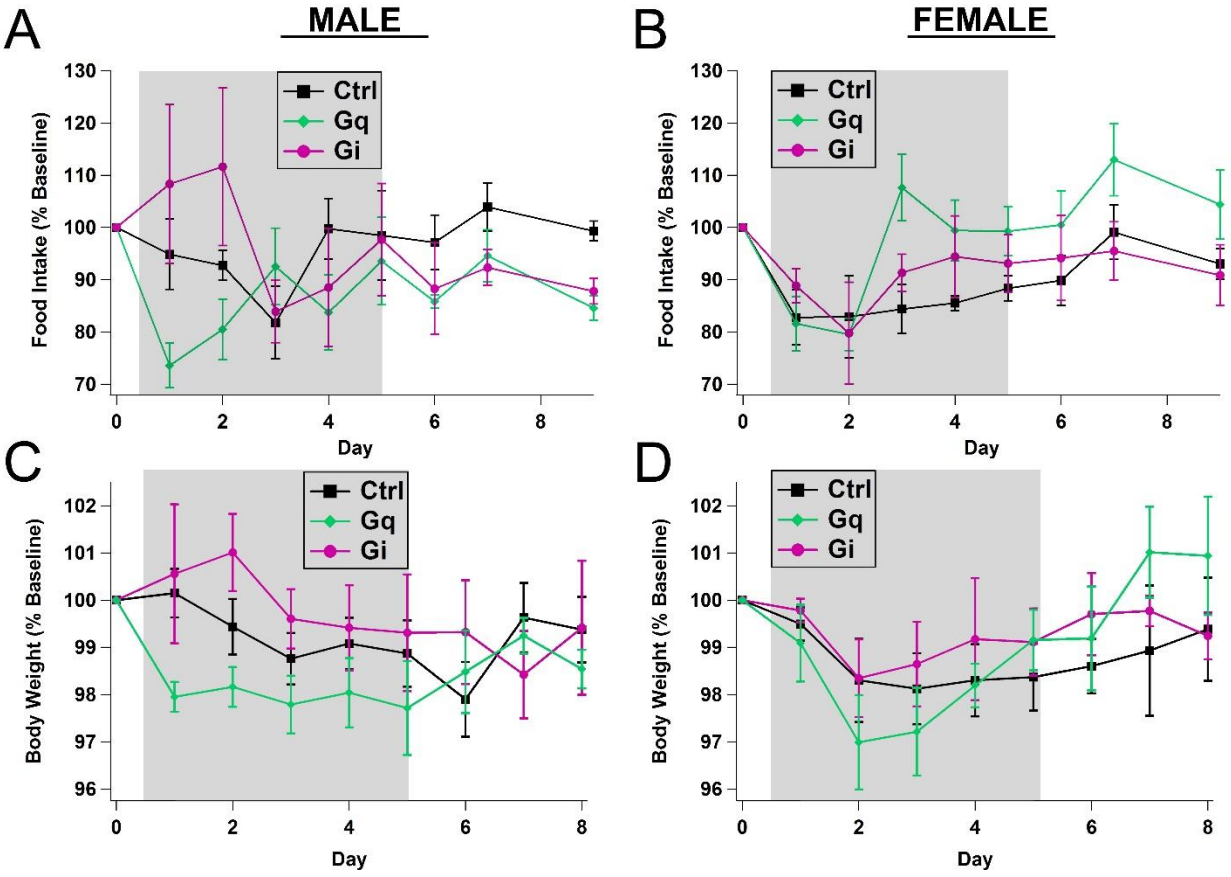

Figure 3.5. Effects of chronic activation and inhibition of VTA MC3R neurons on food intake and body weight by sex.

A-B. Mean daily food intake (normalized to baseline) for males (A) and females (B) with chronic activation or inhibition of VTA MC3R neurons. **C-D**. Mean body weight (% baseline) for males (C) and (D) females with chronic activation or inhibition of VTA MC3R neurons. Gray box highlights chronic CNO treatment. Control ('Ctrl', black squares): male n=6, female n=5; VTA MC3R neuron activation ('Gq', green circles): male n=3, female n=4; VTA MC3R neuron inhibition ('Gi', magenta circles): male n=3; female n=4.

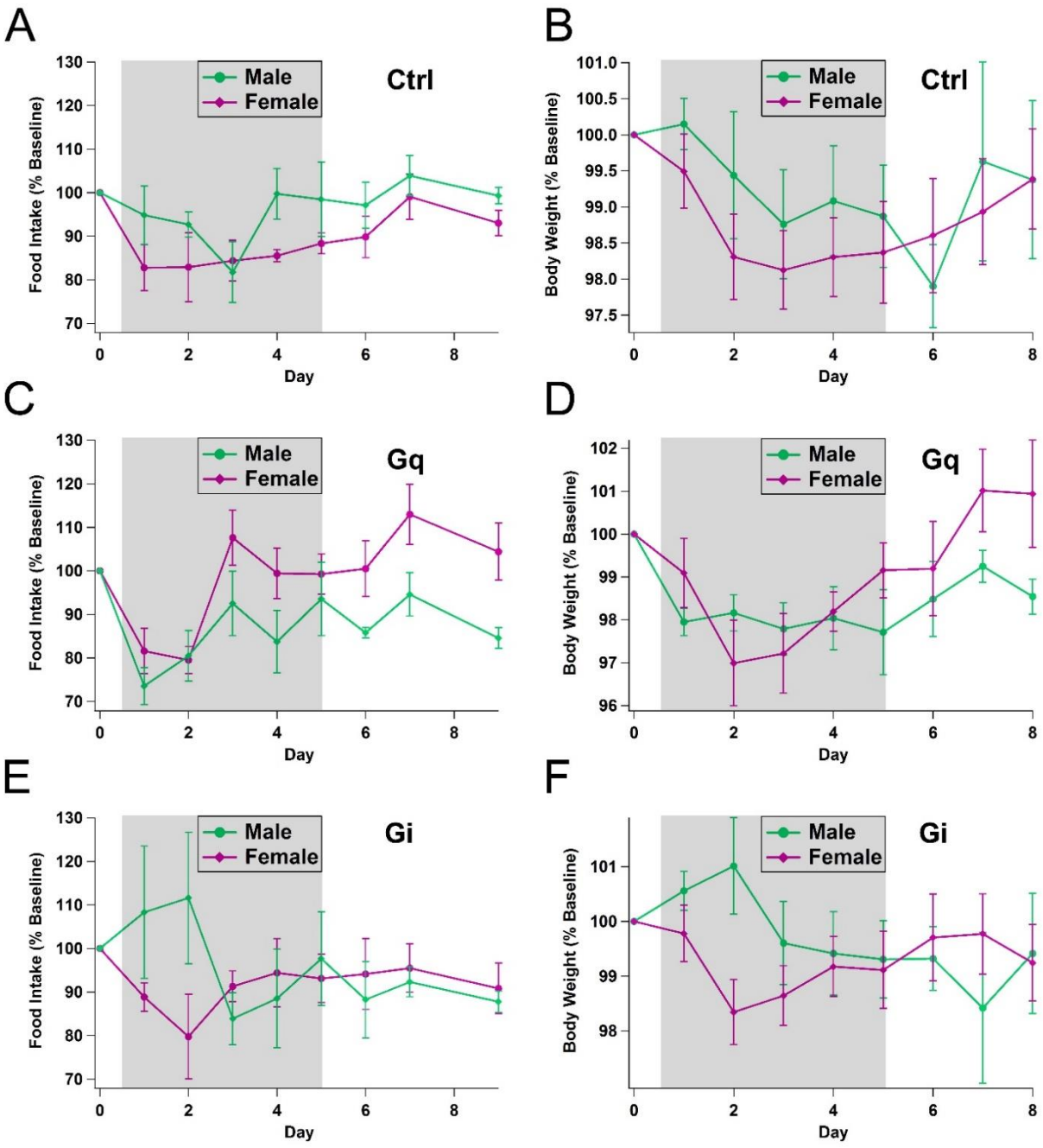

Figure 3.6. Comparison of chronic activation and inhibition of VTA MC3R neurons on food intake and body weight between males and females for each treatment.

A-B. Mean food intake (A) and body weight (B) of control ('Ctrl') mice. **C-D**. Mean food intake (C) and body weight (D) following VTA MC3R neuron activation ('Gq'). **E-F.** Mean food intake

(E) and body weight (F) following VTA MC3R neuron inhibition ('Gi'). Gray box highlights chronic CNO treatment. Males = green, Females = magenta. Control: male n=6, female n=5; VTA MC3R neuron activation ('Gq') male n=3, female n=4; VTA MC3R neuron inhibition ('Gi'): male n=3, female n=4.

MC3Rs have been implicated in altered nutrient partitioning [125; 126; 152]. Thus, to determine if chronic activation or inhibition of VTA MC3R neurons affected the distribution of fat and lean mass, we measured body composition 4 days before the initiation of chronic CNO treatment (baseline) and 24 hours after the last CNO injection (post-chronic treatment). Analysis demonstrated a significant time*group*sex interaction for lean mass with no effect on fat mass (not shown). *Post hoc* analysis demonstrated that chronic VTA MC3R neuron activation in male mice resulted in lower lean mass after the last chronic CNO injection (not shown).

3.5 Discussion

In these studies, we tested the effects of acute and chronic activation and inhibition of VTA MC3R neurons on food intake and body weight and analyzed whether there were sex differences in any of the parameters tested. There was a trend for reduced food intake and body weight with both acute activation and inhibition of VTA MC3R neurons when all mice were analyzed together (Figure 3.2). Further examination of these responses revealed interesting and divergent sex differences, however, with acute activation of VTA MC3R neurons inhibiting feeding only in females, and acute inhibition of VTA MC3R neurons inhibiting feeding only in males (Figure 3.2). Chronic activation of VTA MC3R neurons caused a transient (1-2 days), but significant reduction in feeding and body weight that returned to baseline levels despite the continued activation of VTA MC3R neurons (Figure 3.3), and there was a trend toward increased feeding and body weight following inhibition of VTA MC3R neurons. Although there were no significant main effects of sex following chronic activation or inhibition of VTA MC3R neurons, the changes in food intake and body weight appeared to be driven mainly by males

(Figure 3.5-3.6). Thus, VTA MC3R neurons appear to control feeding and body weight in an activity- and sex-dependent manner.

One of the most interesting results of these studies was the robust sex differences in the response to acute activation and inhibition of the VTA MC3R neurons (Figure 3.2) and the potential sex differences in the responses to chronic CNO treatment (Figure 3.5-3.6). The presence of sexually dimorphic feeding responses produced by the activation and inhibition of VTA MC3R neurons is not surprising given the existence of clear sex differences in the regulation of feeding and energy homeostasis [225; 226] and the presence of sexual dimorphisms and estrous cycle variations in the melanocortin [227; 228] and the mesolimbic systems [229-231]. For example, daily caloric intake of males is greater, even when normalized for body weight and metabolic differences [232], and males gain more weight when fed a high-fat diet [233; 234]. Consistent with their lower food intake, the female arcuate nucleus also has a stronger expression of POMC mRNA, denser POMC neuron processes [235], and female POMC neurons fire at a higher frequency [236]. There are also well-known dimorphisms in the responses to drugs of abuse, with females being affected more than males. For example, females have higher drug intake, escalation of drug use, and motivation for drugs, with more unpleasant withdrawal symptoms and greater reinstatement [230]. Furthermore, sex differences were previously noted in the regulation of reward-related feeding by the melanocortin system, as global MC3R knockout decreased sucrose preference and increased DA turnover in female, but not male mice [157]. Despite these reported sex differences, it was still surprising that the sex differences observed here also depended on VTA MC3R neuron activity, as acute activation only affected feeding in females and acute inhibition only affected feeding in males. Thus, altering VTA MC3R neuron activity interacts with sex via an undefined mechanism to regulate feeding and body weight. It should be noted that due to the exclusion of a large number of mice in these studies as a result of technical issues and our strict inclusion criteria (see Methods section 2.11 and Table 1), these experiments had a limited number of animals of each sex.

Thus, it is possible that sex-dependent effects would become more apparent in the chronic paradigm with the inclusion of higher numbers of mice in each group. Further studies will be required to dissect these sex- and activity-dependent changes in feeding, however.

The ability of acute and chronic activation of VTA MC3R neurons to reduce feeding and body weight is in agreement with a model where α-MSH binds MC3Rs in the VTA to increase the activity of VTA MC3R neurons, resulting in increasing dopamine release and a subsequent decrease in feeding and body weight. In the VTA, MC3R is the likely target for α-MSH and AgRP because it is the predominant receptor subtype in the VTA and there is little expression of MC4Rs in the VTA [136; 137; 157; 237]. MC3Rs functionally couple to G_s, and activation of the MC3Rs by α-MSH stimulates the cAMP/PKA pathway [137; 238; 239]. Therefore, α-MSH signaling should result in activation of VTA MC3R neurons, whereas antagonism of MC3Rs by AgRP should reduce the activity of these neurons. In support of this, our laboratory recently showed that α-MSH increases the firing rate of VTA MC3R neurons in acute brain slices [162] and previous reports have shown that injection of α-MSH into the VTA increases DA release [158; 159; 161]. In addition, intra-VTA administration of MC3R/MC4R agonists decreased both homeostatic and reward-based feeding [163; 165] as well as food reinforcement [164] while administration of MC3R/MC4R antagonists increased food intake and body weight [163]. Thus, the reduction in feeding and body weight following both acute and chronic activation of VTA MC3R neurons (Figure 3.2-3.3) observed here combined with these prior studies supports a model where α-MSH decreases feeding and body weight by activating VTA MC3R neurons and increasing dopamine release.

The reduction in food intake following acute inhibition of VTA MC3R neurons appears to contradict this model for VTA MC3R neuron regulated feeding. These results do agree with a general model for the role of dopamine in the control of feeding, however, whereby both increases and decreases in dopamine levels result in a reduction in feeding (*i.e.* an inverted U response). Dopamine appears to be necessary for feeding and food reward as shown by the

fact that dopamine deficient mice that do not eat and die of starvation unless treated with L-DOPA [28], which is separate from DA's regulation of activity [54], and pharmacological antagonism of dopamine receptors was previously shown to devaluate sucrose reward [240] and to decrease the frequency and duration of feeding [241]. Furthermore, both anorexigenic (feeding inhibiting) and orexigenic (feeding stimulating) peptides have been shown to increase dopamine neuron activity while food intake [242] and different anorexigenic peptides decrease food intake or food reward-associated behaviors by either increasing or decreasing dopamine neuron activity and dopamine release [242]. For example, leptin decreases VTA DA neuron firing rate and decreases food intake [172], whereas neuropeptide Y inhibits VTA DA neurons [243; 244] while increasing operant responding for food [245], and corticotropin-releasing factor increases VTA DA neuron firing [246] while reducing the motivation for food reward [247]. Thus, DA has a complex role in the regulation of feeding, which may explain the seemingly contradictory effects of acute activation and inhibition of VTA MC3R neurons.

Another important factor that could help explain the diversity in these results is the heterogeneity in the neurotransmitters released from VTA MC3R neurons. Approximately 40-60% of VTA MC3R neurons express tyrosine hydroxylase, suggesting that they are dopamine neurons [157], with the remaining 40% of MC3Rs expressed in undefined non-DA neurons. The VTA has classically been considered to consist of ~55-65% dopamine neurons, ~30% GABA neurons, and ~5% glutamate neurons [66; 68; 70; 206; 248], but recent research has indicated that the neurotransmitter phenotype of VTA neurons is more complex [249]. For example, VTA neurons co-releasing DA and glutamate [75; 100], DA and GABA [67; 82; 250], or glutamate and GABA [79; 249; 251] have been identified. Thus, VTA MC3R neurons may release a diverse set of neurotransmitters that could be distinctly regulated by different stimuli. Much like VTA dopamine neurons, VTA GABA and glutamate neurons have been shown to participate in the regulation of both reward- and aversion-associated behaviors [67; 71; 72]. For example, activation of different types of VTA neurons, activation of the same neural type projecting to

different targets, or activation using different stimulating parameters have all been shown to produce opposite effects. For example, VTA glutamate neuron activation is rewarding [103], yet activation of VTA glutamate neuron terminals in the lateral habenula [71] or nucleus accumbens [252] induces aversion in real-time place conditioning protocols. In addition, brief optogenetic stimulation of VTA glutamate neurons or their terminals was shown to be reinforcing, whereas sustained stimulation-induced behavioral avoidance [251]. Similarly, VTA GABA neuron activation is sufficient to disrupt reward consumption or to induce avoidance [72; 253], yet activation of VTA GABAergic projections to the lateral habenula is rewarding [67]. Thus, VTA GABA and glutamate neurons have complex roles in the regulation of reward-related behavior. In general, the exact role for each of these different neurotransmitters released from the VTA in the control of feeding and body weight has not been examined, however. Thus, because VTA MC3Rs are expressed in DA and non-DA neurons, a complex interplay between dopamine, glutamate, and GABA release may be responsible for some of the effects and discrepancies observed in these experiments, and further experiments will be required to identify which neurotransmitters are released by VTA MC3R neurons and how the release of each of these neurotransmitters contributes to VTA MC3R neurons' effects on feeding and body weight.

The robust increase in feeding on the third day of chronic CNO treatment and its subsequent return to baseline on the following days despite continued CNO treatment was surprising. Although the exact cause of these effects is unknown, there are several potential explanations. Because feeding is an essential behavior, there is a lot of redundancy in the circuitry controlling feeding. Therefore, it is possible that the increase in feeding following the initial suppression was caused by a compensatory mechanism driven by other feeding circuits. Alternatively, as discussed above, VTA MC3R neurons are likely to co-release multiple neurotransmitters [67; 75; 79; 82; 100; 249-251]. Thus, a shift in balance of the neurotransmitters released from VTA MC3R neurons might have resulted in a switch from suppression of feeding to its promotion in response to the same stimulus (activation of VTA

MC3R neurons). It appears unlikely, however, that the observed changes in feeding were caused by the loss of the effect of CNO, as CNO has been widely used in chronic paradigms in other systems (*i.e.* [111]). Further study will be required to identify the mechanisms behind the drastic reversal of these effects, however.

Despite the interesting results of these studies, some factors limit the interpretation of the results. First, we did not measure locomotor activity during these studies. Both mesolimbic and melanocortin systems are involved in the regulation of locomotion and activity. For example, DA deficient mice are hypoactive, a condition that can be reversed by L-DOPA administration [28; 254; 255], and chemogenetic activation of VTA DA neurons was shown to produce hyperactivity [222]. Mice with MC3R deficiency also show decreased spontaneous physical activity [126] as well as decreased dark phase wheel running [125]. Therefore, it is possible that alterations in activity could have influenced some of the results of our studies. For example, we cannot exclude the possibility that the decreases in food intake observed in response to acute VTA MC3R neuron silencing (Figure 3.2A) were due to a decrease in locomotion. This possibility appears unlikely, however, because the chronic 5-day inhibition of this neuronal population in the same animals did not produce a decrease and instead caused a slight increase in food intake and body weight (Figure 3.3). Another limitation of these studies is that we did not measure any metabolic parameters. MC3R deficient mice have defects in nutrient partitioning and have been reported to have metabolic imbalances. For example, deletion of MC3R produces a loss of lean mass and an increase in fat mass [125; 126]. Also, MC3R null mice have an increase in respiratory quotient when eating a high fat diet, suggesting a reduction in fat to carbohydrate oxidation [106], and these mice have blunted fasting-induced mobilization of fatty acids from adipose tissue [147]. Because metabolic parameters were not measured, we cannot discount metabolic effects of chronic activation or silencing of VTA MC3R-expressing neurons on body weight. Finally, we did not monitor the estrous cycle during these experiments, which could have influenced the differential responses in males *vs*. females.

Mice have a 4-5 day estrous cycle [225] and eat the least during the preovulatory phase and the most during the diestrus phase of the cycle [256]. In the acute phase of our experiment, mice received injections of CNO or vehicle on Monday and Thursday, so it is possible that mice were injected with CNO and saline during different cycle phases. Our use of counterbalanced injections during the acute experiments should have mitigated any potential effects of differences in estrus cycle, however.

In summary, we have demonstrated that acute activation and inhibition of the VTA MC3R neurons decreased feeding in a sex-dependent manner. Furthermore, chronic activation of VTA MC3R neurons transiently (2 days) decreased feeding and body weight, with potential sex differences in the effects of chronic activation and inhibition as well. Overall, these studies have made a significant contribution to our understanding of the central mechanisms controlling feeding and body weight and have provided new insight into how the melanocortin and the mesolimbic systems may interact to regulate energy homeostasis.

4 DISCUSSION

Anatomical, electrophysiological, and behavioral evidence suggest that the melanocortin and the mesocorticolimbic systems can interact to regulate feeding and body weight, but the underlying mechanisms including the main site of their interaction are not understood. MC3Rs are highly expressed in the VTA and thus VTA MC3R neurons may be a key site for this interaction. Therefore, the focus of this dissertation was to establish circuit connectivity of VTA MC3R neurons and to determine the effects of changes in their activity on feeding and body weight. In these studies, I identified the efferent targets of VTA MC3R neurons as well as the brain regions providing afferent input to this neuronal population and demonstrated that despite the presence of Arc POMC and AgRP neuron projections to the VTA, Arc neurons form few direct synapses with any of the major neuron subtypes in the VTA, including VTA MC3R neurons. I also demonstrated that VTA MC3R neurons acutely control feeding in a sex- and activity-dependent manner. α-MSH increases VTA MC3R neuron activity and decreases feeding, body weight, and food self-administration when injected into the VTA [162-165]. The decrease in feeding produced by DREADD-mediated chronic activation and acute activation in females is consistent with the previously shown effects of nonselective melanocortin receptor agonists suggesting that the VTA MC3R neurons may be the key point of interaction between the melanocortin and the mesocorticolimbic systems. The mechanism by which α-MSH acts in the VTA to decrease feeding appears paradoxical at first glance, as α-MSH increases VTA MC3R neuron activity [162], increases DA release in VTA targets [158; 159], yet decreases feeding, body weight, and food self-administration [163-165]. Interestingly, psychostimulants such as cocaine and amphetamine also increase DA transmission while decreasing feeding, and both α-MSH and psychostimulants increase other DA-dependent behaviors such as locomotion. Thus, the reduction in feeding produced by α-MSH and these drugs of abuse may occur by similar mechanisms and involve the same circuitry. In the following sections, I propose that the underlying circuitry of VTA MC3R neurons, as well as the target-specific differences in

neurotransmitter released by VTA MC3R neurons, may be responsible for the ability of these neurons to control feeding, and I discuss potential roles that some of the components of the VTA MC3R neuron circuitry may play in feeding regulation. Furthermore, the potential sources of sex differences in feeding response to acute changes in activity of VTA MC3R neurons as well as the consequences of volume rather than synaptic transmission of Arc peptides in the VTA are discussed below.

4.1 Potential circuits underlying VTA MC3R neuron control of feeding

Although much of the input-output circuit connectivity of the VTA and the behaviors regulated by these circuits are still unknown, several distinct neural loops have been classified. For example, Beier *et al.* identified two populations of VTA dopamine neurons with distinct connectivity, including dopamine neurons involved in reinforcement and reciprocally connected with lateral NAcc shell and dorsal striatum, and another population of dopamine neurons receiving input from DR and medial NAcc shell and projecting back to the medial NAcc shell as well as the VP, septum, amygdala, and PFC, although the role of this circuit has not been identified [93]. VTA MC3R neurons appear to be a part of the latter circuit as they receive extensive input from DR and send dense projections to the medial NAcc shell, LSI, VP, BST, and BLP, and their connectivity with lateral NAcc or the dorsal striatum was weak. In addition, based on the visual comparison of the location of VTA MC3R neuron soma in my experiments to the results of tracing performed by Lammel et al., the topographical organization of VTA MC3R neurons appears to overlap with VTA dopamine neuron populations projecting to PFC, amygdala, medial shell and core of NAcc but not with those projecting to the dorsal striatum and lateral NAcc shell [65]. However, VTA MC3R neurons appear to mostly belong to the mesolimbic and not mesocortical pathway as they send very sparse projections to the prefrontal cortex. The ability of α-MSH to increase activity of VTA MC3R neurons [162] coupled with decreases in feeding following activation of this neuronal population observed in my

experiments puts forth an idea that the increase in activity of VTA MC3R neurons decreases feeding either by inhibiting food intake-promoting circuits, activating circuits that suppress feeding, or activating those that promote aversion. I have identified VTA MC3R neuron axons in multiple brain areas previously shown to be involved in feeding and reward, and the potential interactions of VTA MC3R neurons with these circuits in regulation of feeding and aversion are discussed below.

VTA MC3R neurons sent moderate to strong projections to brain regions previously known to be involved in feeding regulation including the LH, LS, and BST. The LH contains both glutamate and GABA neurons as well as multiple peptidergic systems [257] which have been shown to have opposing effects on feeding, such that activation of LH GABA neurons promotes feeding whereas activation of LH glutamate neurons suppresses feeding [257]. BST GABA neurons promote feeding through inhibition of LH glutamate neurons [258], and recently, both BST and LH GABA neurons have been shown to promote feeding by inhibiting the ventrolateral periaqueductal gray (vlPAG) [259] (Figure 4.1A). Both BST and LH receive input from VTA GABA neurons, but little to no input from VTA glutamate neurons [98; 206], raising the possibility that GABAergic VTA MC3R neurons could decrease feeding via disinhibition of LH glutamate neurons through inactivation of BST GABA neurons or disinhibition of vlPAG through inhibition of GABA release from BST or LH as shown in Figure 4.1A. Furthermore, activation of LS GABA neurons targeting LH GABA neurons has been shown to inhibit feeding [200] (Figure 4.1B). Therefore, another possibility is that feeding is decreased by glutamatergic transmission from VTA MC3R neurons in the LS which activates LS GABA neurons producing subsequent inhibition of LH GABA neurons. The mechanism of interaction of VTA MC3R neurons with these circuits, specifically, the neurotransmitter phenotype released by the VTA MC3R terminals and the behavioral implications of this release will need to be tested in future experiments.

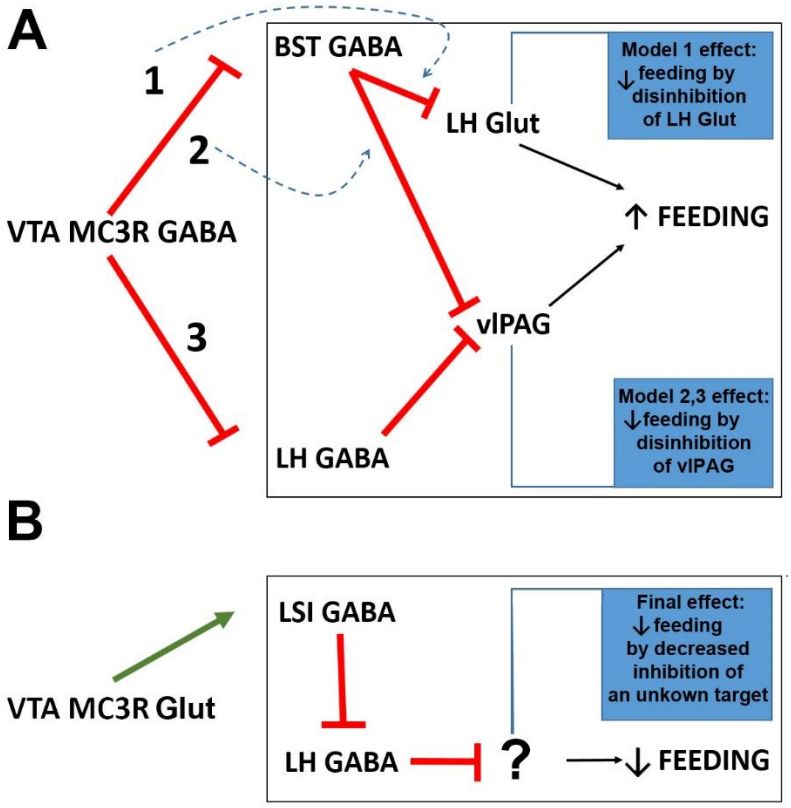

5

Figure 4.1. Models for VTA MC3R neuron-dependent decrease in feeding via excitatory and inhibitory effects on the previously characterized feeding circuits.

Depicted are previously characterized circuits (outlined in black) and the potential downstream effects of VTA MC3R GABA or glutamate neuron activity (blue captions). **A.** Models of VTA MC3R GABA neuron-dependent decrease in feeding via inhibitory effects on the circuits previously shown to increase feeding. VTA MC3R GABA neurons may decrease feeding through indirect disinhibition of LH glutamate neurons via inactivation of BST GABA neurons (1) or indirect disinhibition of vlPAG via inactivation of either BST GABA neurons (2) or LH GABA neurons (3). B. Model of VTA MC3R glutamate neuron-dependent decrease in feeding via activation of a previously characterized inhibitory LS to LH GABA circuit that suppresses feeding.

The DR is one of the most prominent input regions of the VTA [84] and, from my afferent tracing study, is one of the regions providing the most input to VTA MC3R neurons. Like the VTA, the DR is also heterogeneous in anatomy and function and is composed of serotonin (5-HT), dopamine, glutamate, and GABA neurons as well as neurons co-expressing multiple markers (reviewed in [260]). DR glutamate, GABA, and 5-HT neurons are all involved in feeding regulation. For example, fasting activates DR GABA neurons whereas re-feeding after a fast activates DR glutamate neurons, and optogenetic activation of DR GABA neurons increases whereas optogenetic activation of DR glutamate neurons suppresses feeding [261]. Therefore, glutamate released by DR neurons and α-MSH released by Arc POMC neurons may work in tandem on VTA MC3R neurons to increase their activity and decrease feeding. DR 5-HT neurons are also important regulators of feeding as whole-brain enhancement of 5-HT signaling reduces feeding [262] and operant responding for food [263], at least partially through its action in the VTA. For example, $5HT_{2C}$ receptor agonist increases *c-fos* expression in the VTA neurons, and pharmacological and chemogenetic activation of $5HT_{2C}$-expressing VTA neurons decreases food intake and food self-administration [264; 265]. However, Browne *et al.* showed that optogenetic activation of DR 5-HT terminals in the VTA had no effect on sucrose self-administration unless the animals were also treated with citalopram, a selective serotonin reuptake inhibitor [266]. This suggests that 5-HT action in the VTA may be coupled with another neuromodulatory system to exert its effects on feeding and food reward. Therefore, another potential mechanism of feeding suppression could involve a synergistic effect of α-MSH and 5-HT, in which α-MSH acts through the MC3R to enhance the effects of 5-HT. Future studies will be required to determine the subtypes of DR neurons providing input to the VTA MC3R neurons and the behavioral correlates of DR neuron interaction with the VTA MC3R neurons, however.

VTA MC3R neurons were also strongly connected with areas previously shown to be involved in aversion encoding which provides anatomical support for the idea that feeding may be reduced by VTA MC3R neurons through aversive mechanisms, although this hypothesis was

not tested in my experiments. VTA MC3R neurons projected to the aversion center of the brain, the LHb, and activation of glutamatergic VTA terminals in LHb has been shown to generate real-time and conditioned place aversion [71]. Aversion has also been shown to be promoted by photoactivation of VTA glutamatergic fibers in the NAcc suggesting that glutamate released by VTA neurons provides a significant contribution to aversion encoding through its action on multiple brain regions, including regions receiving input from VTA MC3R neurons. Because VTA MC3Rs are expressed in dopamine and non-dopamine neurons [157] and markers of glutamate neurons are co-expressed with TH [74], MC3Rs may be expressed in VTA glutamate neurons and may facilitate α-MSH-mediated activation of these neurons, including those projecting to LHb and NAcc, which would result in a reduction in feeding through aversion. The anatomical location of VTA MC3R neuron soma supports this hypothesis, as many of the MC3R-expressing neurons are located in the medial vGlut2-enriched VTA subnuclei [63], and preliminary studies conducted in our laboratory showed that optogenetic stimulation of VTA MC3R terminals resulted in predominately glutamatergic transmission in the NAcc and LHb. VTA MC3R neurons also received a large amount of input from LHb and activation of LHb terminals in VTA produces conditioned place aversion (CPA) [267] through an increase in activity of VTA DA neurons projecting to PFC, an important mediator of aversion [267; 268]. Although VTA MC3R neurons received extensive input from LHb, they sent very few projections to PFC and therefore are unlikely to mediate aversive behavior directly through this circuit. Future experiments will be required to determine whether VTA MC3R neurons encode aversion and if aversion contributes to the VTA MC3R neuron activation-mediated decrease in feeding. Furthermore, the projection-specific neurotransmitter phenotype of VTA MC3R neurons, the behaviors produced by target-specific activation of these neurons, and the role of the extensive afferent input from LHb will need to be determined in the future. Taken together, the circuitry of VTA MC3R neurons is well-positioned to regulate feeding through multiple mechanisms and the anatomy described in this dissertation puts forth several models to be examined in future experiments.

4.2. Potential sources of sex differences in the response to the chemogenetic activation and inhibition of VTA MC3R neurons

The mesocorticolimbic system is highly sexually dimorphic with clear sex differences in the activity of DA neurons, DA dynamics, and resulting behavior. Many underlying causes have been identified for these differences including differences in gonadal steroid environment and the response to gonadal steroids, differences in circuit connectivity, structure of VTA perikarya, gonadal steroid-independent perinatal imprinting, and sex chromosome-dependent genetic effects. Additionally, sex differences were previously noted in the regulation of reward-related feeding and mesocorticolimbic system physiology by the melanocortin system, as global MC3R knockout decreased sucrose preference and increased DA turnover in female, but not male mice [157]. In these mice, DA levels were normalized by ovariectomy but altered DA content was also observed in prepubescent mice suggesting that, in addition to the role of the interaction of MC3Rs and ovarian gonadal steroids in dopamine function, MC3Rs may also play a role in the development of the mesocorticolimbic system. Similarly, behavioral experiments described here revealed robust sex differences in the feeding in response to acute activation and inhibition of VTA MC3R neurons. The potential causes of these sex differences are discussed below.

Compared to males, dopamine release and uptake are faster in females [269] and higher dopamine levels are found in females treated with drugs that target DAT such as cocaine and amphetamine [269; 270]. The mesocorticolimbic activity is also higher in females as shown by two-fold enhancement of electrically stimulated dopamine efflux by haloperidol, a presynaptic auto-inhibitory D2R blocker [269]. These differences are reflected in sexually dimorphic behavioral responses to drugs of abuse, with females being affected more than males. For example, females have higher drug intake, drug intake-associated side effects, escalation of drug use, and motivation for drugs, with greater withdrawal symptoms upon abstinence and greater reinstatement [230; 271]. The most obvious difference between the sexes is the post-

pubertal gonadal steroid environment in which circulating testosterone is continuously elevated in males whereas females undergo cyclic changes in estradiol and progesterone. Rodent experiments empirically established that gonadal steroids can affect the mesocorticolimbic system and behavior. For example, baseline activity of dopamine neurons is enhanced in estrus rats [231] and basal amphetamine-stimulated striatal dopamine concentration and dopamine-dependent behaviors fluctuate across the estrous cycle [272; 273], in an effect attenuated by ovariectomy which can be reversed by estradiol treatment [272; 274; 275]. Furthermore, dopamine synthesis and turnover are increased and striatal DAT density is decreased by estradiol [276; 277]. This raises the possibility that estradiol may affect the responses of VTA MC3R neurons to activation or inhibition, including the physiological effects facilitated by melanocortins, resulting in cycle stage-dependent and sexually differential behavioral responses.

The typical rodent ovarian cycle lasts 4-5 days. At the beginning stages of the cycle, in metestrus and diestrus, estradiol is low and begins to slowly rise until it peaks in the late afternoon of proestrus and stimulates a GnRH and subsequent LH surge responsible for ovulation which happens during the estrus phase, 12-24 hours after the LH surge [225]. In the experiments testing the effects of acute DREADD-mediated activation and inhibition of VTA MC3R neurons, CNO and saline injections were performed in a counterbalanced manner such that half of the animals were injected with CNO on the first day of testing, and the same animals were injected with saline on the second day of testing, 72 hours later (or vice versa). With this experimental design, even if the cycle stage was consistent between the animals, as cycle synchronization is known to occur in colony-housed animals, some females receiving CNO (and saline) injections should have been in different phases of their ovarian cycle and therefore would have been experiencing different estradiol environment. If estradiol was facilitating the response of VTA MC3R neurons to chemogenetic activation or inhibition, the low estradiol level in females in metestrus and diestrus would be expected to produce a behavioral response

similar to that seen in males (for example, an increase in feeding following activation) whereas the elevated estradiol in females in proestrus and estrus would produce an opposite effect. Averaging the data acquired from mice in different stages of the ovarian cycle would be expected to produce no net effect which is not what was observed in my experiments. Additionally, no differences were seen in the control animals. Together, these observations suggest that post-pubertal ovarian hormones (1) do not contribute to responses following acute activation and inhibition of VTA MC3R neurons in females, (2) are not responsible for sex differences in feeding produced by acute activation and inhibition of VTA MC3R neurons, and (3) do not appear to facilitate cycle-dependent changes in chow feeding.

Fundamental differences in the anatomy of the mesocorticolimbic system could potentially be the source of the sex differences observed in my experiments. For example, large sex differences in the proportions of dopamine neurons projecting to the prelimbic, primary motor, and premotor cortices had been previously reported [278]. However, my anatomical experiments did not reveal any significant sex differences in the projections of VTA MC3R neurons or in the afferent inputs to this neuronal population, although subtle differences in circuit connectivity, especially efferent connectivity, could have been missed by the gross approach used in my studies and will need to be examined further in the future. VTA perikarya also appears to be sexually dimorphic as a preferential shift in the caudal direction has been previously shown for both VTA volume and distribution of TH+ neurons in females compared to males [279]. These sex differences in rostrocaudal distribution of VTA neurons are of particular interest as fewer MC3Rs are present in the rostral VTA compared to the middle and caudal VTA (my unpublished observation and [157]). Therefore, it is possible that females have more VTA MC3R-expressing neurons and that these anatomical differences contribute to sex differences observed in my experiments. Furthermore, the VTA of female rats has been shown to contain more TH+ neurons and higher VTA volume which is not fully accounted for by an increase in TH+ neurons, suggesting that VTA neuron subtypes other than TH-expressing neurons, such as

TH- GABA or glutamate neurons, might be enriched in females [279]. As VTA GABA and glutamate neurons have been shown to participate in the regulation of both reward-associated and aversive behaviors [67; 71; 72], the sex differences in the number of DA neurons expressing MC3Rs, or the proportion of DA *vs* non-DA MC3R neurons could be responsible for the sex differences observed in my experiments. Additionally, many different intersectional phenotypes of VTA neurons exist including glutamate or GABA co-expressing dopamine neurons, or those co-expressing glutamate and GABA in a single neuron. In these neurons, the mechanisms of release of one neurotransmitter over the other or the dynamics of co-release are not understood. It is possible that these mechanics differ in the two sexes and can further contribute to sex differences. Taken together, the sex differences observed in my experiments might due to sexual dimorphisms in (1) the number of VTA MC3R neurons, (2) the phenotype of the VTA MC3R neurons, (3) the neurotransmitter released by the co-releasing VTA MC3R neurons, or (4) the neurotransmitter release dynamics, although these possibilities will need to be tested directly.

Prenatal or perinatal as well as genetic factors may also be responsible for the sex differences in feeding produced by changes in the activity of VTA MC3R neurons. Genetic males (XY) express the *SRY* gene on the Y chromosome which facilitates testicular development. A transient perinatal rise in testosterone produced by the developing testes masculinizes the male brain and lack thereof feminizes the female brain. These differences in hormonal environment during the prenatal development are responsible for many of the sexually dimorphic features of the brain. However, factors other than sex steroids also contribute to sexual differentiation of midbrain DA neurons. For example, primary mesencephalic cell cultures derived from mice prior to the organizational testosterone surge still develop sexually dimorphic characteristics as measured by the number of cells expressing TH, DA levels in the culture medium, and DAT activity [280]. Also, the *SRY* gene product is expressed in the mesencephalic dopamine neurons, is colocalized with TH in some neurons [281; 282], and SRY protein has

been shown to regulate the expression of enzymes involved in DA synthesis [282; 283]. Taken together, the sexual differentiation and function of the mesocorticolimbic dopamine system are very complex. These complexities are reflected in the interaction of this system with the melanocortin system and the explanation of the sex-dependent mechanisms will require further studies.

4.3. Peptidergic transmission and behavior

POMC and AgRP neurons monitor energy state and release their peptide neurotransmitters to maintain energy homeostasis. When energy needs are met, in fed state, POMC neurons release α-MSH which acts on the melanocortin receptors and causes a decrease in energy intake and an increase in energy expenditure. In conditions of energy deficit, AgRP neurons release AgRP, an antagonist/inverse agonist of melanocortin receptors, which promotes feeding while reducing energy expenditure. In addition to peptidergic signaling, Arc POMC and AgRP neurons also co-express glutamate and GABA [120-122] and release of these fast neurotransmitters is involved in the regulation of energy homeostasis [123; 124]. For example, 4th ventricle administration of a $GABA_A$ agonist restored AgRP neuron ablation-induced anorexia [211] and selective deletion of vGat, vesicular transporter for GABA and Glycine, from AgRP neurons produces lean, obesity-resistant mice [123]. AgRP and GABA transmission appear to play different roles in feeding regulation and to work on different timescales. For example, GABA released by AgRP neurons rapidly stimulates feeding, whereas AgRP induces feeding in a delayed but prolonged manner [114; 124; 284]. Similarly, POMC neuron activity over several hours is required to reduce feeding [114; 284; 285]. In my experiments, very few synaptic contacts between any of the Arc and VTA neuron subtypes tested, including those expressing MC3R, were found, suggesting that classical neurotransmitter signaling does not play a large role in the melanocortin system's effect on mesocorticolimbic circuitry, at least at the level of the VTA.

Several different modes of transmission are used by neuropeptides including synaptic transmission and extrasynaptic transmission over short (nm) or long (mm) distances. Studies using genetic markers coupled with electron microscopy showed that, in the PVN, both POMC and AgRP boutons exhibit synaptic and nonsynaptic architecture and that their synaptic release sites contained both small (presumably containing amino acid neurotransmitters) and large vesicles (presumably containing peptides) [197], with non-synaptic sites primarily containing large vesicles, signifying that Arc POMC and AgRP neurons are capable of exerting both synaptic and extrasynaptic peptide-driven effects. However, the low amount of synaptic connectivity between Arc and VTA neurons found in my experiments suggests that in the VTA, α-MSH and AgRP released by POMC and AgRP neurons likely work extra-synaptically. Furthermore, this lack of synaptic connectivity, coupled with the robust labeling of POMC and AgRP neurons by the fluorescent microspheres injected to the VTA, and the previously reported presence of AgRP fibers in close proximity to the putative dopamine neurons [156], implies that Arc feeding peptides act on the VTA circuitry via short-distance diffusion. This anatomical organization is suggestive of a broad action of the melanocortins in the VTA, which likely play modulatory and tuning functions rather that produce a direct action-outcome effect. This hypothesis is supported by the fact that in brain slices, the increase in firing rate of VTA MC3R neurons produced by α-MSH is dependent on activity [162]. Furthermore, the behavioral effects produced by chronic MC3R neuron activation were transient and modest and perhaps would be enhanced by activation of other circuits.

NPY, another orexigenic neuropeptide, is expressed in all AgRP neurons (Figure 1.2) [192; 193] and, similar to GABA released by AgRP neurons, drives fast feeding responses [124]. Analogous to Arc POMC and AgRP neurons, NPY neurons also project to the VTA [156] and NPY receptors are expressed in VTA neurons [243; 286; 287]. NPY has been shown to act on the VTA DA neurons through multiple mechanisms including direct inhibition and presynaptic modulation of excitatory and inhibitory inputs onto DA neurons [244] and intra-VTA

administration of NPY increases motivated behavior towards food [245]. Synaptic NPY release has been previously suggested due to its fast effects on feeding [124; 284] and NPY puncta colocalization with the sites of GABA release [288]. However, the low amount of synaptic contact between VTA DA, GABA, or glutamate neurons and Arc AgRP neurons (AgRP/NPY neurons) observed in my experiments argues against synaptic release of NPY in VTA and suggests that, similar to melanocortin peptides, NPY released by AgRP neurons produces a broad effect on VTA neurons.

The broad action of Arc feeding peptides in the VTA suggested by the anatomy coupled with delayed and long-lasting temporal dynamics of α-MSH and AgRP puts forth a model in which melanocortins set a constant background tone communicating the energy state of the organism to VTA MC3R neurons which allows the nutritive state to influence the response of VTA MC3R neurons to the signals coming from their various presynaptic partners. Therefore, it is possible that the primary role of the interaction between the melanocortin and mesocorticolimbic systems is not for the mesocorticolimbic system to directly modulate feeding (or affect the homeostatic functions), but instead for Arc neurons to relay the energy state to the mesocorticolimbic system to modulate reward sensitivity, whereas the effects produced by the VTA on feeding are secondary.

4.4. Conclusion summary

In the studies in this dissertation I have shown that VTA MC3R neurons have a unique efferent and afferent circuit connectivity which is well-positioned to regulate feeding through multiple potential mechanisms and that VTA MC3R neurons can control feeding and body weight *in vivo* in a sex- and activity-dependent manner, suggesting that this neural population may be a key point of integration of homeostatic and reward information. I have proposed several neural loops and mechanisms through which feeding can be regulated by VTA MC3R

neurons including VTA dopamine and non-dopamine regulated aversive and feeding-related circuits, and I have discussed the potential sources of sex differences produced by changes in the activity of VTA MC3R neurons, including differences in anatomy, neurotransmitter phenotype, and prenatal programming. Furthermore, my experiments revealed an important anatomical feature of the connectivity between the Arc and VTA. Specifically, I showed that despite strong projections to the VTA, Arc neurons form few direct synapses on any of the VTA neuron subtypes, and I discussed the neurochemical and physiological implications of this finding. Taken together, the role of VTA MC3R neurons in feeding appears to be complex, but the data presented here greatly contribute to our understanding of central mechanisms controlling feeding and body weight and provide new insights into how the melanocortin and the mesolimbic systems may interact to regulate energy homeostasis.

4.5. Future directions

Although these studies have provided important information on the anatomy and physiology of the interaction between the melanocortin and the mesocorticolimbic systems, there are still some important unanswered questions. In my experiments, I determined that changes in activity of VTA MC3R neurons can alter feeding but whether the actions of α-MSH and AgRP in the VTA are physiologically relevant remains to be determined. I have designed vectors that can selectively knockdown MC3R expression and, in pilot studies, knockdown of MC3Rsin the VTA produced an interesting diet-dependent effect on feeding and body weight suggesting that VTA MC3Rs differentially modulate intake of different diets. These experiments will need to be repeated with more animals and animals of both sexes, given the sex differences seen in my experiments and by Lippert *et al.* [157]. Furthermore, the effects of VTA MC3R knockdown on reward-associated behaviors will need to be examined in the future.

Approximately 40-60% of MC3Rs are expressed in TH+ VTA neurons (putative dopamine neurons) with the remaining 40% expressed in non-DA neurons of an unknown phenotype [157]. Because the VTA consists of dopamine, glutamate, and GABA neurons [66; 68; 70; 206; 248], the non-dopamine MC3R-expressing neurons could be glutamatergic, GABAergic, or both. Given the differential regulation of feeding and other behaviors by VTA glutamate and GABA neurons, it is important to fully classify the neurotransmitter phenotype of VTA MC3R neurons. Also, because DA, glutamate, and GABA neurons may project to the same target or even be released from the same axon, the phenotype of the neurotransmitters released by VTA MC3R terminals need to be identified in the major targets to begin understanding the target-specific behavioral implications of VTA MC3R neuron activation. Moreover, it is unknown whether VTA MC3R neurons affect feeding behavior through their action on a particular target or if they act on multiple targets in concerted fashion. Therefore, further work is necessary to understand the specific behavioral impact of stimulating or silencing of VTA MC3R terminals in individual projection targets. VTA MC3R neurons receive input from several highly heterogenous brain regions such as LH and DR. It is important to determine the identity of the neurons providing input to the VTA MC3R neurons to begin understanding the conditions which may contribute to the effects of VTA MC3R signaling. Recently, several molecularly distinct populations of VTA neurons with different projections and behavioral correlates have been identified [201; 202] and VTA MC3R neurons appear to overlap with some of these populations in the location of their soma and efferent projections. Future experiments classifying the molecular markers expressed in the VTA MC3R neurons are needed to identify potential mechanisms of VTA MC3R neuron effects on feeding and other behaviors.

Because the VTA is the primary regulator of reward and also contributes to the regulation of aversive behaviors and VTA MC3R neurons are reciprocally innervated with both reward- and aversion- associated brain regions, the role this VTA neuron population plays in these behaviors need to be determined. Some of the experiments that may clarify the functional implication of

VTA MC3R neuron activity include determining the percentage of VTA MC3R neurons responding to rewarding stimuli, including food reward, compared to aversive stimuli, determining whether VTA MC3R activation is rewarding or aversive (or neither) in real-time place preference protocol, determining if activation of VTA MC3R neurons cause conditioned place preference or aversion (or neither), and examining the role of VTA MC3R neuron activity in operant conditioning. It has been suggested that melanocortins preferentially affect intake and motivation for fat [289; 290], although the effects on sugar intake and responding in self-administration protocol have also been reported [164; 165; 291]. It is therefore important to analyze the effects of changes in activity of the VTA MC3R neurons on consumption of diets composed of different macronutrients (high fat vs high sugar *vs* high fat/high sugar).

The sex differences in feeding produced by acute changes in the activity of VTA MC3R neurons appear to not be dependent on the activational properties of gonadal steroids. Therefore, investigating differences in anatomy might shine some light on the causes of sexual dimorphism. For example, the number of dopamine and non-dopamine neurons expressing VTA MC3Rs, including the ratio of different subtypes of VTA neurons, needs to be compared between the two sexes. Although no apparent sex differences were observed in the efferent projections of VTA MC3R neurons, sex differences in the type of neurotransmitter released or the dynamics of neurotransmitter release need to be investigated in the major VTA MC3R neuron targets. Furthermore, it is possible that male and female animals respond differently to DREADD activation or that DREADDs are differentially expressed in the male and female brains. Therefore, the number of DREADD neurons activated by c-fos in response to CNO needs to be compared between the two sexes.

REFERENCES

[1] Ogden, C.L., Carroll, M.D., Kit, B.K., Flegal, K.M., 2014. Prevalence of childhood and adult obesity in the United States, 2011-2012. JAMA 311(8):806-814.

[2] Afshin, A., Forouzanfar, M.H., Reitsma, M.B., Sur, P., Estep, K., Lee, A., et al., 2017. Health Effects of Overweight and Obesity in 195 Countries over 25 Years. N Engl J Med 377(1):13-27.

[3] Heron, M., 2018. Deaths: Leading causes for 2016. MD: National Center for Health Statistics 67(6).

[4] Finkelstein, E.A., Trogdon, J.G., Cohen, J.W., Dietz, W., 2009. Annual medical spending attributable to obesity: payer-and service-specific estimates. Health Aff (Millwood) 28(5):w822-831.

[5] Finkelstein, E.A., Ruhm, C.J., Kosa, K.M., 2005. Economic causes and consequences of obesity. Annu Rev Public Health 26:239-257.

[6] Swinburn, B., Sacks, G., Ravussin, E., 2009. Increased food energy supply is more than sufficient to explain the US epidemic of obesity. Am J Clin Nutr 90(6):1453-1456.

[7] Swinburn, B.A., Sacks, G., Hall, K.D., McPherson, K., Finegood, D.T., Moodie, M.L., et al., 2011. The global obesity pandemic: shaped by global drivers and local environments. Lancet 378(9793):804-814.

[8] Hurt, R.T., Kulisek, C., Buchanan, L.A., McClave, S.A., 2010. The obesity epidemic: challenges, health initiatives, and implications for gastroenterologists. Gastroenterol Hepatol (N Y) 6(12):780-792.

[9] Kenny, P.J., 2011. Reward mechanisms in obesity: new insights and future directions. Neuron 69(4):664-679.

[10] Palmiter, R.D., 2007. Is dopamine a physiologically relevant mediator of feeding behavior? Trends in Neurosciences 30(8):375-381.

[11] Sharma, S., Hryhorczuk, C., Fulton, S., 2012. Progressive-ratio responding for palatable high-fat and high-sugar food in mice. J Vis Exp(63):e3754.

[12] Barbano, M.F., Cador, M., 2005. Various aspects of feeding behavior can be partially dissociated in the rat by the incentive properties of food and the physiological state. Behavioral Neuroscience 119(5):1244-1253.

[13] Wise, R.A., 2004. Dopamine, learning and motivation. Nat Rev Neurosci 5(6):483-494.

[14] Lammel, S., Lim, B.K., Malenka, R.C., 2014. Reward and aversion in a heterogeneous midbrain dopamine system. Neuropharmacology 76:351-359.

[15] Kenny, P.J., 2011. Common cellular and molecular mechanisms in obesity and drug addiction. Nat Rev Neurosci 12(11):638-651.

[16] Wise, R.A., 2006. Role of brain dopamine in food reward and reinforcement. Philos Trans R Soc Lond B Biol Sci 361(1471):1149-1158.

[17] Grace, A.A., Floresco, S.B., Goto, Y., Lodge, D.J., 2007. Regulation of firing of dopaminergic neurons and control of goal-directed behaviors. Trends Neurosci 30(5):220-227.

[18] Paladini, C.A., Roeper, J., 2014. Generating bursts (and pauses) in the dopamine midbrain neurons. Neuroscience 282:109-121.

[19] Morikawa, H., Paladini, C.A., 2011. Dynamic regulation of midbrain dopamine neuron activity: intrinsic, synaptic, and plasticity mechanisms. Neuroscience 198:95-111.

[20] Olds, J., Milner, P., 1954. Positive reinforcement produced by electrical stimulation of septal area and other regions of rat brain. J Comp Physiol Psychol 47(6):419-427.

[21] Stutz, R.M., Rossi, R.R., Bowring, A.M., 1971. Competition between food and rewarding brain shock. Physiol Behav 7(5):753-757.

[22] Garris, P.A., Kilpatrick, M., Bunin, M.A., Michael, D., Walker, Q.D., Wightman, R.M., 1999. Dissociation of dopamine release in the nucleus accumbens from intracranial self-stimulation. Nature 398(6722):67-69.

[23] Hollerman, J.R., Schultz, W., 1998. Dopamine neurons report an error in the temporal prediction of reward during learning. Nat Neurosci 1(4):304-309.

[24] Bromberg-Martin, E.S., Matsumoto, M., Hikosaka, O., 2010. Dopamine in Motivational Control: Rewarding, Aversive, and Alerting. Neuron 68(5):815-834.

[25] Schultz, W., 2016. Dopamine reward prediction-error signalling: a two-component response. Nat Rev Neurosci 17(3):183-195.

[26] Schultz, W., 2007. Multiple dopamine functions at different time courses. Annu Rev Neurosci 30:259-288.

[27] Schultz, W., Dayan, P., Montague, P.R., 1997. A neural substrate of prediction and reward. Science 275(5306):1593-1599.

[28] Zhou, Q.Y., Palmiter, R.D., 1995. Dopamine-deficient mice are severely hypoactive, adipsic, and aphagic. Cell 83(7):1197-1209.

[29] Volkow, N.D., Wang, G.J., Baler, R.D., 2011. Reward, dopamine and the control of food intake: implications for obesity. Trends Cogn Sci 15(1):37-46.

[30] DiLeone, R.J., Taylor, J.R., Picciotto, M.R., 2012. The drive to eat: comparisons and distinctions between mechanisms of food reward and drug addiction. Nat Neurosci 15(10):1330-1335.

[31] Nirenberg, M.J., Waters, C., 2006. Compulsive eating and weight gain related to dopamine agonist use. Mov Disord 21(4):524-529.

[32] Cornelius, J.R., Tippmann-Peikert, M., Slocumb, N.L., Frerichs, C.F., Silber, M.H., 2010. Impulse control disorders with the use of dopaminergic agents in restless legs syndrome: a case-control study. Sleep 33(1):81-87.

[33] Small, D.M., Jones-Gotman, M., Dagher, A., 2003. Feeding-induced dopamine release in dorsal striatum correlates with meal pleasantness ratings in healthy human volunteers. Neuroimage 19(4):1709-1715.

[34] Schur, E.A., Kleinhans, N.M., Goldberg, J., Buchwald, D., Schwartz, M.W., Maravilla, K., 2009. Activation in brain energy regulation and reward centers by food cues varies with choice of visual stimulus. Int J Obes (Lond) 33(6):653-661.

[35] Stice, E., Spoor, S., Bohon, C., Veldhuizen, M.G., Small, D.M., 2008. Relation of reward from food intake and anticipated food intake to obesity: a functional magnetic resonance imaging study. J Abnorm Psychol 117(4):924-935.

[36] Wang, G.J., Volkow, N.D., Logan, J., Pappas, N.R., Wong, C.T., Zhu, W., et al., 2001. Brain dopamine and obesity. Lancet 357(9253):354-357.

[37] van der Zwaal, E.M., de Weijer, B.A., van de Giessen, E.M., Janssen, I., Berends, F.J., van de Laar, A., et al., 2016. Striatal dopamine D2/3 receptor availability increases after long-term bariatric surgery-induced weight loss. Eur Neuropsychopharmacol.

[38] Weingarten, H.P., 1983. Conditioned cues elicit feeding in sated rats: a role for learning in meal initiation. Science 220(4595):431-433.

[39] Petrovich, G.D., 2013. Forebrain networks and the control of feeding by environmental learned cues. Physiol Behav 121:10-18.

[40] Lenoir, M., Serre, F., Cantin, L., Ahmed, S.H., 2007. Intense sweetness surpasses cocaine reward. PLoS One 2(8):e698.

[41] Oswald, K.D., Murdaugh, D.L., King, V.L., Boggiano, M.M., 2011. Motivation for palatable food despite consequences in an animal model of binge eating. Int J Eat Disord 44(3):203-211.

[42] Foo, H., Mason, P., 2005. Sensory suppression during feeding. Proc Natl Acad Sci U S A 102(46):16865-16869.

[43] Cabanac, M., Johnson, K.G., 1983. Analysis of a conflict between palatability and cold exposure in rats. Physiol Behav 31(2):249-253.

[44] Yager, L.M., Robinson, T.E., 2010. Cue-induced reinstatement of food seeking in rats that differ in their propensity to attribute incentive salience to food cues. Behav Brain Res 214(1):30-34.

[45] Hernandez, L., Hoebel, B.G., 1988. Food reward and cocaine increase extracellular dopamine in the nucleus accumbens as measured by microdialysis. Life Sci 42(18):1705-1712.

[46] Roitman, M.F., Stuber, G.D., Phillips, P.E., Wightman, R.M., Carelli, R.M., 2004. Dopamine operates as a subsecond modulator of food seeking. J Neurosci 24(6):1265-1271.

[47] Liang, N.C., Hajnal, A., Norgren, R., 2006. Sham feeding corn oil increases accumbens dopamine in the rat. Am J Physiol Regul Integr Comp Physiol 291(5):R1236-1239.

[48] Hajnal, A., Smith, G.P., Norgren, R., 2004. Oral sucrose stimulation increases accumbens dopamine in the rat. Am J Physiol Regul Integr Comp Physiol 286(1):R31-37.

[49] Schultz, W., 1998. Predictive reward signal of dopamine neurons. J Neurophysiol 80(1):1-27.

[50] Salamone, J.D., Correa, M., Mingote, S., Weber, S.M., 2003. Nucleus accumbens dopamine and the regulation of effort in food-seeking behavior: implications for studies of natural motivation, psychiatry, and drug abuse. J Pharmacol Exp Ther 305(1):1-8.

[51] Salamone, J.D., Cousins, M.S., Snyder, B.J., 1997. Behavioral functions of nucleus accumbens dopamine: empirical and conceptual problems with the anhedonia hypothesis. Neurosci Biobehav Rev 21(3):341-359.

[52] Salamone, J.D., Steinpreis, R.E., McCullough, L.D., Smith, P., Grebel, D., Mahan, K., 1991. Haloperidol and nucleus accumbens dopamine depletion suppress lever pressing for food but increase free food consumption in a novel food choice procedure. Psychopharmacology (Berl) 104(4):515-521.

[53] Koch, M., Schmid, A., Schnitzler, H.U., 2000. Role of nucleus accumbens dopamine D1 and D2 receptors in instrumental and Pavlovian paradigms of conditioned reward. Psychopharmacology (Berl) 152(1):67-73.

[54] Szczypka, M.S., Mandel, R.J., Donahue, B.A., Snyder, R.O., Leff, S.E., Palmiter, R.D., 1999. Viral gene delivery selectively restores feeding and prevents lethality of dopamine-deficient mice. Neuron 22(1):167-178.

[55] Wise, R.A., Colle, L.M., 1984. Pimozide attenuates free feeding: best scores analysis reveals a motivational deficit. Psychopharmacology (Berl) 84(4):446-451.

[56] Wise, R.A., Spindler, J., deWit, H., Gerberg, G.J., 1978. Neuroleptic-induced "anhedonia" in rats: pimozide blocks reward quality of food. Science 201(4352):262-264.

[57] Wise, R.A., Spindler, J., Legault, L., 1978. Major attenuation of food reward with performance-sparing doses of pimozide in the rat. Can J Psychol 32(2):77-85.

[58] Phillips, A.G., Nikaido, R.S., 1975. Disruption of brain stimulation-induced feeding by dopamine receptor blockade. Nature 258(5537):750-751.

[59] Hernandez, L., Hoebel, B.G., 1988. Feeding and hypothalamic stimulation increase dopamine turnover in the accumbens. Physiol Behav 44(4-5):599-606.

[60] Church, W.H., Justice, J.B., Neill, D.B., 1987. Detecting behaviorally relevant changes in extracellular dopamine with microdialysis. Brain Res 412(2):397-399.

[61] Pal, G.K., Thombre, D.P., 1993. Modulation of feeding and drinking by dopamine in caudate and accumbens nuclei in rats. Indian J Exp Biol 31(9):750-754.

[62] Sanchez-Catalan, M.J., Kaufling, J., Georges, F., Veinante, P., Barrot, M., 2014. The antero-posterior heterogeneity of the ventral tegmental area. Neuroscience 282C:198-216.

[63] Morales, M., Margolis, E.B., 2017. Ventral tegmental area: cellular heterogeneity, connectivity and behaviour. Nat Rev Neurosci 18(2):73-85.

[64] Li, X., Qi, J., Yamaguchi, T., Wang, H.L., Morales, M., 2013. Heterogeneous composition of dopamine neurons of the rat A10 region: molecular evidence for diverse signaling properties. Brain Struct Funct 218(5):1159-1176.

[65] Lammel, S., Hetzel, A., Haeckel, O., Jones, I., Liss, B., Roeper, J., 2008. Unique properties of mesoprefrontal neurons within a dual mesocorticolimbic dopamine system. Neuron 57(5):760-773.

[66] Morales, M., Root, D.H., 2014. Glutamate neurons within the midbrain dopamine regions. Neuroscience 282C:60-68.

[67] Stamatakis, A.M., Jennings, J.H., Ung, R.L., Blair, G.A., Weinberg, R.J., Neve, R.L., et al., 2013. A Unique Population of Ventral Tegmental Area Neurons Inhibits the Lateral Habenula to Promote Reward. Neuron 80(4):1039-1053.

[68] Yamaguchi, T., Sheen, W., Morales, M., 2007. Glutamatergic neurons are present in the rat ventral tegmental area. Eur J Neurosci 25(1):106-118.

[69] Margolis, E.B., Lock, H., Hjelmstad, G.O., Fields, H.L., 2006. The ventral tegmental area revisited: is there an electrophysiological marker for dopaminergic neurons? J Physiol 577(Pt 3):907-924.

[70] Nair-Roberts, R.G., Chatelain-Badie, S.D., Benson, E., White-Cooper, H., Bolam, J.P., Ungless, M.A., 2008. Stereological estimates of dopaminergic, gabaergic and glutamatergic neurons in the ventral tegmental area, substantia nigra and retrorubral field in the rat. Neuroscience 152(4):1024-1031.

[71] Root, D.H., Mejias-Aponte, C.A., Qi, J., Morales, M., 2014. Role of Glutamatergic Projections from Ventral Tegmental Area to Lateral Habenula in Aversive Conditioning. Journal of Neuroscience 34(42):13906-13910.

[72] van Zessen, R., Phillips, J.L., Budygin, E.A., Stuber, G.D., 2012. Activation of VTA GABA neurons disrupts reward consumption. Neuron 73(6):1184-1194.

[73] Yamaguchi, T., Qi, J., Wang, H.L., Zhang, S., Morales, M., 2015. Glutamatergic and dopaminergic neurons in the mouse ventral tegmental area. Eur J Neurosci 41(6):760-772.

[74] Yamaguchi, T., Wang, H.L., Li, X., Ng, T.H., Morales, M., 2011. Mesocorticolimbic glutamatergic pathway. J Neurosci 31(23):8476-8490.

[75] Zhang, S., Qi, J., Li, X., Wang, H.L., Britt, J.P., Hoffman, A.F., et al., 2015. Dopaminergic and glutamatergic microdomains in a subset of rodent mesoaccumbens axons. Nat Neurosci 18(3):386-392.

[76] Hnasko, T.S., Chuhma, N., Zhang, H., Goh, G.Y., Sulzer, D., Palmiter, R.D., et al., 2010. Vesicular glutamate transport promotes dopamine storage and glutamate corelease in vivo. Neuron 65(5):643-656.

[77] Gadziola, M.A., Wesson, D.W., 2016. The Neural Representation of Goal-Directed Actions and Outcomes in the Ventral Striatum's Olfactory Tubercle. Journal of Neuroscience 36(2):548-560.

[78] Root, D.H., Hoffman, A.F., Good, C.H., Zhang, S., Gigante, E., Lupica, C.R., et al., 2015. Norepinephrine activates dopamine D4 receptors in the rat lateral habenula. J Neurosci 35(8):3460-3469.

[79] Root, D.H., Mejias-Aponte, C.A., Zhang, S., Wang, H.L., Hoffman, A.F., Lupica, C.R., et al., 2014. Single rodent mesohabenular axons release glutamate and GABA. Nat Neurosci.

[80] Berrios, J., Stamatakis, A.M., Kantak, P.A., McElligott, Z.A., Judson, M.C., Aita, M., et al., 2016. Loss of UBE3A from TH-expressing neurons suppresses GABA co-release and enhances VTA-NAc optical self-stimulation. Nat Commun 7:10702.

[81] Tritsch, N.X., Oh, W.J., Gu, C., Sabatini, B.L., 2014. Midbrain dopamine neurons sustain inhibitory transmission using plasma membrane uptake of GABA, not synthesis. Elife 3:e01936.

[82] Kim, J.I., Ganesan, S., Luo, S.X., Wu, Y.W., Park, E., Huang, E.J., et al., 2015. Aldehyde dehydrogenase 1a1 mediates a GABA synthesis pathway in midbrain dopaminergic neurons. Science 350(6256):102-106.

[83] Anderegg, A., Poulin, J.-F., Awatramani, R., 2015. Molecular heterogeneity of midbrain dopaminergic neurons - Moving toward single cell resolution. Febs Letters 589(24):3714-3726.

[84] Faget, L., Osakada, F., Duan, J., Ressler, R., Johnson, A.B., Proudfoot, J.A., et al., 2016. Afferent Inputs to Neurotransmitter-Defined Cell Types in the Ventral Tegmental Area. Cell Rep 15(12):2796-2808.

[85] Carr, D.B., Sesack, S.R., 2000. Projections from the rat prefrontal cortex to the ventral tegmental area: target specificity in the synaptic associations with mesoaccumbens and mesocortical neurons. J Neurosci 20(10):3864-3873.

[86] Charara, A., Smith, Y., Parent, A., 1996. Glutamatergic inputs from the pedunculopontine nucleus to midbrain dopaminergic neurons in primates: Phaseolus vulgaris-leucoagglutinin anterograde labeling combined with postembedding glutamate and GABA immunohistochemistry. J Comp Neurol 364(2):254-266.

[87] Omelchenko, N., Sesack, S.R., 2005. Laterodorsal tegmental projections to identified cell populations in the rat ventral tegmental area. J Comp Neurol 483(2):217-235.

[88] Omelchenko, N., Bell, R., Sesack, S.R., 2009. Lateral habenula projections to dopamine and GABA neurons in the rat ventral tegmental area. European Journal of Neuroscience 30(7):1239-1250.

[89] Omelchenko, N., Sesack, S.R., 2010. Periaqueductal Gray Afferents Synapse onto Dopamine and GABA Neurons in the Rat Ventral Tegmental Area. Journal of Neuroscience Research 88(5):981-991.

[90] Georges, F., Aston-Jones, G., 2001. Potent regulation of midbrain dopamine neurons by the bed nucleus of the stria terminalis. J Neurosci 21(16):RC160.

[91] Qi, J., Zhang, S., Wang, H.L., Wang, H., de Jesus Aceves Buendia, J., Hoffman, A.F., et al., 2014. A glutamatergic reward input from the dorsal raphe to ventral tegmental area dopamine neurons. Nat Commun 5:5390.

[92] Jhou, T.C., Fields, H.L., Baxter, M.G., Saper, C.B., Holland, P.C., 2009. The Rostromedial Tegmental Nucleus (RMTg), a GABAergic Afferent to Midbrain Dopamine Neurons, Encodes Aversive Stimuli and Inhibits Motor Responses. Neuron 61(5):786-800.

[93] Beier, K.T., Steinberg, E.E., DeLoach, K.E., Xie, S., Miyamichi, K., Schwarz, L., et al., 2015. Circuit Architecture of VTA Dopamine Neurons Revealed by Systematic Input-Output Mapping. Cell 162(3):622-634.

[94] Nieh, E.H., Matthews, G.A., Allsop, S.A., Presbrey, K.N., Leppla, C.A., Wichmann, R., et al., 2015. Decoding Neural Circuits that Control Compulsive Sucrose Seeking. Cell 160(3):528-541.

[95] Hjelmstad, G.O., Xia, Y., Margolis, E.B., Fields, H.L., 2013. Opioid modulation of ventral pallidal afferents to ventral tegmental area neurons. J Neurosci 33(15):6454-6459.

[96] Bocklisch, C., Pascoli, V., Wong, J.C., House, D.R., Yvon, C., de Roo, M., et al., 2013. Cocaine disinhibits dopamine neurons by potentiation of GABA transmission in the ventral tegmental area. Science 341(6153):1521-1525.

[97] Kudo, T., Uchigashima, M., Miyazaki, T., Konno, K., Yamasaki, M., Yanagawa, Y., et al., 2012. Three Types of Neurochemical Projection from the Bed Nucleus of the Stria Terminalis to the Ventral Tegmental Area in Adult Mice. Journal of Neuroscience 32(50):18035-18046.

[98] Taylor, S.R., Badurek, S., Dileone, R.J., Nashmi, R., Minichiello, L., Picciotto, M.R., 2014. GABAergic and Glutamatergic Efferents of the Mouse Ventral Tegmental Area. Journal of Comparative Neurology 522(14):3308-3334.

[99] Brown, M.T., Tan, K.R., O'Connor, E.C., Nikonenko, I., Muller, D., Lüscher, C., 2012. Ventral tegmental area GABA projections pause accumbal cholinergic interneurons to enhance associative learning. Nature 492(7429):452-456.

[100] Stuber, G.D., Hnasko, T.S., Britt, J.P., Edwards, R.H., Bonci, A., 2010. Dopaminergic terminals in the nucleus accumbens but not the dorsal striatum corelease glutamate. J Neurosci 30(24):8229-8233.

[101] Qi, J., Zhang, S., Wang, H.L., Barker, D.J., Miranda-Barrientos, J., Morales, M., 2016. VTA glutamatergic inputs to nucleus accumbens drive aversion by acting on GABAergic interneurons. Nat Neurosci.

[102] Dobi, A., Margolis, E.B., Wang, H.L., Harvey, B.K., Morales, M., 2010. Glutamatergic and nonglutamatergic neurons of the ventral tegmental area establish local synaptic contacts with dopaminergic and nondopaminergic neurons. J Neurosci 30(1):218-229.

[103] Wang, H.L., Qi, J., Zhang, S., Wang, H., Morales, M., 2015. Rewarding Effects of Optical Stimulation of Ventral Tegmental Area Glutamatergic Neurons. J Neurosci 35(48):15948-15954.

[104] Cone, R.D., 2005. Anatomy and regulation of the central melanocortin system. Nat Neurosci 8(5):571-578.

[105] Cone, R.D., 2006. Studies on the physiological functions of the melanocortin system. Endocr Rev 27(7):736-749.

[106] Butler, A.A., 2006. The melanocortin system and energy balance. Peptides 27(2):281-290.

[107] Hill, J.M., Lesniak, M.A., Pert, C.B., Roth, J., 1986. Autoradiographic localization of insulin receptors in rat brain: prominence in olfactory and limbic areas. Neuroscience 17(4):1127-1138.

[108] Scott, M.M., Lachey, J.L., Sternson, S.M., Lee, C.E., Elias, C.F., Friedman, J.M., et al., 2009. Leptin targets in the mouse brain. J Comp Neurol 514(5):518-532.

[109] Zigman, J.M., Jones, J.E., Lee, C.E., Saper, C.B., Elmquist, J.K., 2006. Expression of ghrelin receptor mRNA in the rat and the mouse brain. J Comp Neurol 494(3):528-548.

[110] Wang, D., He, X., Zhao, Z., Feng, Q., Lin, R., Sun, Y., et al., 2015. Whole-brain mapping of the direct inputs and axonal projections of POMC and AgRP neurons. Front Neuroanat 9:40.

[111] Krashes, M.J., Koda, S., Ye, C., Rogan, S.C., Adams, A.C., Cusher, D.S., et al., 2011. Rapid, reversible activation of AgRP neurons drives feeding behavior in mice. J Clin Invest 121(4):1424-1428.

[112] Liu, T., Kong, D., Shah, B.P., Ye, C., Koda, S., Saunders, A., et al., 2012. Fasting activation of AgRP neurons requires NMDA receptors and involves spinogenesis and increased excitatory tone. Neuron 73(3):511-522.

[113] Yang, Y., Atasoy, D., Su, H.H., Sternson, S.M., 2011. Hunger states switch a flip-flop memory circuit via a synaptic AMPK-dependent positive feedback loop. Cell 146(6):992-1003.

[114] Aponte, Y., Atasoy, D., Sternson, S.M., 2011. AGRP neurons are sufficient to orchestrate feeding behavior rapidly and without training. Nat Neurosci 14(3):351-355.

[115] Fan, W., Boston, B.A., Kesterson, R.A., Hruby, V.J., Cone, R.D., 1997. Role of melanocortinergic neurons in feeding and the agouti obesity syndrome. Nature 385(6612):165-168.

[116] Pierroz, D.D., Ziotopoulou, M., Ungsunan, L., Moschos, S., Flier, J.S., Mantzoros, C.S., 2002. Effects of acute and chronic administration of the melanocortin agonist MTII in mice with diet-induced obesity. Diabetes 51(5):1337-1345.

[117] Graham, M., Shutter, J.R., Sarmiento, U., Sarosi, I., Stark, K.L., 1997. Overexpression of Agrt leads to obesity in transgenic mice. Nat Genet 17(3):273-274.

[118] Rossi, M., Kim, M.S., Morgan, D.G., Small, C.J., Edwards, C.M., Sunter, D., et al., 1998. A C-terminal fragment of Agouti-related protein increases feeding and antagonizes the

effect of alpha-melanocyte stimulating hormone in vivo. Endocrinology 139(10):4428-4431.

[119] Ollmann, M.M., Wilson, B.D., Yang, Y.K., Kerns, J.A., Chen, Y., Gantz, I., et al., 1997. Antagonism of central melanocortin receptors in vitro and in vivo by agouti-related protein. Science 278(5335):135-138.

[120] Horvath, T.L., Bechmann, I., Naftolin, F., Kalra, S.P., Leranth, C., 1997. Heterogeneity in the neuropeptide Y-containing neurons of the rat arcuate nucleus: GABAergic and non-GABAergic subpopulations. Brain Res 756(1-2):283-286.

[121] Hentges, S.T., Otero-Corchon, V., Pennock, R.L., King, C.M., Low, M.J., 2009. Proopiomelanocortin expression in both GABA and glutamate neurons. J Neurosci 29(43):13684-13690.

[122] Dicken, M.S., Tooker, R.E., Hentges, S.T., 2012. Regulation of GABA and glutamate release from proopiomelanocortin neuron terminals in intact hypothalamic networks. J Neurosci 32(12):4042-4048.

[123] Tong, Q., Ye, C.P., Jones, J.E., Elmquist, J.K., Lowell, B.B., 2008. Synaptic release of GABA by AgRP neurons is required for normal regulation of energy balance. Nat Neurosci 11(9):998-1000.

[124] Krashes, M.J., Shah, B.P., Koda, S., Lowell, B.B., 2013. Rapid versus delayed stimulation of feeding by the endogenously released AgRP neuron mediators GABA, NPY, and AgRP. Cell Metab 18(4):588-595.

[125] Butler, A.A., Kesterson, R.A., Khong, K., Cullen, M.J., Pelleymounter, M.A., Dekoning, J., et al., 2000. A unique metabolic syndrome causes obesity in the melanocortin-3 receptor-deficient mouse. Endocrinology 141(9):3518-3521.

[126] Chen, A.S., Marsh, D.J., Trumbauer, M.E., Frazier, E.G., Guan, X.M., Yu, H., et al., 2000. Inactivation of the mouse melanocortin-3 receptor results in increased fat mass and reduced lean body mass. Nat Genet 26(1):97-102.

[127] Chen, A.S., Metzger, J.M., Trumbauer, M.E., Guan, X.M., Yu, H., Frazier, E.G., et al., 2000. Role of the melanocortin-4 receptor in metabolic rate and food intake in mice. Transgenic Res 9(2):145-154.

[128] Huszar, D., Lynch, C.A., Fairchild-Huntress, V., Dunmore, J.H., Fang, Q., Berkemeier, L.R., et al., 1997. Targeted disruption of the melanocortin-4 receptor results in obesity in mice. Cell 88(1):131-141.

[129] Sutton, G.M., Trevaskis, J.L., Hulver, M.W., McMillan, R.P., Markward, N.J., Babin, M.J., et al., 2006. Diet-genotype interactions in the development of the obese, insulin-resistant phenotype of C57BL/6J mice lacking melanocortin-3 or -4 receptors. Endocrinology 147(5):2183-2196.

[130] Krude, H., Biebermann, H., Luck, W., Horn, R., Brabant, G., Grüters, A., 1998. Severe early-onset obesity, adrenal insufficiency and red hair pigmentation caused by POMC mutations in humans. Nat Genet 19(2):155-157.

[131] Farooqi, I.S., Yeo, G.S., Keogh, J.M., Aminian, S., Jebb, S.A., Butler, G., et al., 2000. Dominant and recessive inheritance of morbid obesity associated with melanocortin 4 receptor deficiency. J Clin Invest 106(2):271-279.

[132] Vaisse, C., Clement, K., Durand, E., Hercberg, S., Guy-Grand, B., Froguel, P., 2000. Melanocortin-4 receptor mutations are a frequent and heterogeneous cause of morbid obesity. J Clin Invest 106(2):253-262.

[133] Lee, Y.S., Poh, L.K., Loke, K.Y., 2002. A novel melanocortin 3 receptor gene (MC3R) mutation associated with severe obesity. J Clin Endocrinol Metab 87(3):1423-1426.

[134] Savastano, D.M., Tanofsky-Kraff, M., Han, J.C., Ning, C., Sorg, R.A., Roza, C.A., et al., 2009. Energy intake and energy expenditure among children with polymorphisms of the melanocortin-3 receptor. Am J Clin Nutr 90(4):912-920.

[135] Obregón, A.M., Amador, P., Valladares, M., Weisstaub, G., Burrows, R., Santos, J.L., 2010. Melanocortin-3 receptor gene variants: association with childhood obesity and eating behavior in Chilean families. Nutrition 26(7-8):760-765.

[136] Kishi, T., Aschkenasi, C.J., Lee, C.E., Mountjoy, K.G., Saper, C.B., Elmquist, J.K., 2003. Expression of melanocortin 4 receptor mRNA in the central nervous system of the rat. J Comp Neurol 457(3):213-235.

[137] Roselli-Rehfuss, L., Mountjoy, K.G., Robbins, L.S., Mortrud, M.T., Low, M.J., Tatro, J.B., et al., 1993. Identification of a receptor for gamma melanotropin and other proopiomelanocortin peptides in the hypothalamus and limbic system. Proc Natl Acad Sci U S A 90(19):8856-8860.

[138] Bagnol, D., Lu, X.Y., Kaelin, C.B., Day, H.E., Ollmann, M., Gantz, I., et al., 1999. Anatomy of an endogenous antagonist: relationship between Agouti-related protein and proopiomelanocortin in brain. J Neurosci 19(18):RC26.

[139] Jégou, S., Boutelet, I., Vaudry, H., 2000. Melanocortin-3 receptor mRNA expression in pro-opiomelanocortin neurones of the rat arcuate nucleus. J Neuroendocrinol 12(6):501-505.

[140] Cowley, M.A., Smart, J.L., Rubinstein, M., Cerdán, M.G., Diano, S., Horvath, T.L., et al., 2001. Leptin activates anorexigenic POMC neurons through a neural network in the arcuate nucleus. Nature 411(6836):480-484.

[141] Atalayer, D., Robertson, K.L., Haskell-Luevano, C., Andreasen, A., Rowland, N.E., 2010. Food demand and meal size in mice with single or combined disruption of melanocortin type 3 and 4 receptors. Am J Physiol Regul Integr Comp Physiol 298(6):R1667-1674.

[142] Huo, L., Gamber, K., Greeley, S., Silva, J., Huntoon, N., Leng, X.H., et al., 2009. Leptin-dependent control of glucose balance and locomotor activity by POMC neurons. Cell Metab 9(6):537-547.

[143] Zhou, L., Sutton, G.M., Rochford, J.J., Semple, R.K., Lam, D.D., Oksanen, L.J., et al., 2007. Serotonin 2C receptor agonists improve type 2 diabetes via melanocortin-4 receptor signaling pathways. Cell Metab 6(5):398-405.

[144] Lee, B., Koo, J., Yun Jun, J., Gavrilova, O., Lee, Y., Seo, A.Y., et al., 2016. A mouse model for a partially inactive obesity-associated human MC3R variant. Nat Commun 7:10522.

[145] Marsh, D.J., Hollopeter, G., Huszar, D., Laufer, R., Yagaloff, K.A., Fisher, S.L., et al., 1999. Response of melanocortin-4 receptor-deficient mice to anorectic and orexigenic peptides. Nat Genet 21(1):119-122.

[146] Rowland, N.E., Schaub, J.W., Robertson, K.L., Andreasen, A., Haskell-Luevano, C., 2010. Effect of MTII on food intake and brain c-Fos in melanocortin-3, melanocortin-4, and double MC3 and MC4 receptor knockout mice. Peptides 31(12):2314-2317.

[147] Renquist, B.J., Murphy, J.G., Larson, E.A., Olsen, D., Klein, R.F., Ellacott, K.L., et al., 2012. Melanocortin-3 receptor regulates the normal fasting response. Proc Natl Acad Sci U S A 109(23):E1489-1498.

[148] Ghamari-Langroudi, M., Cakir, I., Lippert, R.N., Sweeney, P., Litt, M.J., Ellacott, K.L.J., et al., 2018. Regulation of energy rheostasis by the melanocortin-3 receptor. Sci Adv 4(8):eaat0866.

[149] Girardet, C., Marks, D.L., Butler, A.A., 2018. Melanocortin-3 Receptors Expressed on Agouti-Related Peptide Neurons Inhibit Feeding Behavior in Female Mice. Obesity (Silver Spring) 26(12):1849-1855.

[150] Mavrikaki, M., Girardet, C., Kern, A., Faruzzi Brantley, A., Miller, C.A., Macarthur, H., et al., 2016. Melanocortin-3 receptors in the limbic system mediate feeding-related motivational responses during weight loss. Mol Metab 5(7):566-579.

[151] Begriche, K., Sutton, G.M., Butler, A.A., 2011. Homeostastic and non-homeostatic functions of melanocortin-3 receptors in the control of energy balance and metabolism. Physiol Behav 104(4):546-554.

[152] Begriche, K., Levasseur, P.R., Zhang, J., Rossi, J., Skorupa, D., Solt, L.A., et al., 2011. Genetic dissection of the functions of the melanocortin-3 receptor, a seven-transmembrane G-protein-coupled receptor, suggests roles for central and peripheral receptors in energy homeostasis. J Biol Chem 286(47):40771-40781.

[153] Sutton, G.M., Perez-Tilve, D., Nogueiras, R., Fang, J., Kim, J.K., Cone, R.D., et al., 2008. The Melanocortin-3 Receptor Is Required for Entrainment to Meal Intake. Journal of Neuroscience 28(48):12946-12955.

[154] Marks, D.L., Butler, A.A., Turner, R., Brookhart, G., Cone, R.D., 2003. Differential role of melanocortin receptor subtypes in cachexia. Endocrinology 144(4):1513-1523.

[155] King, C.M., Hentges, S.T., 2011. Relative number and distribution of murine hypothalamic proopiomelanocortin neurons innervating distinct target sites. PLoS One 6(10):e25864.

[156] Dietrich, M.O., Bober, J., Ferreira, J.G., Tellez, L.A., Mineur, Y.S., Souza, D.O., et al., 2012. AgRP neurons regulate development of dopamine neuronal plasticity and nonfood-associated behaviors. Nat Neurosci 15(8):1108-1110.

[157] Lippert, R.N., Ellacott, K.L., Cone, R.D., 2014. Gender-specific roles for the melanocortin-3 receptor in the regulation of the mesolimbic dopamine system in mice. Endocrinology 155(5):1718-1727.

[158] Torre, E., Celis, M.E., 1986. Alpha msh injected into the substantia nigra or intraventricularly alters behavior and the striatal dopaminergic activity. Neurochemistry International 9(1):85-90.

[159] Torre, E., Celis, M.E., 1988. Cholinergic mediation in the ventral tegmental area of alpha melanotropin induced excessive grooming changes of the dopamine activity in the nucleus accumbens and caudate putamen. Life Sciences 42(17):1651-1658.

[160] Klusa, V., Svirskis, S., Opmane, B., Muceniece, R., Wikberg, J.E.S., 1999. Behavioural responses of gamma-MSH peptides administered into the rat ventral tegmental area. Acta Physiologica Scandinavica 167(2):99-104.

[161] Sanchez, M.S., Barontini, M., Armando, I., Celis, M.E., 2001. Correlation of increased grooming behavior and motor activity with alterations in nigrostriatal and mesolimbic catecholamines after alpha-melanotropin and neuropeptide glutamine-isoleucine injection in the rat ventral tegmental area. Cellular and Molecular Neurobiology 21(5):523-533.

[162] West, K.S., Lu, C., Olson, D.P., Roseberry, A.G., 2019. α-MSH increases the activity of MC3R-expressing neurons in the ventral tegmental area. J Physiol.

[163] Roseberry, A.G., 2013. Altered feeding and body weight following melanocortin administration to the ventral tegmental area in adult rats. Psychopharmacology (Berl) 226(1):25-34.

[164] Shanmugarajah, L., Dunigan, A.I., Frantz, K.J., Roseberry, A.G., 2017. Altered sucrose self-administration following injection of melanocortin receptor agonists and antagonists into the ventral tegmental area. Psychopharmacology (Berl).

[165] Yen, H.H., Roseberry, A.G., 2014. Decreased consumption of rewarding sucrose solutions after injection of melanocortins into the ventral tegmental area of rats. Psychopharmacology (Berl).

[166] Hyland, B.I., Reynolds, J.N., Hay, J., Perk, C.G., Miller, R., 2002. Firing modes of midbrain dopamine cells in the freely moving rat. Neuroscience 114(2):475-492.

[167] Inoue, K., Kiriike, N., Kurioka, M., Fujisaki, Y., Iwasaki, S., Yamagami, S., 1997. Bromocriptine enhances feeding behavior without changing dopamine metabolism. Pharmacol Biochem Behav 58(1):183-188.

[168] Webber, E.S., Bonci, A., Krashes, M.J., 2015. The elegance of energy balance: Insight from circuit-level manipulations. Synapse 69(9):461-474.

[169] Lindblom, J., Opmane, B., Mutulis, F., Mutule, I., Petrovska, R., Klusa, V., et al., 2001. The MC4 receptor mediates alpha-MSH induced release of nucleus accumbens dopamine. Neuroreport 12(10):2155-2158.

[170] Jansone, B., Bergstrom, L., Svirskis, S., Lindblom, J., Klusa, V., Wikberg, J.E.S., 2004. Opposite effects of gamma(1)- and gamma(2)-melanocyte stimulating hormone on regulation of the dopaminergic mesolimbic system in rats. Neuroscience Letters 361(1-3):68-71.

[171] Osakada, F., Mori, T., Cetin, A.H., Marshel, J.H., Virgen, B., Callaway, E.M., 2011. New rabies virus variants for monitoring and manipulating activity and gene expression in defined neural circuits. Neuron 71(4):617-631.

[172] Hommel, J.D., Trinko, R., Sears, R.M., Georgescu, D., Liu, Z.-W., Gao, X.-B., et al., 2006. Leptin receptor signaling in midbrain dopamine neurons regulates feeding. Neuron 51(6):801-810.

[173] Pei, H., Patterson, C.M., Sutton, A.K., Burnett, K.H., Myers, M.G., Olson, D.P., 2019. Lateral Hypothalamic Mc3R-Expressing Neurons Modulate Locomotor Activity, Energy Expenditure, and Adiposity in Male Mice. Endocrinology 160(2):343-358.

[174] van den Pol, A.N., Yao, Y., Fu, L.Y., Foo, K., Huang, H., Coppari, R., et al., 2009. Neuromedin B and gastrin-releasing peptide excite arcuate nucleus neuropeptide Y neurons in a novel transgenic mouse expressing strong Renilla green fluorescent protein in NPY neurons. J Neurosci 29(14):4622-4639.

[175] Savitt, J.M., Jang, S.S., Mu, W., Dawson, V.L., Dawson, T.M., 2005. Bcl-x is required for proper development of the mouse substantia nigra. J Neurosci 25(29):6721-6728.

[176] Vong, L., Ye, C., Yang, Z., Choi, B., Chua, S., Lowell, B.B., 2011. Leptin action on GABAergic neurons prevents obesity and reduces inhibitory tone to POMC neurons. Neuron 71(1):142-154.

[177] Taniguchi, H., He, M., Wu, P., Kim, S., Paik, R., Sugino, K., et al., 2011. A resource of Cre driver lines for genetic targeting of GABAergic neurons in cerebral cortex. Neuron 71(6):995-1013.

[178] Preibisch, S., Saalfeld, S., Tomancak, P., 2009. Globally optimal stitching of tiled 3D microscopic image acquisitions. Bioinformatics 25(11):1463-1465.

[179] Hein, L.R., De Oliveira, J.A., De Campos, K.A., Caltabiano, P.C., 2012. Extended depth from focus reconstruction using NIH ImageJ plugins: quality and resolution of elevation maps. Microsc Res Tech 75(11):1593-1607.

[180] Paxinos, G., Franklin, K.B.J., 2001. The Mouse Brain in Stereotaxic Coordinates. 2nd ed. Academic: San Diego, CA.

[181] Sato, Y., Nakajima, S., Shiraga, N., Atsumi, H., Yoshida, S., Koller, T., et al., 1998. Three-dimensional multi-scale line filter for segmentation and visualization of curvilinear structures in medical images. Med Image Anal 2(2):143-168.

[182] Rueden, C.T., Schindelin, J., Hiner, M.C., DeZonia, B.E., Walter, A.E., Arena, E.T., et al., 2017. ImageJ2: ImageJ for the next generation of scientific image data. BMC Bioinformatics 18(1):529.

[183] Sears, J.C., Broihier, H.T., 2016. FoxO regulates microtubule dynamics and polarity to promote dendrite branching in Drosophila sensory neurons. Dev Biol 418(1):40-54.

[184] Schindelin, J., Arganda-Carreras, I., Frise, E., Kaynig, V., Longair, M., Pietzsch, T., et al., 2012. Fiji: an open-source platform for biological-image analysis. Nature Methods 9(7):676-682.

[185] Soille, P., Vincent, L.M., 1990. Determining watersheds in digital pictures via flooding simulations. Proc. SPIE 1360:240-250.

[186] Yetnikoff, L., Lavezzi, H.N., Reichard, R.A., Zahm, D.S., 2014. An update on the connections of the ventral mesencephalic dopaminergic complex. Neuroscience.

[187] Aransay, A., Rodriguez-Lopez, C., Garcia-Amado, M., Clasca, F., Prensa, L., 2015. Long-range projection neurons of the mouse ventral tegmental area: a single-cell axon tracing analysis. Frontiers in Neuroanatomy 9.

[188] Beier, K.T., Gao, X.J., Xie, S., DeLoach, K.E., Malenka, R.C., Luo, L., 2019. Topological Organization of Ventral Tegmental Area Connectivity Revealed by Viral-Genetic Dissection of Input-Output Relations. Cell Rep 26(1):159-167.e156.

[189] Wickersham, I.R., Finke, S., Conzelmann, K.K., Callaway, E.M., 2007. Retrograde neuronal tracing with a deletion-mutant rabies virus. Nat Methods 4(1):47-49.

[190] Wickersham, I.R., Lyon, D.C., Barnard, R.J., Mori, T., Finke, S., Conzelmann, K.K., et al., 2007. Monosynaptic restriction of transsynaptic tracing from single, genetically targeted neurons. Neuron 53(5):639-647.

[191] Watabe-Uchida, M., Zhu, L., Ogawa, S.K., Vamanrao, A., Uchida, N., 2012. Whole-Brain Mapping of Direct Inputs to Midbrain Dopamine Neurons. Neuron 74(5):858-873.

[192] Shutter, J.R., Graham, M., Kinsey, A.C., Scully, S., Lüthy, R., Stark, K.L., 1997. Hypothalamic expression of ART, a novel gene related to agouti, is up-regulated in obese and diabetic mutant mice. Genes Dev 11(5):593-602.

[193] Hahn, T.M., Breininger, J.F., Baskin, D.G., Schwartz, M.W., 1998. Coexpression of Agrp and NPY in fasting-activated hypothalamic neurons. Nat Neurosci 1(4):271-272.

[194] Zupanc, G.K., 1996. Peptidergic transmission: from morphological correlates to functional implications. Micron 27(1):35-91.

[195] van den Pol, A.N., 2012. Neuropeptide transmission in brain circuits. Neuron 76(1):98-115.

[196] Ludwig, M., Leng, G., 2006. Dendritic peptide release and peptide-dependent behaviours. Nat Rev Neurosci 7(2):126-136.

[197] Atasoy, D., Betley, J.N., Li, W.P., Su, H.H., Sertel, S.M., Scheffer, L.K., et al., 2014. A genetically specified connectomics approach applied to long-range feeding regulatory circuits. Nat Neurosci 17(12):1830-1839.

[198] Ikemoto, S., 2007. Dopamine reward circuitry: Two projection systems from the ventral midbrain to the nucleus accumbens-olfactory tubercle complex. Brain Research Reviews 56(1):27-78.

[199] Yang, H., de Jong, J.W., Tak, Y., Peck, J., Bateup, H.S., Lammel, S., 2018. Nucleus Accumbens Subnuclei Regulate Motivated Behavior via Direct Inhibition and Disinhibition of VTA Dopamine Subpopulations. Neuron 97(2):434-449.e434.

[200] Sweeney, P., Yang, Y., 2016. An Inhibitory Septum to Lateral Hypothalamus Circuit That Suppresses Feeding. J Neurosci 36(44):11185-11195.

[201] Khan, S., Stott, S.R., Chabrat, A., Truckenbrodt, A.M., Spencer-Dene, B., Nave, K.A., et al., 2017. Survival of a Novel Subset of Midbrain Dopaminergic Neurons Projecting to the Lateral Septum Is Dependent on NeuroD Proteins. J Neurosci 37(9):2305-2316.

[202] Poulin, J.F., Caronia, G., Hofer, C., Cui, Q., Helm, B., Ramakrishnan, C., et al., 2018. Mapping projections of molecularly defined dopamine neuron subtypes using intersectional genetic approaches. Nat Neurosci 21(9):1260-1271.

[203] Jennings, J.H., Ung, R.L., Resendez, S.L., Stamatakis, A.M., Taylor, J.G., Huang, J., et al., 2015. Visualizing hypothalamic network dynamics for appetitive and consummatory behaviors. Cell 160(3):516-527.

[204] Barbano, M.F., Wang, H.L., Morales, M., Wise, R.A., 2016. Feeding and Reward Are Differentially Induced by Activating GABAergic Lateral Hypothalamic Projections to VTA. J Neurosci 36(10):2975-2985.

[205] Nieh, E.H., Vander Weele, C.M., Matthews, G.A., Presbrey, K.N., Wichmann, R., Leppla, C.A., et al., 2016. Inhibitory Input from the Lateral Hypothalamus to the Ventral Tegmental Area Disinhibits Dopamine Neurons and Promotes Behavioral Activation. Neuron 90(6):1286-1298.

[206] Hnasko, T.S., Hjelmstad, G.O., Fields, H.L., Edwards, R.H., 2012. Ventral tegmental area glutamate neurons: electrophysiological properties and projections. J Neurosci 32(43):15076-15085.

[207] Brinschwitz, K., Dittgen, A., Madai, V.I., Lommel, R., Geisler, S., Veh, R.W., 2010. Glutamatergic axons from the lateral habenula mainly terminate on GABAergic neurons of the ventral midbrain. Neuroscience 168(2):463-476.

[208] Stamatakis, A.M., Stuber, G.D., 2012. Activation of lateral habenula inputs to the ventral midbrain promotes behavioral avoidance. Nat Neurosci 15(8):1105-1107.

[209] Rosen, A.M., Victor, J.D., Di Lorenzo, P.M., 2011. Temporal coding of taste in the parabrachial nucleus of the pons of the rat. J Neurophysiol 105(4):1889-1896.

[210] Boughter, J.D., Lu, L., Saites, L.N., Tokita, K., 2019. Sweet and bitter taste stimuli activate VTA projection neurons in the parabrachial nucleus. Brain Res 1714:99-110.

[211] Wu, Q., Boyle, M.P., Palmiter, R.D., 2009. Loss of GABAergic signaling by AgRP neurons to the parabrachial nucleus leads to starvation. Cell 137(7):1225-1234.

[212] Wu, Q., Clark, M.S., Palmiter, R.D., 2012. Deciphering a neuronal circuit that mediates appetite. Nature 483(7391):594-597.

[213] Carter, M.E., Soden, M.E., Zweifel, L.S., Palmiter, R.D., 2013. Genetic identification of a neural circuit that suppresses appetite. Nature 503(7474):111-114.

[214] Ricardo, J.A., Koh, E.T., 1978. Anatomical evidence of direct projections from the nucleus of the solitary tract to the hypothalamus, amygdala, and other forebrain structures in the rat. Brain Res 153(1):1-26.

[215] Herbert, H., Moga, M.M., Saper, C.B., 1990. Connections of the parabrachial nucleus with the nucleus of the solitary tract and the medullary reticular formation in the rat. J Comp Neurol 293(4):540-580.

[216] Karimnamazi, H., Travers, S.P., Travers, J.B., 2002. Oral and gastric input to the parabrachial nucleus of the rat. Brain Res 957(2):193-206.

[217] Campos, C.A., Bowen, A.J., Roman, C.W., Palmiter, R.D., 2018. Encoding of danger by parabrachial CGRP neurons. Nature 555(7698):617-622.

[218] Flegal, K.M., Carroll, M.D., Ogden, C.L., Curtin, L.R., 2010. Prevalence and trends in obesity among US adults, 1999-2008. JAMA 303(3):235-241.

[219] Flegal, K.M., Kruszon-Moran, D., Carroll, M.D., Fryar, C.D., Ogden, C.L., 2016. Trends in Obesity Among Adults in the United States, 2005 to 2014. Jama-Journal of the American Medical Association 315(21):2284-2291.

[220] Khaodhiar, L., McCowen, K.C., Blackburn, G.L., 1999. Obesity and its comorbid conditions. Clin Cornerstone 2(3):17-31.

[221] Hajnal, A., Norgren, R., 2001. Accumbens dopamine mechanisms in sucrose intake. Brain Res 904(1):76-84.

[222] Wang, S., Tan, Y., Zhang, J.E., Luo, M., 2013. Pharmacogenetic activation of midbrain dopaminergic neurons induces hyperactivity. Neurosci Bull 29(5):517-524.

[223] Runegaard, A.H., Sørensen, A.T., Fitzpatrick, C.M., Jørgensen, S.H., Petersen, A.V., Hansen, N.W., et al., 2018. Locomotor- and Reward-Enhancing Effects of Cocaine Are Differentially Regulated by Chemogenetic Stimulation of Gi-Signaling in Dopaminergic Neurons. eNeuro 5(3).

[224] Sandhu, E.C., Fernando, A.B.P., Irvine, E.E., Tossell, K., Kokkinou, M., Glegola, J., et al., 2018. Phasic Stimulation of Midbrain Dopamine Neuron Activity Reduces Salt Consumption. eNeuro 5(2).

[225] Asarian, L., Geary, N., 2013. Sex differences in the physiology of eating. American Journal of Physiology-Regulatory Integrative and Comparative Physiology 305(11):R1215-R1267.

[226] Shi, H., Seeley, R.J., Clegg, D.J., 2009. Sexual differences in the control of energy homeostasis. Front Neuroendocrinol 30(3):396-404.

[227] Stincic, T.L., Rønnekleiv, O.K., Kelly, M.J., 2018. Diverse actions of estradiol on anorexigenic and orexigenic hypothalamic arcuate neurons. Horm Behav 104:146-155.

[228] Hubbard, K., Shome, A., Sun, B., Pontré, B., McGregor, A., Mountjoy, K.G., 2019. Chronic High-Fat Diet Exacerbates Sexually Dimorphic Pomctm1/tm1 Mouse Obesity. Endocrinology 160(5):1081-1096.

[229] Morissette, M., Di Paolo, T., 1993. Sex and estrous cycle variations of rat striatal dopamine uptake sites. Neuroendocrinology 58(1):16-22.

[230] Becker, J.B., 2016. Sex differences in addiction. Dialogues Clin Neurosci 18(4):395-402.

[231] Calipari, E.S., Juarez, B., Morel, C., Walker, D.M., Cahill, M.E., Ribeiro, E., et al., 2017. Dopaminergic dynamics underlying sex-specific cocaine reward. Nat Commun 8:13877.

[232] Woodward, C.J., Emery, P.W., 1989. Energy balance in rats given chronic hormone treatment. 2. Effects of corticosterone. Br J Nutr 61(3):445-452.

[233] Benz, V., Bloch, M., Wardat, S., Böhm, C., Maurer, L., Mahmoodzadeh, S., et al., 2012. Sexual dimorphic regulation of body weight dynamics and adipose tissue lipolysis. PLoS One 7(5):e37794.

[234] Yang, Y., Smith, D.L., Keating, K.D., Allison, D.B., Nagy, T.R., 2014. Variations in body weight, food intake and body composition after long-term high-fat diet feeding in C57BL/6J mice. Obesity (Silver Spring) 22(10):2147-2155.

[235] Nohara, K., Zhang, Y., Waraich, R.S., Laque, A., Tiano, J.P., Tong, J., et al., 2011. Early-life exposure to testosterone programs the hypothalamic melanocortin system. Endocrinology 152(4):1661-1669.

[236] Wang, C., He, Y., Xu, P., Yang, Y., Saito, K., Xia, Y., et al., 2018. TAp63 contributes to sexual dimorphism in POMC neuron functions and energy homeostasis. Nat Commun 9(1):1544.

[237] Liu, H., Kishi, T., Roseberry, A.G., Cai, X., Lee, C.E., Montez, J.M., et al., 2003. Transgenic mice expressing green fluorescent protein under the control of the melanocortin-4 receptor promoter. J Neurosci 23(18):7143-7154.

[238] Gantz, I., Konda, Y., Tashiro, T., Shimoto, Y., Miwa, H., Munzert, G., et al., 1993. Molecular cloning of a novel melanocortin receptor. J Biol Chem 268(11):8246-8250.

[239] Gantz, I., Miwa, H., Konda, Y., Shimoto, Y., Tashiro, T., Watson, S.J., et al., 1993. Molecular cloning, expression, and gene localization of a fourth melanocortin receptor. J Biol Chem 268(20):15174-15179.

[240] Schneider, L.H., 1986. Selective D-1 or D-2 receptor antagonists inhibit sucrose sham feeding in rats. Appetite. 7(3):294.

[241] Baldo, B.A., Sadeghian, K., Basso, A.M., Kelley, A.E., 2002. Effects of selective dopamine D1 or D2 receptor blockade within nucleus accumbens subregions on ingestive behavior and associated motor activity. Behav Brain Res 137(1-2):165-177.

[242] Liu, S., Borgland, S.L., 2015. Regulation of the mesolimbic dopamine circuit by feeding peptides. Neuroscience 289C:19-42.

[243] Korotkova, T.M., Brown, R.E., Sergeeva, O.A., Ponomarenko, A.A., Haas, H.L., 2006. Effects of arousal- and feeding-related neuropeptides on dopaminergic and GABAergic neurons in the ventral tegmental area of the rat. Eur J Neurosci 23(10):2677-2685.

[244] West, K.S., Roseberry, A.G., 2017. Neuropeptide-Y alters VTA dopamine neuron activity through both pre- and postsynaptic mechanisms. J Neurophysiol 118(1):625-633.

[245] Pandit, R., Luijendijk, M.C., Vanderschuren, L.J., la Fleur, S.E., Adan, R.A., 2014. Limbic substrates of the effects of neuropeptide Y on intake of and motivation for palatable food. Obesity (Silver Spring) 22(5):1216-1219.

[246] Wanat, M.J., Hopf, F.W., Stuber, G.D., Phillips, P.E., Bonci, A., 2008. Corticotropin-releasing factor increases mouse ventral tegmental area dopamine neuron firing through a protein kinase C-dependent enhancement of Ih. J Physiol 586(8):2157-2170.

[247] Wanat, M.J., Bonci, A., Phillips, P.E., 2013. CRF acts in the midbrain to attenuate accumbens dopamine release to rewards but not their predictors. Nat Neurosci 16(4):383-385.

[248] Steffensen, S.C., Svingos, A.L., Pickel, V.M., Henriksen, S.J., 1998. Electrophysiological characterization of GABAergic neurons in the ventral tegmental area. J Neurosci 18(19):8003-8015.

[249] Root, D.H., Zhang, S., Barker, D.J., Miranda-Barrientos, J., Liu, B., Wang, H.L., et al., 2018. Selective Brain Distribution and Distinctive Synaptic Architecture of Dual Glutamatergic-GABAergic Neurons. Cell Rep 23(12):3465-3479.

[250] Tritsch, N.X., Ding, J.B., Sabatini, B.L., 2012. Dopaminergic neurons inhibit striatal output through non-canonical release of GABA. Nature 490(7419):262-266.

[251] Yoo, J.H., Zell, V., Gutierrez-Reed, N., Wu, J., Ressler, R., Shenasa, M.A., et al., 2016. Ventral tegmental area glutamate neurons co-release GABA and promote positive reinforcement. Nat Commun 7:13697.

[252] Qi, J., Zhang, S., Wang, H.-L., Barker, D.J., Miranda-Barrientos, J., Morales, M., 2016. VTA glutamatergic inputs to nucleus accumbens drive aversion by acting on GABAergic interneurons. Nat Neurosci advance online publication.

[253] Tan, K.R., Yvon, C., Turiault, M., Mirzabekov, J.J., Doehner, J., Labouèbe, G., et al., 2012. GABA neurons of the VTA drive conditioned place aversion. Neuron 73(6):1173-1183.

[254] Zigmond, M.J., Stricker, E.M., 1972. Deficits in feeding behavior after intraventricular injection of 6-hydroxydopamine in rats. Science 177(4055):1211-1214.

[255] Szczypka, M.S., Rainey, M.A., Kim, D.S., Alaynick, W.A., Marck, B.T., Matsumoto, A.M., et al., 1999. Feeding behavior in dopamine-deficient mice. Proc Natl Acad Sci U S A 96(21):12138-12143.

[256] Petersen, S., 1976. The temporal pattern of feeding over the oestrous cycle of the mouse. Animal behaviour 24(4):939-955.

[257] Stuber, G.D., Wise, R.A., 2016. Lateral hypothalamic circuits for feeding and reward. Nat Neurosci 19(2):198-205.

[258] Jennings, J.H., Rizzi, G., Stamatakis, A.M., Ung, R.L., Stuber, G.D., 2013. The inhibitory circuit architecture of the lateral hypothalamus orchestrates feeding. Science 341(6153):1517-1521.

[259] Hao, S., Yang, H., Wang, X., He, Y., Xu, H., Wu, X., et al., 2019. The Lateral Hypothalamic and BNST GABAergic Projections to the Anterior Ventrolateral Periaqueductal Gray Regulate Feeding. Cell Rep 28(3):616-624.e615.

[260] Luo, M., Zhou, J., Liu, Z., 2015. Reward processing by the dorsal raphe nucleus: 5-HT and beyond. Learn Mem 22(9):452-460.

[261] Nectow, A.R., Schneeberger, M., Zhang, H.X., Field, B.C., Renier, N., Azevedo, E., et al., 2017. Identification of a Brainstem Circuit Controlling Feeding. Cell 170(3):429-+.

[262] Goudie, A.J., Thornton, E.W., Wheeler, T.J., 1976. Effects of Lilly 110140, a specific inhibitor of 5-hydroxytryptamine uptake, on food intake and on 5-hydroxytryptophan-induced anorexia. Evidence for serotoninergic inhibition of feeding. J Pharm Pharmacol 28(4):318-320.

[263] Sanders, A.C., Hussain, A.J., Hen, R., Zhuang, X., 2007. Chronic blockade or constitutive deletion of the serotonin transporter reduces operant responding for food reward. Neuropsychopharmacology 32(11):2321-2329.

[264] Faton, S., Tassin, J.P., Duranton, F., Bagnol, D., Lajoix, A.D., 2018. 5-HT. Behav Brain Res 347:234-241.

[265] Valencia-Torres, L., Olarte-Sanchez, C.M., Lyons, D.J., Georgescu, T., Greenwald-Yarnell, M., Myers, M.G., Jr., et al., 2016. Activation of Ventral Tegmental Area 5-HT2C Receptors Reduces Incentive Motivation. Neuropsychopharmacology : official publication of the American College of Neuropsychopharmacology.

[266] Browne, C.J., Abela, A.R., Chu, D., Li, Z., Ji, X., Lambe, E.K., et al., 2019. Dorsal raphe serotonin neurons inhibit operant responding for reward via inputs to the ventral tegmental area but not the nucleus accumbens: evidence from studies combining optogenetic stimulation and serotonin reuptake inhibition. Neuropsychopharmacology 44(4):793-804.

[267] Lammel, S., Lim, B.K., Ran, C., Huang, K.W., Betley, M.J., Tye, K.M., et al., 2012. Input-specific control of reward and aversion in the ventral tegmental area. Nature 491(7423):212-217.

[268] Lammel, S., Ion, D.I., Roeper, J., Malenka, R.C., 2011. Projection-specific modulation of dopamine neuron synapses by aversive and rewarding stimuli. Neuron 70(5):855-862.

[269] Walker, Q.D., Ray, R., Kuhn, C.M., 2006. Sex differences in neurochemical effects of dopaminergic drugs in rat striatum. Neuropsychopharmacology 31(6):1193-1202.

[270] Virdee, K., McArthur, S., Brischoux, F., Caprioli, D., Ungless, M.A., Robbins, T.W., et al., 2014. Antenatal glucocorticoid treatment induces adaptations in adult midbrain dopamine neurons, which underpin sexually dimorphic behavioral resilience. Neuropsychopharmacology 39(2):339-350.

[271] Becker, J.B., McClellan, M.L., Reed, B.G., 2017. Sex differences, gender and addiction. J Neurosci Res 95(1-2):136-147.

[272] Becker, J.B., 1999. Gender differences in dopaminergic function in striatum and nucleus accumbens. Pharmacology Biochemistry and Behavior 64(4):803-812.

[273] Fink, G., Sumner, B.E., Rosie, R., Grace, O., Quinn, J.P., 1996. Estrogen control of central neurotransmission: effect on mood, mental state, and memory. Cell Mol Neurobiol 16(3):325-344.

[274] Xiao, L., Becker, J.B., 1994. Quantitative microdialysis determination of extracellular striatal dopamine concentration in male and female rats: effects of estrous cycle and gonadectomy. Neurosci Lett 180(2):155-158.

[275] Ohtani, H., Nomoto, M., Douchi, T., 2001. Chronic estrogen treatment replaces striatal dopaminergic function in ovariectomized rats. Brain Res 900(2):163-168.

[276] Pasqualini, C., Olivier, V., Guibert, B., Frain, O., Leviel, V., 1995. Acute stimulatory effect of estradiol on striatal dopamine synthesis. J Neurochem 65(4):1651-1657.

[277] McArthur, S., Murray, H.E., Dhankot, A., Dexter, D.T., Gillies, G.E., 2007. Striatal susceptibility to a dopaminergic neurotoxin is independent of sex hormone effects on cell survival and DAT expression but is exacerbated by central aromatase inhibition. J Neurochem 100(3):678-692.

[278] Kritzer, M.F., Creutz, L.M., 2008. Region and sex differences in constituent dopamine neurons and immunoreactivity for intracellular estrogen and androgen receptors in mesocortical projections in rats. Journal of Neuroscience 28(38):9525-9535.

[279] McArthur, S., McHale, E., Gillies, G.E., 2007. The size and distribution of midbrain dopaminergic populations are permanently altered by perinatal glucocorticoid exposure in a sex- region- and time-specific manner. Neuropsychopharmacology 32(7):1462-1476.

[280] Sibug, R., Küppers, E., Beyer, C., Maxson, S.C., Pilgrim, C., Reisert, I., 1996. Genotype-dependent sex differentiation of dopaminergic neurons in primary cultures of embryonic mouse brain. Brain Res Dev Brain Res 93(1-2):136-142.

[281] Dewing, P., Chiang, C.W., Sinchak, K., Sim, H., Fernagut, P.O., Kelly, S., et al., 2006. Direct regulation of adult brain function by the male-specific factor SRY. Curr Biol 16(4):415-420.

[282] Czech, D.P., Lee, J., Sim, H., Parish, C.L., Vilain, E., Harley, V.R., 2012. The human testis-determining factor SRY localizes in midbrain dopamine neurons and regulates multiple components of catecholamine synthesis and metabolism. J Neurochem 122(2):260-271.

[283] Milsted, A., Serova, L., Sabban, E.L., Dunphy, G., Turner, M.E., Ely, D.L., 2004. Regulation of tyrosine hydroxylase gene transcription by Sry. Neurosci Lett 369(3):203-207.

[284] Atasoy, D., Betley, J.N., Su, H.H., Sternson, S.M., 2012. Deconstruction of a neural circuit for hunger. Nature 488(7410):172-177.

[285] Zhan, C., Zhou, J., Feng, Q., Zhang, J.E., Lin, S., Bao, J., et al., 2013. Acute and long-term suppression of feeding behavior by POMC neurons in the brainstem and hypothalamus, respectively. J Neurosci 33(8):3624-3632.

[286] Kishi, T., Aschkenasi, C.J., Choi, B.J., Lopez, M.E., Lee, C.E., Liu, H., et al., 2005. Neuropeptide Y Y1 receptor mRNA in rodent brain: distribution and colocalization with melanocortin-4 receptor. J Comp Neurol 482(3):217-243.

[287] Wolak, M.L., DeJoseph, M.R., Cator, A.D., Mokashi, A.S., Brownfield, M.S., Urban, J.H., 2003. Comparative distribution of neuropeptide Y Y1 and Y5 receptors in the rat brain by using immunohistochemistry. J Comp Neurol 464(3):285-311.

[288] Ramamoorthy, P., Wang, Q., Whim, M.D., 2011. Cell type-dependent trafficking of neuropeptide Y-containing dense core granules in CNS neurons. J Neurosci 31(41):14783-14788.

[289] Tracy, A.L., Clegg, D.J., Johnson, J.D., Davidson, T.L., Benoit, S.C., 2008. The melanocortin antagonist AgRP (83-132) increases appetitive responding for a fat, but not a carbohydrate, reinforcer. Pharmacol Biochem Behav 89(3):263-271.

[290] Van Den Heuvel, J., Eggels, L., van Rozen, A., Fliers, E., Kalsbeek, A., Adan, R., et al., 2015. Inhibitory effect of the melanocortin receptor agonist melanotan-II (MTII) on feeding depends on dietary fat content and not obesity in rats on free-choice diets. Frontiers in Behavioral Neuroscience 9.

[291] Figlewicz, D.P., Jay, J.L., Acheson, M.A., Magrisso, I.J., West, C.H., Zavosh, A., et al., 2013. Moderate high fat diet increases sucrose self-administration in young rats. Appetite 61(1):19-29.

APPENDICES

Appendix A

Table 0.1. Number of RVdG labeled neurons across the entire brain.

Brain area	Abbr.	Region	Sub-region	RVdG labeling
Field CA3 of hippocampus	CA3	Cerebral cortex	Cortical plate	-
Retrosplenial cortex	RS	Cerebral cortex	Cortical plate	+
Motor cortex	M	Cerebral cortex	Cortical plate	+
Somatosensory cortex	S1/S2	Cerebral cortex	Cortical plate	+
Secondary visual cortex	V2	Cerebral cortex	Cortical plate	-
Secondary auditory cortex	Au	Cerebral cortex	Cortical plate	-
Medial parietal association cortex	MPtA	Cerebral cortex	Cortical plate	-
Insular cortex	ICrtx	Cerebral cortex	Cortical plate	+
Ectorhinal cortex	Ect	Cerebral cortex	Cortical plate	+
Perirhinal cortex	PRh	Cerebral cortex	Cortical plate	+
Temporal association cortex	TeA	Cerebral cortex	Cortical plate	-
Cingulate cortex	Cg	Cerebral cortex	Cortical plate	+
Prelimbic cortex	PrL	Cerebral cortex	Cortical plate	+
Infralimbic cortex	IL	Cerebral cortex	Cortical plate	+
Orbital cortex	OC	Cerebral cortex	Cortical plate	+
Anterior olfactory nucleus	AO	Cerebral cortex	Cortical plate	-
Dorsal peduncular cortex	DP	Cerebral cortex	Cortical plate	+
Dorsal tenia tecta	DTT	Cerebral cortex	Cortical plate	+

Nucleus of the lateral olfactory tract	LOT	Cerebral cortex	Cortical plate	+
Piriform cortex	Pir	Cerebral cortex	Cortical plate	+
Claustrum	Cl	Cerebral cortex	Cortical subplate	+
Endopiriform nucleus	En	Cerebral cortex	Cortical subplate	+
Caudate putamen	CPu	Cerebral nuclei	Striatum	+
Lateral septal nuclei	LS	Cerebral nuclei	Striatum	+
Septofimbrial nucleus	SFi	Cerebral nuclei	Striatum	-
Septohippocampal nucleus	SHi	Cerebral nuclei	Striatum	-
Nucleus accumbens	Acb	Cerebral nuclei	Striatum	+++++
Olfactory tubercle	Tu	Cerebral nuclei	Striatum	+
Lateral stripe of the striatum	LSS	Cerebral nuclei	Striatum	-
IPAC	IPAC	Cerebral nuclei	Striatum	++
Medial globus pallidus	MGP	Cerebral nuclei	Pallidum	+
Lateral globus pallidus	LGP	Cerebral nuclei	Pallidum	+
Medial septal nucleus	MS	Cerebral nuclei	Pallidum	+
Nucleus of the diagonal band	NDB	Cerebral nuclei	Pallidum	+
Triangular septal nucleus	TS	Cerebral nuclei	Pallidum	-
Magnocellular preoptic nucleus	MCPO	Cerebral nuclei	Pallidum	++

BST	BST	Cerebral nuclei	Pallidum	++
Ventral pallidum	VP	Cerebral nuclei	Pallidum	+++++
Substantia innominata	SI	Cerebral nuclei	Pallidum	++
Central amygdala	CeA	Amygdala	Striatum	++
Medial amygdala	MeA	Amygdala	Striatum	+
Basomedial amygdala	BMa	Amygdala	Cortical subplate	+
Basolateral amygdala	BLa	Amygdala	Cortical subplate	+
Cortical amygdalar area	CoA	Amygdala	Cortical plate	+
Anterior amygdaloid area	AA	Amygdala	Striatum	+
Intercalated amygdaloid nucleus	IM	Amygdala	Striatum	-
Amygdalostriatal transition area	Astr	Amygdala	Striatum	-
Lateral habenular nucleus	LHb	Diencephalon	Thalamus	++++
Medial habenular nucleus	MHb	Diencephalon	Thalamus	+
Ethmoid thalamic nucleus	Eth	Diencephalon	Thalamus	+
Retroethmoid nucleus	REth	Diencephalon	Thalamus	-
Supragenicular thalamic nucleus	SG	Diencephalon	Thalamus	-
Anterior group of the dorsal thalamus	ATN	Diencephalon	Thalamus	-

Mediodorsal thalamic nucleus	MD	Diencephalon	Thalamus	-
Submedius thalamic nucleus	Sub	Diencephalon	Thalamus	-
Paratenial thalamic nucleus	PT	Diencephalon	Thalamus	+
Paraventricular thalamic nucleus	PeT	Diencephalon	Thalamus	+
Reuniens thalamic nucleus	Re	Diencephalon	Thalamus	+
Parafascicular thalamic nucleus	PF	Diencephalon	Thalamus	+
Posterior intralaminar thalamic nucleus	PIL	Diencephalon	Thalamus	-
Reticular thalamic nucleus	Rt	Diencephalon	Thalamus	+
Ventromedial thalamic nucleus	VM	Diencephalon	Thalamus	+
Subparafascicular thalamic nucleus	SPF	Diencephalon	Thalamus	+
Peripeduncular nucleus	PP	Diencephalon	Thalamus	+
Geniculate thalamic group	GEN	Diencephalon	Thalamus	+
A14 dopamine cells	A14	Diencephalon	Hypothalamus	-
Anterior commissural nucleus	AC	Diencephalon	Hypothalamus	+

Anterodorsal preoptic nucleus	ADP	Diencephalon	Hypothalamus	+
Median preoptic nucleus	MnPO	Diencephalon	Hypothalamus	-
Parastrial nucleus	PS	Diencephalon	Hypothalamus	+
Ventrolateral preoptic nucleus	VLPO	Diencephalon	Hypothalamus	+
Ventromedial preoptic nucleus	VMPO	Diencephalon	Hypothalamus	-
Medial preoptic nucleus	MPO	Diencephalon	Hypothalamus	++
Supraoptic nucleus	SO	Diencephalon	Hypothalamus	+
Paraventricular hypothalamic nucleus	PVH	Diencephalon	Hypothalamus	++
Periventricular hypothalamic nucleus	PeH	Diencephalon	Hypothalamus	+
Vascular organ of the lamina terminalis	VOLT	Diencephalon	Hypothalamus	+
Suprachiasmatic nucleus	Sch	Diencephalon	Hypothalamus	-
Dorsomedial hypothalamic nucleus	DMH	Diencephalon	Hypothalamus	++
Arcuate hypothalamic nucleus	Arc	Diencephalon	Hypothalamus	+
Anterior hypothalamus	AH	Diencephalon	Hypothalamus	+
Ventromedial hypothalamic nucleus	VMH	Diencephalon	Hypothalamus	+

Tuberomammillary nucleus	VTM	Diencephalon	Hypothalamus	+
Posterior hypothalamic area	PH	Diencephalon	Hypothalamus	++
Mammillary nucleus	MN	Diencephalon	Hypothalamus	++
Premammillary nucleus	PM	Diencephalon	Hypothalamus	+
Supramammillary nucleus	SuM	Diencephalon	Hypothalamus	++
Lateral preoptic area	LPO	Diencephalon	Hypothalamus	+++
Lateral hypothalamic area	LH	Diencephalon	Hypothalamus	+++++
Medial tuberal nucleus	MTu	Diencephalon	Hypothalamus	++
Parasubthalamic nucleus	PSTh	Diencephalon	Hypothalamus	++
Subthalamic nucleus	STh	Diencephalon	Hypothalamus	+
Zona incerta	ZI	Diencephalon	Hypothalamus	++
Interpeduncular nucleus	IP	Midbrain	Behavioral state related	+
Dorsal raphe	DR	Midbrain	Behavioral state related	+++++
Pedunculopontine tegmental nucleus	PPTg	Midbrain	Behavioral state related	++
Substantia nigra	SN	Midbrain	Behavioral state/motor related	+++
Interstitial nucleus of Cajal	InC	Midbrain	Motor related	+
Nucleus of Darkschewitsch	Dk	Midbrain	Motor related	+

Periaqueductal gray	PAG	Midbrain	Motor related	+++
Precommissural nucleus	PrC	Midbrain	Motor related	-
Supraoculomotor periaqueductal gray	Su3	Midbrain	Motor related	+++
Anterior pretectal nucleus	APT	Midbrain	Motor related	+
Nucleus of the posterior commissure	NPC	Midbrain	Motor related	+
Posterior pretectal nucleus	PPT	Midbrain	Motor related	-
Retroparafascicular nucleus	RPF	Midbrain	Motor related	-
Superior colliculus	SC	Midbrain	Motor related	++++
Inferior colliculus	IC	Midbrain	Sensory related	+
Cuneiform nucleus	CnF	Midbrain	Motor related	+
Dorsal terminal nucleus of the accessory optic tract	DT	Midbrain	Motor related	+
Dorsomedial tegmental area	DMTg	Midbrain	Motor related	++
Edinger-Westphal nucleus	EW	Midbrain	Motor related	+
Intercollicular nucleus	InCo	Midbrain	Motor related	+
Medial accessory oculomotor nucleus	MA3	Midbrain	Motor related	-
Midbrain reticular nucleus	MRN	Midbrain	Motor related	+++
Oculomotor nucleus	3N	Midbrain	Motor related	+
Parabigeminal nucleus	PBG	Midbrain	Motor related	-

Paratrochlear nucleus	Pa4	Midbrain	Motor related	+
Red nucleus	RN	Midbrain	Motor related	+
Retrorubral nucleus and field	RR	Midbrain	Motor related	++
Rostral interstitial nucleus of medial longitudinal fasciculus	RI	Midbrain	Motor related	-
Tegmental nucleus	TN	Midbrain	Motor related	++
Sagulum nucleus	Sag	Midbrain	Sensory related	-
Median raphe nucleus	MnR	Hindbrain	Pons	+++
Paramedian raphe nucleus	PMnR	Hindbrain	Pons	++
Pontine reticular nucleus	PRNr	Hindbrain	Pons	++
Laterodorsal tegmental nucleus	LDTg	Hindbrain	Pons	++
Locus coeruleus	LC	Hindbrain	Pons	+
Subcoeruleus nucleus	SubC	Hindbrain	Pons	+
Lateral parabrachial nucleus	LPB	Hindbrain	Pons	++++
Medial parabrachial nucleus	MPB	Hindbrain	Pons	++
Barrington's nucleus	Bar	Hindbrain	Pons	+
Central gray	CG	Hindbrain	Pons	+
Dorsal tegmental nucleus	DTg	Hindbrain	Pons	+

Intertrigeminal nucleus	I5	Hindbrain	Pons	-
Motor trigeminal nucleus	Mo5	Hindbrain	Pons	+
Posterodorsal tegmental nucleus	PDTg	Hindbrain	Pons	+
Reticulotegmental nucleus of the pons	RtTg	Hindbrain	Pons	+
Supratrigeminal nucleus	Su5	Hindbrain	Pons	+
Koelliker-Fuse nucleus	KF	Hindbrain	Pons	+
Nucleus of lateral lemniscus	NLL	Hindbrain	Pons	+
Periolivary region	RPO	Hindbrain	Pons	-
Principal sensory trigeminal nucleus	Pr5	Hindbrain	Pons	+
Raphe magnus nucleus	RMg	Hindbrain	Medulla	++
Raphe pallidus nucleus	RPa	Hindbrain	Medulla	-
Facial nucleus	7N	Hindbrain	Medulla	+
Gigantocellular reticular nucleus	Gi	Hindbrain	Medulla	+
Intermediate reticular nucleus	IRt	Hindbrain	Medulla	+
Paraabducens nucleus	Pa6	Hindbrain	Medulla	-
Paragigantocellular nucleus	PGi	Hindbrain	Medulla	+

Parvicellular reticular nucleus	PCRt	Hindbrain	Medulla	+
Prepositus nucleus	Pr	Hindbrain	Medulla	+
Rostroventrolateral reticular nucleus	RVL	Hindbrain	Medulla	-
Vestibular nuclei	Ve	Hindbrain	Medulla	+
Interposed cerebellar nucleus	Int	Cerebellum	Cerebellar nuclei	+
Lateral (dentate) cerebellar nucleus	Lat	Cerebellum	Cerebellar nuclei	+
Medial (fastigial) cerebellar nucleus	Med	Cerebellum	Cerebellar nuclei	-
medial lemniscus	ml	tract		-
medial longitudinal fasciculus	mlf	tract		-
decussation of the superior cerebellar peduncle	xscp	tract		-
Periventricular fiber system	pv	tract		-
Superior cerebellar peduncle	scp	tract		-
cerebral peduncle	cp	tract		-
dorsal fornix	df	tract		-

tectospinal tract	ts	tract		-
commissure of the superior colliculus	csc	tract		+
commissure of the inferior colliculus	cic	tract		+
cingulum	cg	tract		+
Probst's bundle	prb	tract		+
internal capsule	ic	tract		+
Mammillothalamic tract	mt	tract		+

Legend: - <1; + 1-26; ++27-89, +++90-153, ++++154-218; +++++219-564

Appendix B

Table 0.2. Results of Statistical Analyses for DREADD data.

Acute CNO: cumulative food intake

Interactions:

time * drug * GROUP: F(8,76)=1.445, p=0.192

drug * GROUP * sex: F(2,19)=6.263, p=0.008

time * drug * GROUP * sex: F(8,76)=3.019, p=0.005

post hoc tests:

drug * GROUP * sex (drug)

	group	***sex***	***comparison***	***p-value***	***significant***
	Ctrl	M	CNO vs. vehicle	0.733	no
	Ctrl	F	CNO vs. vehicle	0.363	no
	Gq	M	CNO vs. vehicle	0.002	yes
	Gq	F	CNO vs. vehicle	0.03	yes

time * drug * GROUP * sex (drug)

time (hr)	***group***	***sex***	***comparison***	***p-value***	***significant***
1	Gi	M	CNO vs. vehicle	0.002	yes
2	Gi	M	CNO vs. vehicle	0.003	yes
3	Gi	M	CNO vs. vehicle	0.009	yes
4	Gi	M	CNO vs. vehicle	0.005	yes
24	Gi	M	CNO vs. vehicle	0.015	yes

2	Gq	F	CNO vs. vehicle	0.049	yes
3	Gq	F	CNO vs. vehicle	0.083	no (trend)
4	Gq	F	CNO vs. vehicle	0.072	no (trend)
24	Gq	F	CNO vs. vehicle	0.021	yes
24	Gq	M	CNO vs. vehicle	0.015	yes

Acute CNO: Δ body weight

Interactions:

drug * group: F(2,19)=0.592, p=0.563

drug * group * sex: F(2,19)=0.630, p=0.543

Chronic CNO: daily food intake

Interactions:

time * group: F(16,152)=2.109, p=0.010

time * group * sex : F(16,152)=0.795, p=0.689

post hoc tests:

time * group (group)

time (day)	***group***	***sex***	***comparison***	***p-value***	***significant***
1	Gq	all	vs. ctrl	0.096	no (trend)
1	Gq	all	vs. Gi	0.012	yes
2	Gq	all	vs. Gi	0.071	no (trend)
3	Gq	all	vs. ctrl	0.099	no (trend)

Chronic CNO: daily food intake normalized to mean baseline food intake

Interactions:

time * group: F(16,152)=2.130, p=0.010

post hoc tests:

time * group (group)

time (day)	***group***	***sex***	***comparison***	***p-value***	***significant***
1	Gq	all	vs. Gi	0.013	yes
2	Gq	all	vs. Gi	0.069	no (trend)
3	Gq	all	vs. ctrl	0.013	yes
3	Gq	all	vs. Gi	0.085	no (trend)

time * group (time)

time (day)	***group***	***sex***	***comparison***	***p-value***	***significant***
baseline	ctrl	all	vs. day 1	0.017	yes
baseline	ctrl	all	vs. day 2	0.015	yes
baseline	ctrl	all	vs. day 3	0	yes
baseline	ctrl	all	vs. day 4	0.078	no (trend)
1	ctrl	all	vs. day 0	0.017	yes
1	ctrl	all	vs. day 7	0.029	yes
2	ctrl	all	vs. day 0	0.015	yes
2	ctrl	all	vs. day 7	0.022	yes
3	ctrl	all	vs. day 0	0	yes

3	ctrl	all	vs. day 6	0.097	no (trend)
3	ctrl	all	vs. day 7	0.005	yes
3	ctrl	all	vs. day 8	0.009	yes
4	ctrl	all	vs. day 0	0.078	no (trend)
4	ctrl	all	vs. day 7	0.04	yes
6	ctrl	all	vs. day 3	0.097	no (trend)
6	ctrl	all	vs. day 7	0.069	no (trend)
7	ctrl	all	vs. day 1	0.029	yes
7	ctrl	all	vs. day 2	0.022	yes
7	ctrl	all	vs. day 3	0.005	yes
7	ctrl	all	vs. day 4	0.04	yes
7	ctrl	all	vs. day 6	0.069	no (trend)
8	ctrl	all	vs. day 3	0.009	yes
0	Gq	all	vs. day 1	0.001	yes
0	Gq	all	vs. day 2	0.003	yes
1	Gq	all	vs. day 0	0.001	yes
1	Gq	all	vs. day 3	0.017	yes
1	Gq	all	vs. day 4	0.053	no (trend)
1	Gq	all	vs. day 5	0.004	yes
1	Gq	all	vs. day 6	0.014	yes
1	Gq	all	vs. day 7	0.001	yes
1	Gq	all	vs. day 8	0.013	yes
2	Gq	all	vs. day 0	0.003	yes
2	Gq	all	vs. day 3	0.01	yes

2	Gq	all	vs. day 4	0.052	no (trend)
2	Gq	all	vs. day 5	0.022	yes
2	Gq	all	vs. day 6	0.063	no (trend)
2	Gq	all	vs. day 7	0.003	yes
2	Gq	all	vs. day 8	0.054	no (trend)
3	Gq	all	vs. day 1	0.017	yes
3	Gq	all	vs. day 2	0.01	yes
4	Gq	all	vs. day 1	0.053	no (trend)
4	Gq	all	vs. day 2	0.052	no (trend)
4	Gq	all	vs. day 7	0.027	yes
5	Gq	all	vs. day 1	0.004	yes
5	Gq	all	vs. day 2	0.022	yes
6	Gq	all	vs. day 1	0.014	yes
6	Gq	all	vs. day 2	0.063	no (trend)
6	Gq	all	vs. day 7	0.057	no (trend)
7	Gq	all	vs. day 1	0.001	yes
7	Gq	all	vs. day 2	0.003	yes
7	Gq	all	vs. day 4	0.027	yes
7	Gq	all	vs. day 6	0.057	no (trend)
7	Gq	all	vs. day 8	0.03	yes
8	Gq	all	vs. day 0	0.094	no (trend)
8	Gq	all	vs. day 1	0.013	yes
8	Gq	all	vs. day 2	0.054	no (trend)
8	Gq	all	vs. day 7	0.03	yes

0	Gi	all	vs. day 3	0.019	yes
0	Gi	all	vs. day 6	0.084	no (trend)
0	Gi	all	vs. day 8	0.003	yes
3	Gi	all	vs. day 0	0.019	yes
6	Gi	all	vs. day 0	0.084	no (trend)
8	Gi	all	vs. day 0	0.003	yes

Chronic CNO: cumulative Δ change in body weight

Interactions:

time * group: F(16,152)=1.722, p=0.048

time * group * sex: F(16,152)=0.879, p=0.594

post hoc tests:

time * group (group)

time (day)	***group***	***sex***	***comparison***	***p-value***	***significant***
1	Gq	all	vs. ctrl	0.041	yes
1	Gq	all	vs. Gi	0.011	yes
2	Gq	all	vs. Gi	0.024	yes
3	Gq	all	vs. Gi	0.092	no (trend)

Chronic CNO: daily body weight normalized to mean baseline body weight

Interactions:

time * group: F(16,152)=1.950, p=0.020

time * group * sex: F(16,152)=0.830, p=0.650

post hoc tests:

time * group (group)

time (day)	***group***	***sex***	***comparison***	***p-value***	***significant***
1	Gq	all	vs. ctrl	0.037	yes
1	Gq	all	vs. Gi	0.016	yes
2	Gq	all	vs. Gi	0.024	yes
3	Gq	all	vs. Gi	0.061	no (trend)

time * group (time)

time (day)	***group***	***sex***	***comparison***	***p-value***	***significant***
baseline	ctrl	all	day 2	0.038	yes
baseline	ctrl	all	day 3	0.005	yes
baseline	ctrl	all	day 4	0.019	yes
baseline	ctrl	all	day 5	0.01	yes
baseline	ctrl	all	day 6	0.003	yes
1	ctrl	all	day 2	0.073	no (trend)
1	ctrl	all	day 3	0.028	yes
1	ctrl	all	day 4	0.078	no (trend)
1	ctrl	all	day 5	0.047	yes
1	ctrl	all	day 6	0.012	yes
2	ctrl	all	day 0	0.038	yes
2	ctrl	all	day 1	0.073	no (trend)
3	ctrl	all	day 0	0.005	yes

3	ctrl	all	day 1	0.028	yes
3	ctrl	all	day 7	0.069	
3	ctrl	all	day 8	0.042	yes
4	ctrl	all	day 0	0.019	yes
4	ctrl	all	day 1	0.078	no (trend)
5	ctrl	all	day 0	0.01	yes
5	ctrl	all	day 1	0.047	yes
6	ctrl	all	day 0	0.003	yes
6	ctrl	all	day 1	0.012	yes
6	ctrl	all	day 7	0.041	yes
6	ctrl	all	day 8	0.05	no (trend)
7	ctrl	all	day 3	0.069	no (trend)
7	ctrl	all	day 6	0.041	yes
8	ctrl	all	day 3	0.042	yes
8	ctrl	all	day 6	0.05	yes
baseline	Gq	all	day 1	0.004	yes
baseline	Gq	all	day 2	0.001	yes
baseline	Gq	all	day 3	0.001	yes
baseline	Gq	all	day 4	0.006	yes
baseline	Gq	all	day 5	0.016	yes
baseline	Gq	all	day 6	0.078	no (trend)
1	Gq	all	day 0	0.004	yes
1	Gq	all	day 7	0.031	yes
1	Gq	all	day 8	0.063	no (trend)

2	Gq	all	day 0	0.001	yes
2	Gq	all	day 6	0.06	no (trend)
2	Gq	all	day 7	0	yes
2	Gq	all	day 8	0.002	yes
3	Gq	all	day 0	0.001	yes
3	Gq	all	day 4	0.078	no (trend)
3	Gq	all	day 5	0.062	no (trend)
3	Gq	all	day 6	0.03	yes
3	Gq	all	day 7	0	yes
3	Gq	all	day 8	0.001	yes
4	Gq	all	day 0	0.006	yes
4	Gq	all	day 3	0.078	no (trend)
4	Gq	all	day 7	0.003	yes
4	Gq	all	day 8	0.023	yes
5	Gq	all	day 0	0.016	yes
5	Gq	all	day 3	0.062	no (trend)
5	Gq	all	day 7	0.003	yes
5	Gq	all	day 8	0.053	no (trend)
6	Gq	all	day 0	0.078	no (trend)
6	Gq	all	day 2	0.06	no (trend)
6	Gq	all	day 3	0.03	yes
6	Gq	all	day 7	0.036	yes
7	Gq	all	day 1	0.031	yes
7	Gq	all	day 2	0	yes

7	Gq	all	day 3	0	yes
7	Gq	all	day 4	0.003	yes
7	Gq	all	day 5	0.003	yes
7	Gq	all	day 6	0.036	yes
8	Gq	all	day 1	0.063	no (trend)
8	Gq	all	day 2	0.002	yes
8	Gq	all	day 3	0.001	yes
8	Gq	all	day 4	0.023	yes
8	Gq	all	day 5	0.053	no (trend)

Chronic CNO: body composition (fat mass)

Interactions:

time * group: F(2,19)=0.303, p=0.742

time * group * sex: F(2,19)=0.932, p=0.411

Chronic CNO: body composition (lean mass)

Interactions:

time * group: F(2,19)=0.691, p=0.513

time * group * sex: F(2,19)=3.646, p=0.046

post hoc tests:

time * group (group)

time (day)	***group***	***sex***	***comparison***	***p-value***	***significant***

Post-chronic	Gq	M	vs. ctrl	0.05	yes